

Corrosion Protection
by Selective Addressing of Polymer Dispersions to
Electrochemical Active Sites

Von der Fakultät für Naturwissenschaften
Department Chemie
der Universität Paderborn
zur Erlangung des Grades eines
Doktors der Naturwissenschaften
- Dr. rer. nat. -
genehmigte Dissertation

von
Sergej Toews, M.Sc.
aus Orenburg

Paderborn 2010

Erstgutachter:	Prof. Dr. Wolfgang Bremser
Zweitgutachter:	Prof. Dr.-Ing. Guido Grundmeier
Eingereicht am:	18.08.2010
Mündliche Prüfung am:	24.09.2010

*für meine Familie: Marina,
Maximilian Abram und
Leonhard Jakob*

Danksagung

Die vorliegende Arbeit wurde während meiner Tätigkeit als wissenschaftlicher Angestellter am Institut für Polymere, Materialien und Prozesse der Universität Paderborn im Zeitraum von November 2007 bis August 2010 angefertigt. Sie soll mir an dieser Stelle Gelegenheit bieten, mich bei all denen zu bedanken, die mich während meiner Promotionszeit begleitet und unterstützt haben.

Meinem Mentor und Betreuer, Prof. Wolfgang Bremser, gilt mein besonderer Dank für die kontinuierliche Unterstützung, Förderung und Betreuung dieser Dissertation sowie für seine stete Diskussionsbereitschaft und das Interesse am Fortgang dieser Arbeit. Herrn Prof. Guido Grundmeier danke ich für die freundliche Übernahme des Koreferats und für die vielen anregenden Diskussionen.

Der BASF Coatings GmbH gebührt mein besonderer Dank für die fortwährende Unterstützung durch mein gesamtes Studium, sowie für die Finanzierung der vorliegenden Arbeit. Im speziellen möchte ich Herrn Dr. Horst Hintze-Brüning und Herrn Dr. Michael Dornbusch für die interessante Thematik dieser Arbeit und für die intensiven und konstruktiven Diskussionen danken. Mein spezieller Dank gilt Herrn Dr. Sebastian Sinnwell für die anregenden Diskussionen zum Ende dieser Arbeit.

Allen Mitarbeitern des Fachbereiches Chemie und Technologie der Beschichtungsstoffe danke ich für die angenehme Atmosphäre, die Kollegialität, die stete Hilfsbereitschaft und für viele heitere Stunden.

Herrn Dr. Manuel Lohrengel gilt mein besonderer Dank für die freundliche Aufnahme in seiner Arbeitsgruppe für Mikroelektrochemie an der Heinrich-Heine-Universität zur Durchführung von Mikro-Kapillar-Zellen-Messungen.

Mein größter Dank gilt meiner Familie für die anhaltende Unterstützung während meiner Promotionszeit.

Abstract

This study followed the scientific approach of identifying active sites for electrochemical, corrosive processes on hot dipped galvanized steel and the creation of a material with selective deposition properties that could inhibit the corrosive activity of these weak spots. This study firstly involved high lateral resolution investigations on surface element composition and electrochemical micro probe techniques that identified weak zones on HDG steel substrate. Applying scanning electron microscopy and energy dispersive X-ray spectroscopy it was found that aluminum in HDG alloys (ZnAl 0.5 w.-%) segregates not only towards the zinc/iron and zinc/air interface but especially towards the boundaries of zinc grains. Surface high resolution potential mappings utilizing scanning Kelvin probe – force microscopy showed the electrochemical potential difference of grain boundaries (lower potential) compared to the surrounding grain surfaces: a clear indication for higher corrosive activity of these structures. The application of the micro capillary cell showed that grain boundaries tend to dissolve more easily due to corrosive currents that were measured at lower electrochemical potential (-910 mV) than on single grains (-830 mV). The final corrosion test on a coil coated substrate showed the higher corrosion activity of grain boundaries at the corrosion front. In this test corroded grain boundaries could be observed leading up to 200 μm forward from the main corrosion front into the intact coating/substrate interface. From these findings a model of different corrosion pathways was derived, which suggests that the anodic part reaction quickly propagates forward along the grain boundaries and is escorted by the local cathode. It can be said that on the delaminated substrate surface the main corrosion front can spread out more easily. Based on this model the corrosion propagation would decelerate by inhibiting the grain boundary activity. The second part of this study focused on the design of polymeric material and its selective application to grain boundaries. The anodic dissolution ability of grain boundaries and the preferred release of aluminum cations were thus used for the selective application of corrosion inhibiting materials on these active sites. An initial applicability screening of materials towards grain boundaries showed promising results with autophoresis of water-borne dispersions; among phosphating and surface spontaneous polymerization. Based on these results water-borne block-co-polymer dispersions were synthesized containing adhesion promoting groups such as carboxylic acid, phosphonic acid and triethoxysilane. Application of these polymers exclusively on grain boundaries could be realized with a controlled release of aluminum cations from these weak spots. It was shown that in the pH region of 2.5 to 4.0 grain boundaries start to dissolve and that coagulation of dispersed polymer particles is susceptible towards triple charged aluminum cations. This combination led to selective deposition of polymer particles on grain boundaries. The final proof of concept was provided by a comparison of non-grain boundary treated versus grain boundary treated HDG substrates in a salt spray test. The results showed a significant difference in the condition of the grain boundaries at the corrosion front, where the grain boundaries selectively covered with a specifically designed polymer reduced the anodic dissolution along the grain boundaries by a factor of three to twenty. In conclusion, grain boundaries on HDG steel are highly corrosively active and it was possible to block their corrosive activity by applying polymers only to these weak zones. This new method of selective corrosion protection bears high potential as a promising strategy towards smart and environmentally friendly pretreatment of steel goods.

Kurzfassung

Die vorliegende Studie verfolgte einen umfassenden experimentellen Ansatz die im Korrosionsprozess elektrochemisch aktiven Schwachstellen auf feuerverzinktem (HDG) Stahl zu identifizieren und Materialien selektiv auf diesen Stellen abzuscheiden um diese dadurch zu inhibieren. Im ersten Teil dieser Studie wurden hochauflösende Oberflächenanalysemethoden angewendet um die Elementzusammensetzung und die elektrochemisch aktiven Stellen auf solchen heterogenen Oberflächen zu untersuchen. Mittels der Rasterelektronenmikroskopie und der energiedispersiven Röntgenspektroskopie konnte gezeigt werden, dass sich Aluminium aus der Feuerverzinkungslegierung (ZnAl 0,5 gew.-%) neben der Segregation an die Zink/Eisen- und Zink/Luftgrenzfläche sich bevorzugt an den Korngrenzen der feuerverzinkten Stahloberflächen anreichert. Die Raster-Kelvinsonde-Kraftmikroskopie detektierte einen Unterschied im elektrochemischen Potential von Korngrenzen zu den Kornflächen. Dabei trat an den Korngrenzen ein negativeres Potential auf, was auf eine höhere anodische Auflösung dieser Strukturen hinweist. Mittels der Mikro-Kapillar-Zellen-Technik konnten Stromdichte-Potential-Messungen an Korngrenzen und Kornflächen durchgeführt werden. Dabei konnten bereits bei einer Polarisierung des Substrates von -910mV initiale Korrosionsströme an den elektrochemisch aktiven Korngrenzen detektiert werden. Auf den Kornflächen wurden erste Korrosionsströme bei einem Potential von -830 mV gemessen. Dieser Potentialunterschied bestätigte die anodische Auflösungsreaktion der Korngrenzenstrukturen. Im abschließenden Korrosionstest an einem lackierten Substrat konnte gezeigt werden, dass ausgehend von der aktiven Korrosionsfront eine korrosive Schädigungen entlang der Korngrenzen von bis zu 200 µm unter den noch intakten Grenzflächenbereich zwischen Beschichtung und Substrat auftritt. Aus diesen Ergebnissen wurde ein Modell mit zwei verschiedenen Korrosionswegen für das Fortschreiten der Korrosionsfront entlang dieser Grenzfläche entwickelt. Zunächst schreitet die Lokalanode schnell entlang der Korngrenzen voran und wird begleitet von dem komplementären kathodischen Bereich. Die nachfolgende Hauptkorrosionsfront kann somit schneller auf dem vorgeschädigten Substrat voranschreiten. Ausgehend von diesem Modell würde eine Inhibierung der Korngrenzenkorrosion auch eine Verlangsamung der Hauptkorrosionsfront mit sich bringen. Im zweiten Teil dieser Studie wurden Materialien für die gezielte Adressierung an die Korngrenzen synthetisiert und untersucht. Als Steuerungselement wurde hierfür das anodische Auflösungsverhalten der Korngrenzen und die damit verbundene lokale Freisetzung von Aluminiumkationen angewendet. Unter den zunächst untersuchten Techniken wie Phosphatierung und spontane Oberflächenpolymerisation zeigte die autophoretische Polymerabscheidung die vielversprechendsten Ergebnisse bezüglich der Selektivität des Abscheidemechanismus. Basierend auf diesen Erkenntnissen wurden Block-co-polymer-Dispersionen mit funktionalen Haftgruppen für oxidische Substrate (Carboxyl-, Phosphonsäure und Triethoxysilan) für die gezielte Korngrenzenapplikation synthetisiert. Die Abscheidung dieser Polymerdispersionen an den Korngrenzen konnte durch die kontrollierte Freisetzung von Aluminiumkationen im pH-Wertbereich 2,5 - 4,0 erfolgen. Die Destabilisierung der Dispersionspartikel durch dreiwertige Aluminiumkationen führte schließlich zur selektiven Belegung der korrosiven Schwachstellen. Die abschließenden Korrosionstests zeigten eine drei- bis zwanzigfache Verringerung der Schädigung entlang der Korngrenzen, wenn diese gezielt mit den synthetisierten Block-co-polymeren belegt und somit inhibiert wurden. Zusammenfassend konnte gezeigt werden, dass Korngrenzen auf HDG-Stahl eine verstärkte Korrosionsaktivität aufweisen und dass diese durch die gezielte Applikation geeigneter Polymere exklusiv an diesen Schwachstellen herabgesetzt werden kann. Dieses Konzept für selektiven Korrosionsschutz birgt ein hohes Potenzial als Strategie zur ressourcenschonenden und umweltfreundlichen Vorbehandlung von Stahloberflächen.

Content

Danksagung	v
Abstract	vii
Kurzfassung	viii
Chapter 1 – General Introduction	1
1.1 Corrosion impact on economy and society	1
1.2 Scientific approach	3
1.3 Corrosion processes on coated substrates	4
1.4 Adhesion theory	7
1.4.1 Mechanical adhesion	8
1.4.2 Primary and secondary adhesion	9
1.5 Approaches to new conversion methods – a literature survey	14
1.5.1 Rare earth compounds and transition metals	14
1.5.2 Self-healing function	15
1.5.3 Sol-Gel process	16
1.5.4 Self-assembled monolayer	16
1.6 References	18
Chapter 2 – Applied Techniques	23
2.1 Scanning electron microscopy and energy dispersive X-ray spectroscopy	23
2.2 Scanning Kelvin probe – force microscopy	24
2.3 Micro capillary cell	25
2.4 Gel permeation chromatography	28
2.5 Dynamic light scattering and ζ -potential	28
2.6 Surface plasmon resonance spectroscopy, measurements and sensor preparation	29
2.7 References	31
Chapter 3 – Results and Discussion	33
3.1 Substrate characterization	33
3.1.1 Fundamentals	33
3.1.1.1 Aluminum in HDG coating alloys	33
3.1.1.2 Grain boundaries and weak zones	36

3.1.2	Experimental procedures	38
3.1.2.1	Substrate	38
3.1.3	Experimental results	39
3.1.3.1	Surface structure and element distribution on HDG-Steel Al 0.5 w.-%	39
3.1.3.2	Surface potential	43
3.1.3.3	Dissolution activity of grain boundaries vs. grains	45
3.1.3.4	Corrosion behavior of grain boundaries on coated substrates	50
3.1.3.5	Corrosion pathways as a model development	51
3.1.4	Conclusion	55
3.1.5	References	56
3.2	Material survey for grain boundary application	59
3.2.1	Fundamentals	59
3.2.1.1	Phosphating	60
3.2.1.2	Surface spontaneous polymerization	61
3.2.1.3	Polymer deposition	62
3.2.2	Experimental procedure	63
3.2.2.1	Grain boundary dissolution	63
3.2.2.2	Phosphating	63
3.2.2.3	Surface spontaneous polymerization	64
3.2.2.4	Polymer deposition	64
3.2.3	Experimental results	65
3.2.3.1	Grain boundary dissolution	65
3.2.3.2	Phosphating	66
3.2.3.3	Surface spontaneous polymerization	71
3.2.3.4	Polymer deposition	72
3.2.4	Conclusion	76
3.2.5	References	77
3.3	Polymer design for grain boundary application	81
3.3.1	Fundamentals	81
3.3.1.1	Requirements and characteristics of the polymer of choice	81
3.3.1.2	Synthesis of block-co-polymers	82
3.3.1.3	Mechanistic understanding of the block-co-polymer formation in the presence of DPE	85

3.3.2	Experimental procedures	88
3.3.2.1	Materials	88
3.3.2.2	Synthesis of functional block-co-polymers in a hetero phase system	88
3.3.3	Experimental results	89
3.3.3.1	Overview of synthesized block-co-polymers	89
3.3.3.2	GPC and particle size observations	90
3.3.3.3	Conversion ratios of the monomers	93
3.3.3.4	Dispersion stability	96
3.3.4	Conclusion	97
3.3.5	References	98
3.4	Polymer application on grain boundaries	101
3.4.1	Fundamentals	101
3.4.1.1	Colloid stability	101
3.4.2	Experimental procedure	107
3.4.2.1	Titration on ion selectivity	107
3.4.2.2	SPR measurements	107
3.4.2.3	Grain boundary selective polymer application	107
3.4.2.4	Coating application and testing	108
3.4.3	Experimental results	108
3.4.3.1	Polymer ion selectivity	109
3.4.3.2	Polymer particle stability in dependency of pH values	111
3.4.3.3	Polymer particle adsorption to aluminum and zinc oxide surfaces	112
3.4.3.4	Selective deposition on grain boundaries of HDG steel	119
3.4.3.5	Testing results	124
3.4.4	Conclusion	128
3.4.5	References	129
Chapter 4 – Overall Conclusion and Outlook		131
Appendix		<i>xiii</i>
Abbreviations		<i>xiii</i>
Publications		<i>xv</i>

Chapter 1 –

General Introduction



Fig. 1.1: Example of corroded steel surface where the coating has lost its ability to protect the surface from oxygen and humidity [1].

1.1 Corrosion impact on economy and society

Corrosion protection of steel surfaces plays an important role in everyday life. The majority of steel manufactured goods and products are exposed to atmospheric humidity and oxygen in which presence iron follows its natural role to create the most thermodynamically stable compound. The steel oxidizes and

corrosion occurs. In order to protect steel from corrosion it is covered with a multilayer coating system. In the case of galvanized steel, the first layer is metallic zinc. When a corrosive attack on steel occurs that acts as a sacrificial anode and protects the steel from oxidic dissolution. In general, the next layer is a zinc phosphate layer which inhibits electrochemical corrosion processes on the zinc surface and provides adhesion to the following organic coating layer. Aside from the decorative demand for color and appearance, this organic coating layer provides a barrier against humidity, oxygen and corrosive stimulants. Within industry, the phosphating process is well established. It is easy to handle and cheap in terms of the ingredients required. However the overall costs of the phosphating process are in issue, due to a temperature of around 65°C and the toxic sludge that is continuously generated in the phosphating bath. The toxicity from the nickel and fluorides added into the phosphate bath for corrosion improvement are also a major reason that industry is seeking new technologies that would replace the phosphating process. This study will focus on these exact issues. Existing corrosion concepts will be evaluated and a new concept based on water borne polymers will be derived and proved in terms of its usability. In addition, the reduction of the pretreated surface area from a continuous layer to a smart and structured application that is only specific to the weak spots of the substrate, will reduce the total amount of pretreatment material required, which may in turn improve the economic and ecological efficiency.

Fig.1.1 provides an illustration of a corroded steel surface. The annual loss resulting from corrosion in the industrial countries is estimated at 3-4% of GDP [2]. According to these numbers, the annual economic loss for EU countries alone can be calculated at 350 Billion Euro [3]. In addition to the high financial costs the production of steel is very energy intensive and leaves a carbon footprint of 1.35 tones CO₂ per ton of steel [4]. Prolonging the lifetime of steel made goods will thus also lead to a reduction in carbon dioxide emissions. Even though recent studies show that a quarter of these costs could be reduced through the appropriate use of existing corrosion concepts, corrosion still remains a tremendous loss factor. In addition, there is a strong need for the replacement of traditional corrosion concepts based on heavy metals such as lead and chromium, due to environmental and health responsibilities. There is a long history of heavy metals having excellent corrosion protection for steel, but they

are toxic and in the case of hexavalent chromium even strongly carcinogenic [5,6]. In the last decade huge efforts have been made by industry and research institutions towards the development and implementation of new, environmentally friendly corrosion protection systems that eliminate these substances from technical applications. This change in technology is strongly enforced by political directives. In 2000, the European Parliament prohibited the use of chromium compounds for automotive industry, one of the major users of corrosion protective materials [7]. For the aviation industry, a similar policy is being prepared and will be enforced in the near future.

All of these aspects highlight the necessity for a better understanding of corrosion processes and the development of new, environmentally friendly materials and concepts for corrosion protection.

1.2 Scientific approach

The general consideration when inventing coatings for a specific type of substrates e.g. steel, aluminum, or zinc coated steel is that the substrate surface consists of a homogeneous distribution of all alloy containing elements. At the same time, it is general knowledge that the surface of any technical substrate is heterogeneous due to the alloying process. It is also well known that corrosion prefers to start at weak zones. These areas are typically edges, vertices and heterogeneous segregations [8]. It can be assumed that the electrochemical process of corrosion starts at these spots. The aim of this study is to identify the weak zones of a technical substrate of hot dipped galvanized steel (HDG), investigate the electrochemical activity and influence on the corrosion process at the substrate coating interface and develop a polymeric coating material to specifically block and inhibit these weak zones. The approach of adapting the coating material to the heterogeneous surface properties of technical substrates would provide a new concept for environmentally friendly corrosion protection coatings.

1.3 Corrosion processes on coated substrates

Electrochemical processes of corrosion on a coated substrate were primarily investigated by Evans in the 1960s [9]. Evans found that electrochemical corrosion reactions are separated locally into two part reactions; in the so called local cells an anodic and a cathodic area (see Fig. 1.2).

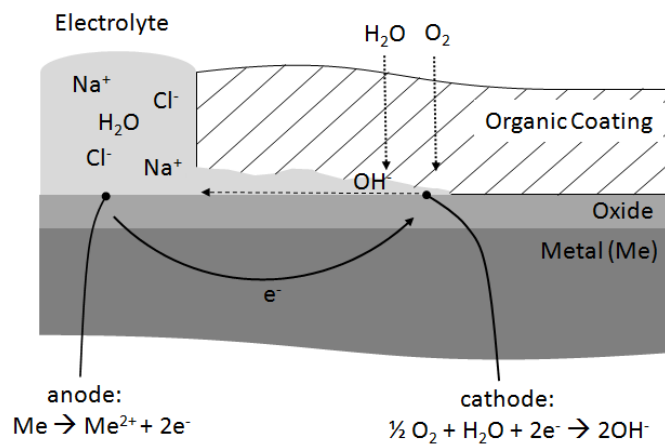
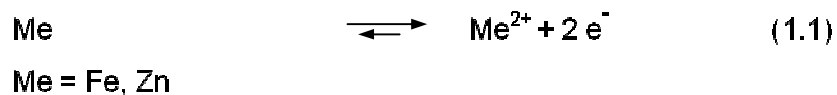
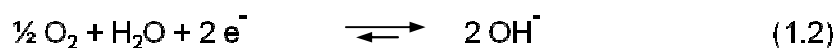


Fig. 1.2: Schematic illustration of the cathodic delamination mechanism, a cross section view [10].

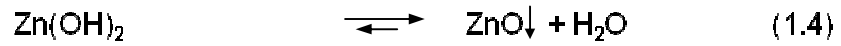
Metal oxidizes in the area of the local anode.



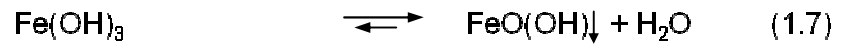
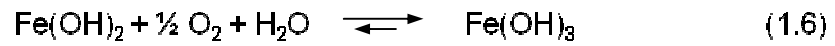
The released electrons from this part of the reaction will flow through the conductive substrate to the local cathode. The oxidized metal atoms become loose in the metallic grid structure and dissolve into the ambient electrolyte. Oxygen is reduced to hydroxyl ions at the local cathode in the presence of water.



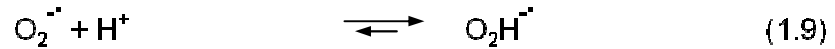
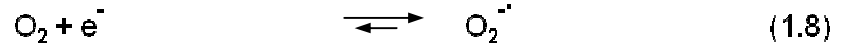
In a cascade of the following reactions, metal ions and hydroxyl ions precipitate.



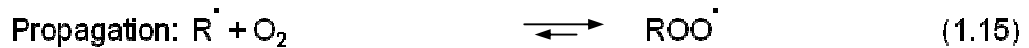
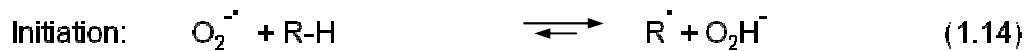
In the case of iron, this process results in rust.



During the oxygen reduction, many short-lived intermediates of hydroxy radicals and peroxy radicals are formed in the cathodic area which is always located in the outermost region of the defect [11,12].



The radical species are highly reactive and therefore prefer to react with the polymeric material of the organic coating.



R = Polymer

The diffusion coefficient of water and electrolytes (10^{-6} cm²/s) along the polymer/metal oxide interface is 100 times higher than through the bulk polymer. This leads to the destruction of the polymeric material particularly at the interface between the coating and metal/metal oxide [13]. This process leads to de-

adhesion of the organic coating and to an uncovered metal substrate, this is the so called cathodic delamination [14]. Cathodic delamination is dominant in high atmospheric humidity and occurs on metals such as iron, but especially on zinc [10]. The most determining factors for the kinetics of the cathodic delamination are highlighted as the pH-stability of the metal oxide, the oxygen permeability and the adhesion of the organic coating as well as the relative humidity of the surrounding atmosphere [13,15-20]. Zinc coatings are applied to low alloy steel sheets in order to improve corrosion resistance by acting as a sacrificial anode [21]. At the same time, the zinc oxide surface is more affected by corrosive delamination. The hydroxyl ions generated in the cathodic area raise the pH value in the local cathode area. In this outermost forefront of the delaminated area the delaminated organic coating is still very close to the substrate which results in a very small free volume. In this area a few hydroxyl ions raise the pH to maximum values. Zinc/zinc oxide is stable up to the pH value of 13.5 but in the forefront of the delaminated area these pH values are exceeded which leads to the dissolution of the amphoteric zinc oxide/hydroxide to zincate species [22-24].



The benefit brought by zinc coating to the steel substrate is combined with the losses, considering the corrosive delamination of the organic coatings. Based on this fundamental understanding a model will be derived for corrosive delamination on the heterogeneous substrate surface of HDG steel within this study (see section 3.1).

In order to decrease the delamination and corrosion process, ongoing public research is approaching the improvement of corrosive delamination from two sides, by modifying the zinc alloy and by improving the organic coating. Scoping of the zinc alloy approach finds recent research results that have shown that doping the zinc alloy with metals of lower electrochemical potential e.g. titanium,

aluminum, or magnesium lower the electron conductivity of the oxide layer significantly [11]. Electrons coming from the local anode are no longer able to come up to the local cathode. Disrupting the cathodic part of the corrosion process leads to a breakdown of the cathodic delamination. The anodic corrosion reaction also then stops, when the electron flow is inhibited. The approach to prevent cathodic delamination from the side of the organic coating faces the major aspects of adhesion and degradation resistance of polymeric materials.

1.4 Adhesion theory

Adhesion theory in general describes adhesive forces at the interface of a solid substrate and a second phase. The second phase can be a molecule, a particle, a droplet or a continuous liquid or solid phase such as a coating [25]. Adhesion theory is based on different models of mechanical, primary and secondary adhesion, due to the different interaction mechanism of these two phases [26]. Considering coatings, adhesion is a complex phenomenon that can only be partially explained by these simplified models; testing coating for adhesion visco-elastic properties of the solidified coating material also provides a dominant factor to the adhesion performance of the coating [27]. Nevertheless, the overall adhesion performance of coatings is predominant for the protection of the metal substrate and is also dependent on the molecular adhesion of the functional groups incorporated into the coating material and addressed to the substrate/coating interface. Molecular adhesion models will therefore be discussed within this chapter. Based on these models, functional monomers have been screened on their adsorption and desorption strength towards oxidic surfaces [28]. These screening results lead to the monomer choice used for the block-co-polymer design for grain boundary application of this study (see section 3.3).

1.4.1 Mechanical adhesion

The theory of mechanical adhesion describes the force-fit interlock of two adhered phases. This mechanism takes place when one of the two adhesive phases is a solid material with a rough or porous surface structure that comes into contact with a penetrating liquid phase, which solidifies after spreading over the surface. A good technical example would be a coating or a sealant applied to a zinc phosphated or defined oxidized metal surface. Van den Brand et al. reported to achieve a well-defined microstructure with good wetting properties on aluminum by creating a pseudoboehmite oxyhydroxide layer through immersion in boiling water [29]. This procedure creates a porous structure with an active surface area increased 14 times [30]. In line with this work, mechanical adhesion would occur in the rough structure of grain boundaries on coated HDG steel samples (see section 3.1). A schematic understanding of the mechanical adhesion models is illustrated in *Fig. 1.3*.

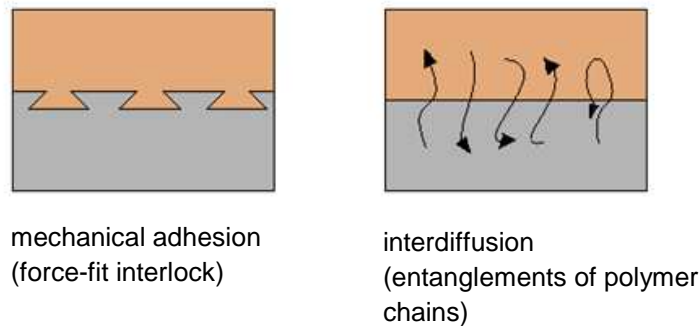


Fig. 1.3: Schematic illustration of the relevant mechanical adhesion models.

On an absolutely planar surface this mechanism of force-fit interlock loses its effectiveness and primary and secondary adhesion models have to be considered. An exception to force-fit interlock on planar surfaces is found in the adhesion of two thermoplastic surfaces. This model for adhesion is based on the

diffusion theory, due to inter-diffusion and entanglements of polymer chains. Even though in corresponding literature polymer chain inter-diffusion is most often considered as an independent model [31-33], in this study it will be subordinated to the mechanical adhesion model based on a general understanding of mechanics. The difference to the model previously discussed is only that the mechanics are expanded to the sub nanometer scale on the molecular level of polymer chains. Polymer chains in the bulk phase of the material have some degree of mobility. This mobility is highly temperature dependent, which makes this mechanism controllable and well suited to industrial applications such as the welding of plastics. The mobility of polymer chains becomes significant for diffusive interpenetration at temperatures above the glass transition temperature. For example, hydrated poly polybutadiene chains with a molecular weight of 105,000 g/mol and a glass transition temperature of 108 °C have a diffusion coefficient of $2.22 \cdot 10^{-11}$ cm²/s at 125 °C. Raising the temperature to 165 °C doubles the diffusion coefficient to $4.52 \cdot 10^{-11}$ cm²/s [34]. The welding process for plastics requires a self-diffusion coefficient above 10^{-8} cm²/s in order to achieve an interpenetrated length of 50 µm within one second [35]. Therefore the resulting entanglements of the single polymer chains can be understood as force-fit interlock and associated to the theory of mechanical adhesion.

1.4.2 Primary and secondary adhesion

Both primary and secondary adhesions are based on the fundamentals of adsorption theory where chemical bonding takes place on a molecular level. These types of adhesions play the most dominant role by designing polymers for a strong bond to the metal/oxide substrate in order to reduce coating delamination processes discussed in section 3.3 of this study. The concept of primary adhesion includes covalent, ionic and metallic interaction. In *Tab. 1.2*, the bonding type, the length and the energy of the molecular are consolidated. *Fig. 1.4* schematically illustrates the chemistry of primary and secondary adhesion.

Tab.1.2: Bonding type, length and energy of molecular interaction in adsorption theory [36].

bonding type	length [nm]	energy [kJ/mol]
<u>primary adhesion</u>		
ionic bonds	0.15 – 0.24	600 – 1100
covalent bonds	0.15 – 0.24	60 – 700
metallic bonds	0.26 – 0.30	110 – 350
<u>secondary adhesion</u>		
hydrogen bridging bonds	0.30 – 0.50	40 – 50
dipole / dipole-interaction (Keesom-Forces)		4 – 21
dipole / induced dipole-interaction (Debye-Forces)		< 2
dispersive interaction (London-Forces)	0.50 – 10.0	4 – 42

These chemical bonds typically have a relatively high bonding energy and are therefore very stable. In the case of covalent bonding and the overlapping of binding, molecular orbitals occur by sharing at least one pair of electrons from one atom of the adhesive molecule and one from the substrate [37]. A good example of covalent bonding in the interface chemistry is the application of thiols or thiolfunctionalized polymers on gold surfaces [38,39]. In the present day, covalent bonding to corrosion susceptible surfaces attracts a great deal of attention in steel pretreatment chemistry. Covalent bonded molecules saturate the chemical reactivity of coordinative centers of the substrate and provide them with a high resistance against further reactions. In addition, the bonded molecules provide these reactive sites with steric hindrance and shield these sites from corrosive attacks. Therefore the outermost atoms of the substrate become stabilized against corrosive dissolution.

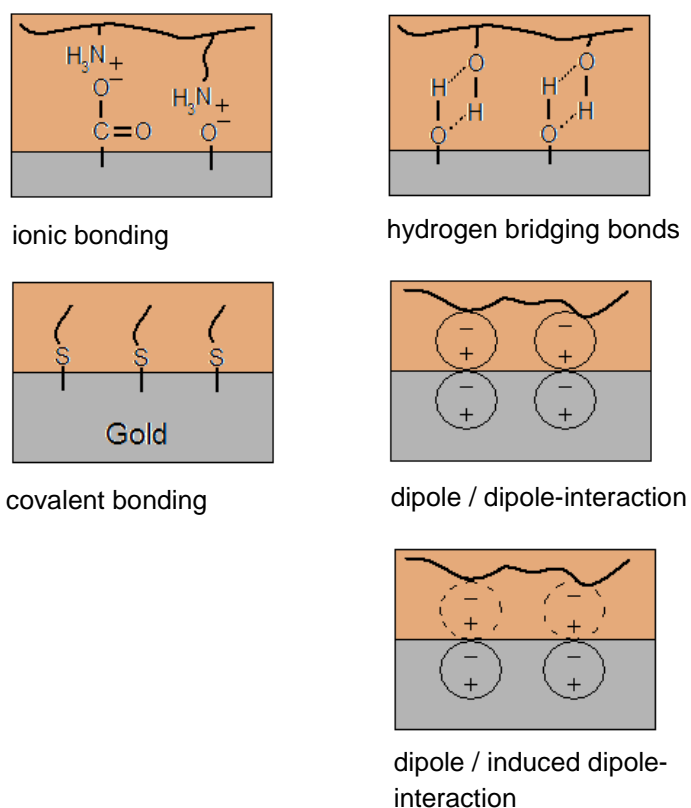


Fig.1.4: Schematic illustration of molecular interaction in the primary and secondary adhesion.

Based on these concepts, over the last decade there have been general developments of conversion systems using silane chemistry to passivate aluminumoxide and zincoxide surfaces. It is postulated that the silanol group when under cleavage of alcohol undergoes a condensation process with a hydroxyl function of the substrate [40,41]. Investigations supporting this theory were provided by finding $^+Si-O-Al$ and $^+Si-O-Fe$ fragments from ToF-SIMS spectra on the substrate surface after removing the conversion layer [42]. However contra to this, recent investigations using the ToF-SIMS-technique showed the same molecule fragment by treating the metal/oxide substrate with a silicon oil polydimethylsiloxane (PDMS) [13]. It is very well known that PDMS is chemically inert and does not react with the oxide surface of the substrate. This means that the conversion chemistry of oxidic surfaces with silanols remain a

research object of high interest. However, good adhesion of silanol conversion layers to metal/metal oxide substrates and the improved corrosion resistance is still undisputable [43,44]. This method of conversion is not fully understood but is formulated to the stage where it is ready to be implemented in the steel coil and automotive industry [45]. Based on the results of the monomer survey silane monomers will also be co-polymerized and applied to grain boundaries within this study.

Ionic bonds are very well known from organic and inorganic salts. The chemical interaction in an ionic bond relies on positive and negative charges. In order to describe the interaction between the adsorbing organic molecule/polymer and the inorganic surface of the substrate, the HSAB-Model (*Hard and Soft Acids and Bases*) has been developed by Pearson [46,47]. This model distinguishes acids as electron pair acceptor molecules defined by Lewis or as proton donor molecules as defined by Brönsted. Bases are the counter molecules to the acids which make them electron pair donor molecules in the case of Lewis and proton acceptor molecules in the case of Brönsted to [48]. The HSAB-Model also distinguishes between hard (hard to polarize) and soft (easy to polarize) acids and bases. Relatively stable acid-base-complexes result from the combination of hard acids with hard bases and from soft acids with soft bases [49]. In the case of a combination of a soft component with a hard component the resulting bond strength is rather weak. Based on these principles the oxide surface of a substrate can react in different ways with the polymeric coating material. Hydroxyl terminated surfaces in general behave as a Brönsted base by donating their protons to a proton acceptor such as an amino group coming from the coating material [50]. In the case where the reactive group from the coating material is a carboxylic acid, the hydroxyl function of the surface can be protonated and leave the metal/oxide surface as a water molecule. The newly created and freely available metal cation on the substrate surface reacts as a Lewis acid with the carboxylic group, the Lewis base and creates a coordinative complex [51]. This observation can be made on zinc substrates as well as aluminum [52]. Review of the two substrates highlights the need to consider that the strengths of these complexes cannot be the same, because carboxylic acids behave as strong Lewis bases in their dissociated form [53]. In this way, the more stable complex of the carboxylic acid function will be performed with the hard Lewis acid, the

Al^{3+} -cation, rather than with the weak Lewis acid, the Zn^{2+} -cation [54]. The fundamental understanding of the interaction between cations and functional groups of polymer dispersion will also be important for the selective deposition of polymer particles on grain boundaries in section 3.4 of this study. As a result of the most recent developments in single molecule desorption using atomic force microscopy it is possible to measure the adhesion force of single functional groups on the specific metal oxide surfaces. In fact not only the type of metal oxide but also the surface orientation due to the crystal structure of the metal/oxide leads to different adhesion strength of the adsorbed molecule. Recent studies by M. Valtiner and G. Grundmeier have shown that the peel force from an acrylic acid function on a hydroxide-stabilized polar $\text{ZnO}(0001)\text{-Zn}$ surface can be measured in the range of 60-80 pN and attributed to secondary adhesion forces. When a carboxylic acid function was peeled off the edges of the zinc oxide surface, peel forces of up to 700 pN were measured. The higher peel force was attributed to coordinative bonding of the carboxylic function to the edge of a polar surface $\text{ZnO}(0001)\text{-Zn}$ surface [55]. These investigations are very important to understand how adhesives adsorb to surfaces such as HDG steel in order to evaluate the stability of the adsorbed functionalities under corrosive conditions. In fact within this study, it will be found that HDG steel surfaces appear as flat grains and grain boundaries can be described as multi edges geometries (see section 3.1). Single molecule peel force investigations are still in the early stages, but will provide important information and knowledge on the adhesion strength of different functionalities and help to design specific polymeric coating materials for the specific need of the different metal/oxide properties in order to improve corrosion protection and resistance for cathodic delamination.

The metallic bond is characteristically known for creating a delocalized electron gas which surrounds the atomic kernels and establishes the adhesive force within a metal substrate. This type of chemical bond is of interest when considering inter and intra-metallic phases. Because of its different focus, it will not be discussed further in this thesis.

The secondary adhesion is based on secondary valences and distinguishes between hydrogen bridging bonds, Keesom forces, Debye forces and London forces. In the case of hydrogen bridging bonds, a hydroxyl terminated surface interacts with the hydroxyl function of the coating polymer or simply with water.

The strength of the bond is dedicated to delocalization of the bridging proton which is entropically stabilized [56]. In the case of Keesom forces, both the adhesive and the substrate bear a dipole moment resulting in an attractive interaction of the contrary charges. Debye forces interact similarly to the Keesom forces with a marginal difference where only one of the reacting partners bears a dipole moment but induces a contrary charge at the surface of its interacting partner.

1.5 Approaches to new conversion methods; a literature survey

Ambitious efforts to eliminate toxic and carcinogenic materials such as hexavalent chrome have led to new approaches in passivation systems for steel, galvanized steel and aluminum over the last few years. The supreme target of these coating materials is to establish highly adhesive, oxygen and water impermeable layers on the surface. The fundamentals of the previously discussed adsorption theory provide the basis for the following innovative conversion layer systems:

- Rare earth compounds and transition metals
- Self-Healing function
- Sol-Gel process
- Self-assembled monolayer

1.5.1 Rare earth compounds and transition metals

The idea of inhibiting corrosion through the use of rare earth compounds and chromes analogous transition metals started where hexavalent chrome showed its effectiveness. Chromium compounds have been used for corrosion protection throughout the last century but were only classified as highly toxic and carcinogenic two decades ago. In the corresponding literature, the properties in terms of corrosion protection in conversion layers of elements such as Cerium, Zirconium, Molybdate or Vanadium have been investigated [57-59]. In all cases, the oxidized form of the elements is the active corrosion inhibiting substance. The

use of trivalent chromium compounds is also reported to provide improved corrosion protection as they are less reactive than the hexavalent chromium and therefore exposure to humans is less harmful. However trivalent chromium could oxidize to its hexavalent species under certain conditions [60]. Cerium for example converts to ceriumhydroxyde at higher pH values, similar to those obtained in the area of the local cathode. The ceriumhydroxide interrupts the electron transport of the local cathode and the corrosion process stops. The conversion of the substrate can be realized either through dipping it into a solution of the corresponding salt or by adding these salts to the coating pretreatment material that is applied to the substrate. Recently developed processes add rare earth compounds to sol-gel coatings and combine both the passivating abilities of the transition metals with the good barrier properties of the sol-gel process. In this case, the oxidized form of the element is directly implemented in the silica-oxygen matrix of the coating layer [58,61]. However, some of the rare earth and transition metals are not sufficiently tested in terms of long-term exposure to the human body. A broad application in industrial manufacturing could lead to the classification of these compounds as critical for the human body. It could be argued that the development of new metal passivation materials should strive towards non-heavy metal compounds.

1.5.2 Self-healing function

The self-healing effect for coating materials in terms of corrosion protection was firstly realized as a result of the addition of organic corrosion inhibitors such as 8-hydroxyquinoline and different types of benzotriazoles and benzothiazoles [62,63]. The inhibitor molecules are not bonded to the polymeric matrix of the coating and are able to diffuse. This mobility is necessary in the case where a defect in the coating layer occurs. Inhibitor molecules can migrate to the bare substrate spot and cover it by establishing chemical bonds to the metal surface. But this mobility has one major disadvantage. The inhibitor is able to leak from the coating and the system will thus within time, lose its self-healing properties. The inhibitor covered defect can also only be protected for a limited quantity of time. The latest developments in this area allow the encapsulation of the inhibitor molecules in nano-container or nano-vesicles which release their content only in

the situation where damage to the coating occurs [64]. This method allows a prolonged self-healing function of the coating layer, however the time period of the healed status in the case of a defect occurring is still limited.

1.5.3 Sol-Gel process

A conversion layer based on the sol-gel technique provides improved corrosion resistance properties on steel [65,66], galvanized steel [67], and aluminum [68]. The conversion layer can be created by any type of coating process e.g. dipping or spraying with a silanol solution. In order to achieve a conversion layer with the desired properties for corrosion protection, the silanol solution should be adjusted to low pH values such as 4 – 5 [69]. The process of film formation is controlled by the pH and is thus going through the steps of pre-condensation, generating oligosilanol molecules and subsequently condensing with residual monomeric silanol on the substrate surface. The deposited film is then finally cured at raised temperatures in order to achieve the high cross link density. Even though chemical bonding of this type of conversion layer is controversial within literature, it provides a good protection toward cathodic delamination and corrosion propagation. These abilities may also be attributed to the high cross link density of the three dimensional network [70] as discussed in the adhesion theory.

1.5.4 Self-assembled monolayer

At an academic level, self-assembling molecules have been intensively investigated as long chain alkylthioles (C_{12}) on gold surfaces [71,72]. These molecules adsorb to the gold surface and create covalent bonds of thiole functionalities with gold atoms from the substrate surface. *Fig. 1.4* shows a schematic illustration of adsorbed SAM molecules to a metal substrate. SAM molecules are tilting to an angle of around 15° and create a dense packaging due to their long backbone chain. The densely packed and highly orientated monolayer hermetically seals the substrate surface [73]. For modern corrosion protection, applications of the molecules are designed with an anchoring group on one side and a head group on the other. The anchoring group is designed for the specific target surface which in the case of aluminum can be a phosphonic

acid [74]. Silane functional anchoring groups in analogy to the sol-gel process are also terms of investigation for usability in terms of corrosion protection. Head groups are designed to create covalent bonds to the top applied organic coating system. A prominent example for such head groups is the amine functionality which is very reactive with epoxy groups from the coating.

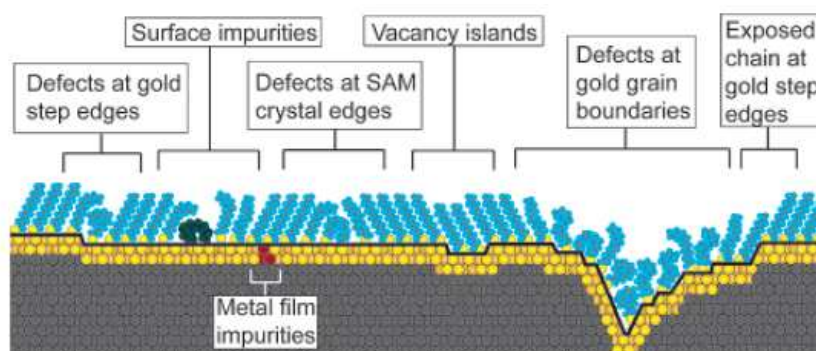


Fig. 1.4: Schematic illustration of some of the intrinsic and extrinsic defects found in SAMs formed on polycrystalline substrates. The dark line at the metal-sulfur interface is a visual guide for the reader and indicates the changing topography of the substrate itself [75].

The same packaging angle that is responsible for the high impermeability of an established SAM is also responsible for the biggest disadvantage of such conversion systems in terms of corrosion protection. At ambient temperatures, the formation of the self-assembled monolayer starts simultaneously at different points and propagates in so called island growth [76]. Whenever two growing SAM crystals hit each other they create an intrinsic defect and are not able to protect the substrate sufficiently. In general, SAMs are weak in covering extrinsic defects arising from the substrate surface such as grain boundaries, impurities due to segregation and unevenness in topography (see Fig. 1.4). Therefore for technical use, short chain molecules such as trimethoxysilyl propylamine (γ -APS), a C_3 – chain molecule, are preferably applied. These molecules cannot create high barrier properties but they act well as an adhesion promoter between the substrate and coating [13].

1.6 References

- [1] Annual Report 2003 IFAM Klebtechnik und Oberflächen (2003)
- [2] Z. Zeng, K. Natesan, Z. Cai, S.B. Darling, *Nature Mat.* 7 (2008) 641
- [3] Eurostat Press Release 55/2010 (2010)
- [4] SteelConstructions.org, NSC 2010 (2010) 32
- [5] W. Machle, F. Gregorius, *Public Health Rep.* 63 (1948) 1114
- [6] T.F. Mancuso, W.C. Hueper, *Ind. Med. Surg.* 20 (1951) 358
- [7] Directive 2000/53/EC of the European Parliament and of the Council of 18 September 2000 on end-of-life vehicles, *Off. J. Europ. Comm.* L269 (2002) 34
- [8] E. Almeida, I. Alves, C. Brites, L. Fedrizzi, *Prog. Org. Coat.* 46 (2003) 8
- [9] U. R. Evans, *An Introduction to Metallic Corrosion*, Hodder-Arnold, London (1963)
- [10] R.Posner, Thesis „Combined Spectroscopic and Electrochemical Studies of Ion Transport and Corrosive de-Adhesion Processes at Polymer/Oxide/Metal Interfaces”, Universität Paderborn (2009)
- [11] R. Hausbrand, *Steel Research Int.*, 74 (2003) 453
- [12] A. Leng, H. Streckel, K. Hofmann, M. Stratmann, *Corr. Sci.* 41 (1999) 599
- [13] K. Wapner, Thesis „Grenzflächenchemische und elektrochemische Untersuchungen zur Haftung und Enthftung an modifizierten Klebstoff/Metall-Grenzflächen“ Ruhr-Universität Bochum (2006)
- [14] P.A. Sorensen, K. Dam-Johansen, C.E. Weinell, S.Kiil, *Prog. Org. Coat.* 67 (2010) 107
- [15] H. Leidheiser, *Corrosion Control by Organic Coatings*, Science Press, Princeton NJ (USA), 1979
- [16] H. Leidheiser, W. Wang, L. Igetoft, *Prog. Org. Coat.* 11 (1983) 19
- [17] M. Stratmann, A. Leng, W. Fürbeth, H. Streckel, H. Gehmecker, K. H. Grosse-Brinkhaus, *Prog. Org. Coat.* 27 (1996) 261
- [18] W. Fürbeth, M. Stratmann, *Prog. Org. Coat.* 39 (2000) 23
- [19] A. Leng, H. Streckel, M. Stratmann, *Corr. Sci.* 41(1999) 547
- [20] A. Leng, H. Streckel, M. Stratmann, *Corr. Sci.* 41(1999) 579
- [21] M. Rohwerder et al, Annual Report 2003, Max-Planck-Institut für Eisenforschung GmbH, Düsseldorf (2003)

-
- [22] W. Fürbeth et al, *Corr. Sci.*, 41 (2001) 207
- [23] W. Fürbeth et al, *Corr. Sci.*, 41 (2001) 229
- [24] W. Fürbeth et al, *Corr. Sci.*, 41 (2001) 243
- [25] A. J. Kinloch, *Adhesion and Adhesives – Science and Technology*, Chapman and Hall, London (1987)
- [26] D. E. Packham, *J. Adhesion*, 39 (1992) 137
- [27] G. Meichsener, T.G. Mezger, J. Schröder, *Coatings Compendien „Lackeigenschaften messen und steuern“* Vincentz, Hannover (2003)
- [28] S. Toews, *Adsorption funktionaler Monomere an oxidischen Grenzflächen*, Master Thesis, Universität Paderborn (2007)
- [29] J.van den Brand, S.van Gils, P.C.J.Beentjes, H.Terryn, V.Sivel, J.H.W.de Wit, *Prog. Org. Coat.*, 51 (2004) 339
- [30] J.van den Brand, O.Blaiev, P.C.J.Beentjes, H.Terryn, J.H.W.de Wit, *Langmuir*, 20 (2004) 6308
- [31] A. J. Kinloch, *Adhesion and Adhesives – Science and Technology*, Chapman and Hall, London (1987)
- [32] W. Possart, *Adhesion-Current Research and Applications*, Wiley-VCH, Weinheim (2005)
- [33] A. V. Pocius, *Adhesion and Adhesives Technology-An Introduction*, 2nd Ed., Hanser, München, Wien (2002)
- [34] C. R. Bartels, *Macromolecules*, 17 (1984) 2702
- [35] H. Potente, *Fügen von Kunststoffen - Grundlagen Verfahren Anwendung*, Hanser, München, Wien (2004)
- [36] L.-H. Lee, *Fundamentals of Adhesion*, Plenum Press, New York, London (1991)
- [37] A. F. Holleman, E. Wieberg, *Lehrbuch der Anorganischen Chemie*, 101 Auflage, deGruyter, Berlin (1995)
- [38] M. Büttner, *J. Phys. Chem. B*, 109 (2005) 5464
- [39] L. D. Unsworth, *J. Coll. Interf. Sci.*, 281 (2005) 112
- [40] M.-L. Abel, *J. Adhes.*, 80 (2004) 291
- [41] J. F. Watts, *Surf. Interface Anal.*, 29 (2000) 115
- [42] J. F. Watts, *Int. J. Adhes. Adhes.*, 16 (1996) 5
- [43] M. F. Montemor et al, *Electrochim Acta*, 52 (2007) 7486
- [44] W. J. van Ooij et al, *Surf. Engineering*, 16 (2000) 386

- [45] P. Schubach, Chemetall GmbH, 2. Korrosionsschutz-Symposium, Grainau (2007)
- [46] A. J. Kinloch, Adhesion and Adhesives – Science and Technology, Chapman and Hall, London (1987)
- [47] A. V. Pocius, Adhesion and Adhesives Technology-An Introduction, 2nd Ed., Hanser, München (2002)
- [48] A. F. Holleman, E. Wieberg, Lehrbuch der Anorganischen Chemie, 101 Auflage, deGruyter, Berlin (1995)
- [49] R. G. Pearson, Coord. Chem. Rev. 100 (1990) 403
- [50] C. Fauquet, Appl. Surf. Sci. 81 (1994) 435
- [51] N. Carciello, J. Mater. Sci., 19 (1984) 4045
- [52] J. H. W. de Wit, Langmuir, 20 (2004) 6308
- [53] K. P. C. Volhardt et al, Organische Chemie, dritte Auflage, Wiley-VCH, Weinheim (2000)
- [54] A. F. Holleman, E. Wieberg, Lehrbuch der Anorganischen Chemie, 101 Auflage, deGruyter, Berlin, (1995)
- [55] M. Valtiner, G. Grundmeier, Langmuir 26 (2010) 815
- [56] C. Tanford, The Hydrophobic Effect: Formation of Micelles and Biological Membranes, Krieger Publishing Comp. Malabar (1991)
- [57] A. J. Davenport, Corr. Sci. 32 (1991) 653
- [58] J. Krömer, Henkel AG & Co. KGaA, 2. Korrosionsschutz-Symposium, Grainau (2007)
- [59] R. L. Cook, Corrosion, 56 (2000) 321
- [60] A.D. Apte, V. Tare, P. Bose, J. Hazard. Mater. 128 (2006) 164
- [61] P. Schubach, Chemetall GmbH, 2. Korrosionsschutz-Symposium, Grainau (2007)
- [62] M. L. Zheludkevich, Electrochem. Comm., 9 (2007) 2622
- [63] S. H. Sanad, Surface Tech., 22 (1984) 29
- [64] M. L. Zheludkevich, Chem. Mater., 19 (2007) 402
- [65] M. Guglielmi, J. Sol-Gel Sci. Technol. 8 (1997) 443
- [66] G. P. Sundararajan, Surf. Eng. 16 (2000) 315
- [67] M. F. Montemor, Prog. Org. Coat. 51 (2004) 188
- [68] A. Franquet, Surf. Interface Anal., 36 (2004) 681
- [69] W. J. van Ooij, J. Adhes. Sci. Technol. 11 (1997) 29
- [70] W. J. van Ooij, J. Adhes. Sci. Technol. 17 (2004) 2191

-
- [71] J. P. Folkers, *J. Adhes. Sci. Technol.* 6 (1992) 1397
- [72] G. M. Whitesides, *J. Am. Chem. Soc.*, 113 (1991) 12
- [73] E. Delamarche, *Langmuir*, 10 (1994) 4103
- [74] P. Thissen, M. Valtiner, G. Grundmeier, *Langmuir* 26 (2010) 156
- [75] J.C. Love, L.A. Estroff, J.K. Kriebel, R.G. Nuzzo, G.M. Whitesides, *Chem. Rev.* 105 (2005) 1103
- [76] B.J. Ravoo, D.N. Reinhoudt, S. Onclin, *Angew. Chem.* 117 (2005) 6438

Chapter 2 – Applied Techniques

2.1 Scanning electron microscopy and energy dispersive X-ray spectroscopy

Scanning Electron Spectroscopy (SEM) images were obtained by means of a NEON 40 FE-SEM (Carl Zeiss SMT AG, Oberkochen, Germany). For Energy Dispersive X-ray (EDX) spectroscopy analysis an UltraDry Silicon Drift X-ray detector from Thermo Scientific was used. Both the imaging and element analysis were obtained using an acceleration voltage of 5.0 kV and an electrode working distance of 5.0 mm.

It is important in this section to highlight the resolution ability of the obtained EDX spectra. With dependency to the accelerating voltage E_0 (in keV), the critical excitation voltage E_C (in keV) and the mean sample density ρ (in g/cm³), the spatial resolution of the obtained EDX analysis can be calculated *with the Equation 2.1* [1].

$$Resolution [\mu m] = 0.231 \frac{(E_0^{2/3} - E_C^{2/3})}{\rho} \quad (2.1)$$

For the two main elements of interest to this thesis, aluminum and zinc, the accelerating voltage of 5.0 keV and the mean sample density of 7.14 g/cm³ (density of zinc, as zinc is the major element of alloy) the spatial resolution is shown in *Tab. 2.1*.

Tab. 2.1: Spatial resolution of the EDX detected element lines [2,3] for an acceleration voltage of 5.0 keV.

Element Line	Critical Excitation Voltage (E_C)	Spatial Resolution
Al_(k-Line)	1.49 keV	0.04 μm
Zn_(l-Line)	1.01 keV	0.06 μm

Under these conditions the resolution of 60 nm was calculated for the analysis of zinc substrates. This spatial resolution is rather high and provides the appropriate dimension for the characterization of HDG steel surface heterogeneities in the top layer of 60 nm and grain boundaries ranging between 100 to 1000 nm.

2.2 Scanning Kelvin probe – force microscopy

The Scanning Kelvin Probe – Force Microscopy (SKP-FM) potential mappings of HDG steel surfaces were generated by a Veeco Dimension Icon (Veeco Instruments Inc., Santa Barbara, USA) using the Veeco Surface Potential imaging tool. The distance between the substrate and the conductive cantilever tip was set to 50 nm and adapted to the surface topography. The excitation

voltage on the cantilever tip was 500 mV. This technique allows measurement of the electrochemical potential of the substrate surface top layer.

2.3 Micro capillary cell

The micro capillary cell, also known as scanning droplet cell, is a tool for spatially resolved electrochemical investigation of metallic surfaces and was developed simultaneously by Lohrengel and Bohni [4,5]. The fundamental idea is to position tiny electrolyte droplets (diameter of $\geq 10 \mu\text{m}$) on the investigated surface. The wetted area on the substrate forms the working electrode (WE), a gold wire within the electrolyte filled capillary is the counter electrode (CE) and silver silver/chloride precipitate provides the reference electrode (RE). A schematic illustration of the micro capillary cell set up is shown in *Fig. 2.1*. The electrolyte was provided by an acetate solution at a pH value of 6. With this three-electrode arrangement, the complete range of common potentiostatic techniques such as impedance, transients or cyclic voltammograms is measurable.

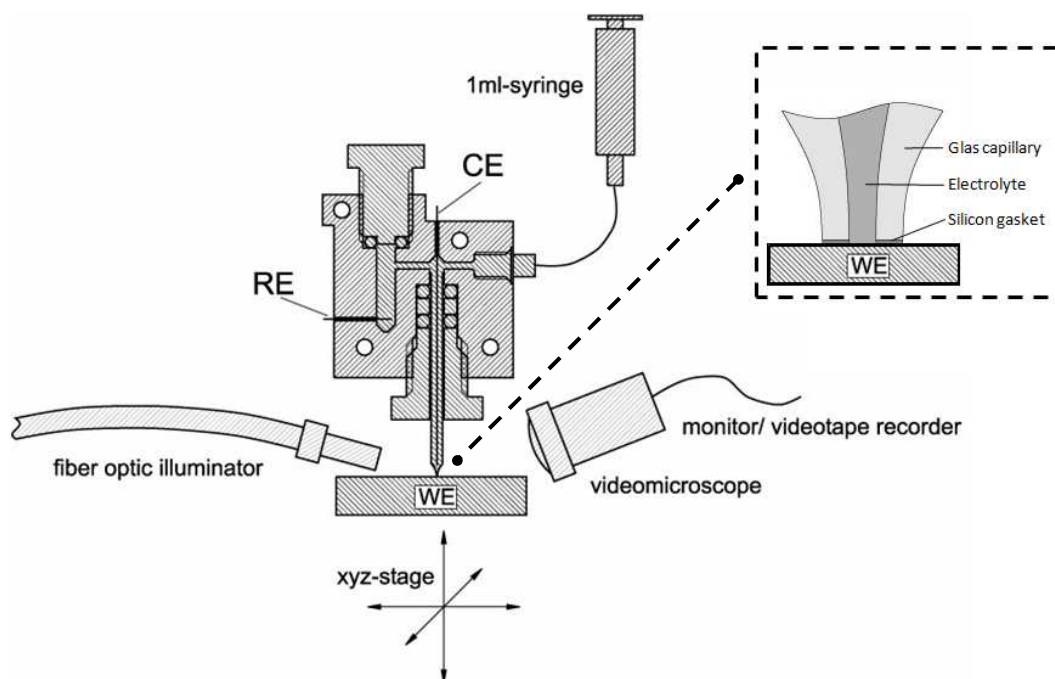


Fig. 2.1: The three-electrode arrangement of the micro capillary cell technique where the substrate is the working electrode (WE), a gold wire within the electrolyte filled micro

capillary is the counter electrode (CE) and silver/silver chloride precipitate is the reference electrode (RE) [6].

In the present study, the micro capillary cell measurements were carried out with a micro capillary cell technique developed at the Institute of Physical Chemistry and Electrochemistry of the Heinrich-Heine Universität Düsseldorf as illustrated in *Fig. 2.1*. The major challenge when applying this technique on small structures such as grain boundaries is to prepare a capillary with a working diameter in the same range as the structure to be investigated. Therefore a conventional capillary with an inner diameter of 1.8 mm is heated at a single spot and pulled apart in a manner so that the melting glass on the spot taper becomes a cone point as shown in *Fig. 2.2. (left)*.

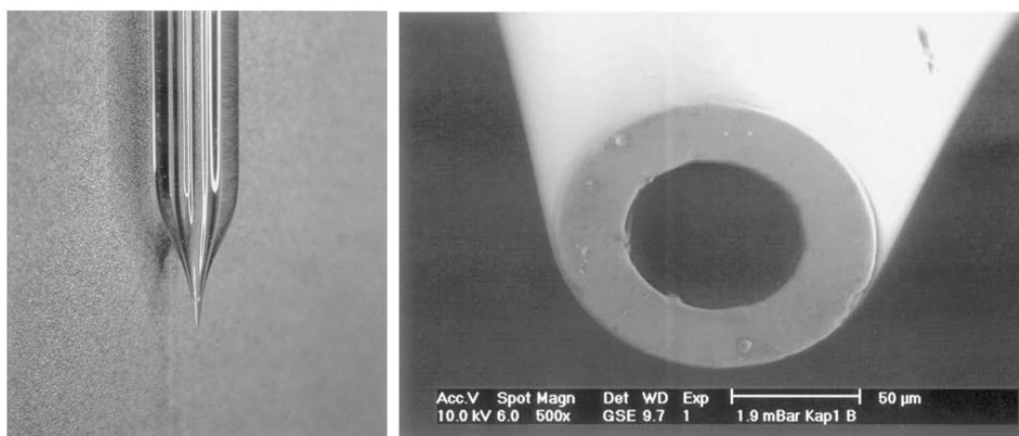


Fig. 2.2: Photograph of the pulled glass capillary to cone point (left) and polished tip of the micro capillary to an mouth diameter of approx. 70 μm (right) [7].

The capillary end (capillary mouth) must be flat in order to provide closed contact with the substrate. Therefore in the conventional capillary preparation method, the capillary mouth must be micro polished. The capillary mouth that typically results is shown in *Fig. 2.2. (right)*. However due to the fragile nature of such small glass pieces, it is very difficult to prepare smaller flat polished taper capillary ends with a diameter of less than 50 μm ; the reproduction of capillaries with the same mouth diameter is also quite difficult.

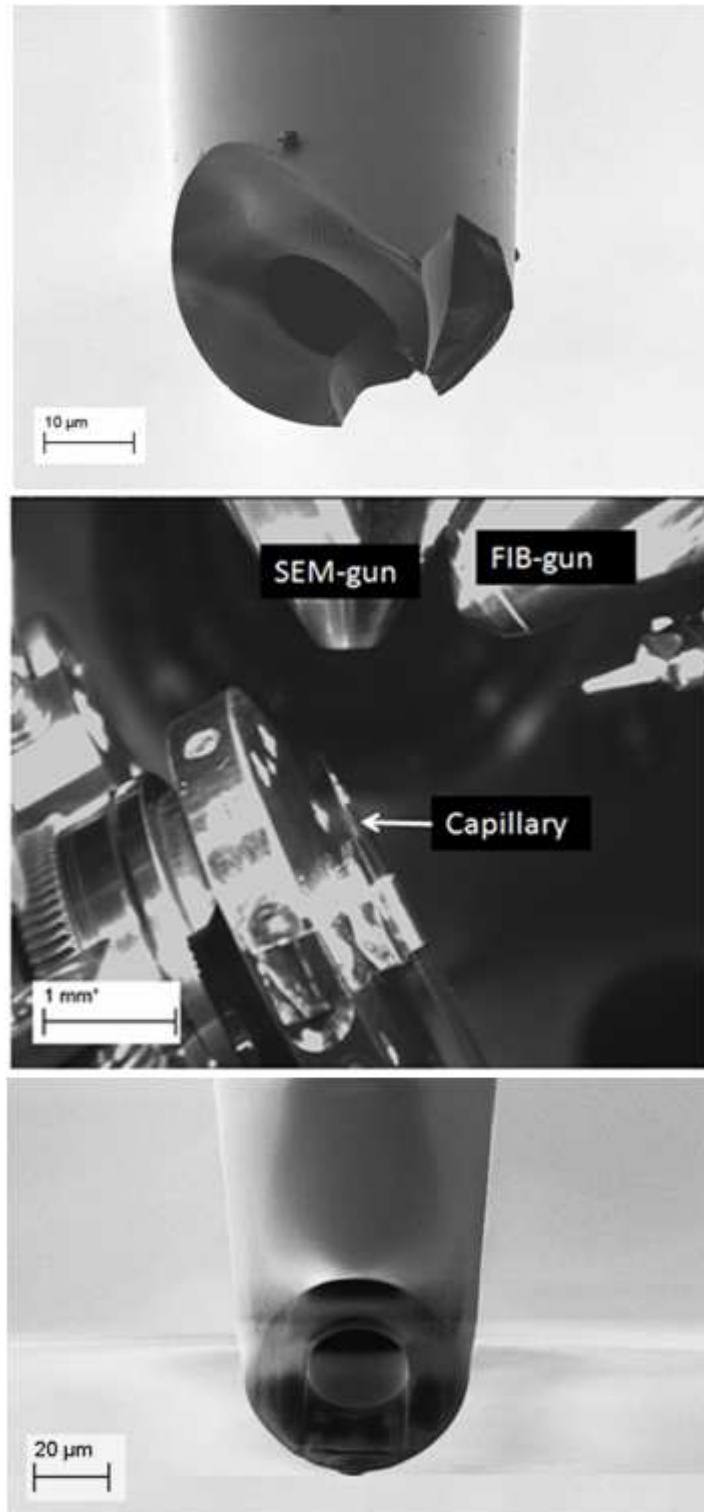


Fig. 2.3: Capillary preparation by Focused Ion Beam cutting. Capillary end as obtained after pulling with an inner diameter of the capillary end of ca. 10 μm (top). Arrangement for the Capillary in the SEM/FIB Chamber in the NEON 40 FE-SEM from Zeiss (middle). Capillary end after cutting with the inner diameter 20 μm (bottom).

A diameter larger than 50 μm would be too large for the electrochemical analysis of grain boundaries as found in HDG steel (see section 3.1). Therefore preparation of the capillary mouth was carried out through the application of the Focused Ion Beam technique (FIB). FIB is a popular tool for the cutting or drilling of micro structures especially in the micro-chip industry [8,9]. It uses a gallium ion beam to remove material from a sample to a precision of a few nanometers, this cutting procedure is shown in *Fig. 2.3*. With this technique, capillaries with any mouth diameter can be obtained. On the other hand, even though diameters smaller than 5 μm could be obtained, such small diameters were difficult to handle during the measurement process. When approaching the substrate surface, breakage of the capillary at the fragile end occurred quite often and thus only a few measurements could be obtained with each capillary. It was found that the smallest diameter for the secure handling of the capillaries was 20 μm . Micro capillaries with a diameter of 20 μm were thus used for the surface characterization.

2.4 Gel permeation chromatography

Gel permeation chromatography (GPC, L-Series from Merck) was used to determine molecular weights and molecular weight distributions, M_w/M_n , of block-co-polymers synthesized in section 3.3: Polymer Design for Grain Boundary Application. Molecular weights are calculated with respect to the polystyrene standards. The measurements were obtained in Tetrahydrofuran (THF) at a temperature of 25°C.

2.5 Dynamic light scattering and ζ -potential

Dynamic light scattering (DLS) and ζ -potential were measured on a Zetasizer Nano-ZS from Malvern. DLS was used to determine the particle size and its distribution in the resulting polymer dispersion. ζ -potentials were measured under standard conditions using the automatic Hückel approach at a temperature of 25°C.

2.6 Surface plasmon resonance spectroscopy measurements and sensor preparation

Surface plasmon resonance (SPR) spectroscopy is an advanced method that probes adsorption phenomenon on metal surfaces [10]. It is widely used on gold surfaces and their variations that have some organic monolayer. This technique has found broad application in biosensing through the use of monolayer chemistry as a receptor for biomolecules [11-12]. Studies monitoring the self-assembly of long chain molecules on aluminum oxide layers using the SPR technique have also been conducted [13,14]. Within section 3.4: Polymer Application on Grain Boundaries of this study, this technique will be used to investigate the adsorption and precipitation of polymer particles to aluminum oxide and zinc oxide surfaces. However SPR devices are based on the detection of refractive index changes in a thin dielectric layer found on top of a noble metal surface and probed by the evanescent field of a laser beam [15]. The reflected intensity of the beam is recorded as a function of incident angle and decreases dramatically as light couples into the plasmon mode of the metal or the waveguide modes of the dielectric. The evanescent tail of the plasmon is very surface sensitive. When adsorption on the surface occurs the plasmon interacts with the additional material. This results in the reflection intensity minimum shifting to higher angles. This method can therefore be used to determine film thickness. In the present study, the SPR technique will be used to detect the adsorption of block-co-polymer dispersions to aluminum oxide and zinc oxide surfaces with a pH dependency. Investigations in this work were carried out on a SPR apparatus Res-Tec GmbH, Framershein. *Fig. 2.5* provides a schematic of the SPR flow cell set up and the resulting spectra information in dependency of the thickness of the adsorbed polymer layer. Going from characters a) to c) in the scheme the adsorbed polymer layer is increasing, resulting in the shift of the reflection minima.

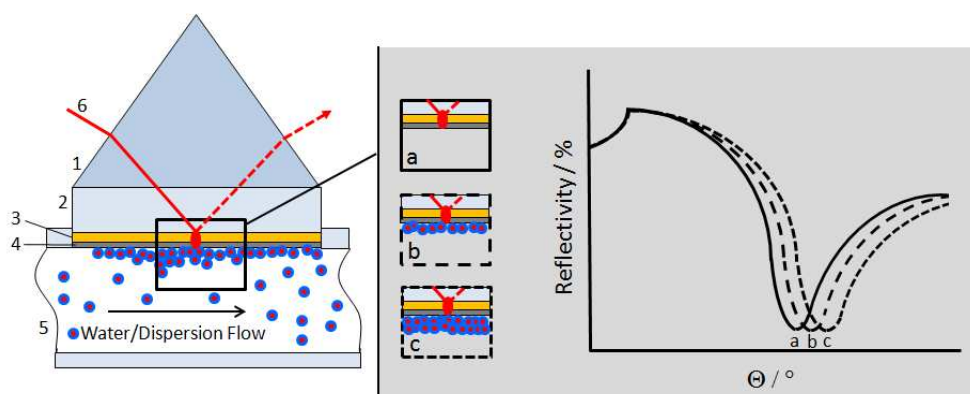


Fig. 2.5: Scheme of the SPR flow cell set up and the spectra obtained by varying the adsorbed polymer layer thickness. 1-Prism; 2-sensor LaSFN9 glass; 3-gold layer; 4-metal oxide layer; 5-flow cell. [a. no adsorbed polymer layer; b. monolayer of polymer particles; c. increased thickness of the adsorbed polymer layer] 6-laser beam.

SPR sensors based on LaSFN9 glass with defined gold layers were purchased from MPI Polymer Research, Mainz. The film build was 0.5 nm Chromium as an adhesion promoter for the 45 nm gold layer. The sensors were finished with a layer of metal oxide obtained through physical vapor deposition (PVD). Findings showed that a layer of zinc or aluminum deposited on the sensor had to be smaller than 10 nm for proper plasmon activity. Higher film builds of zinc or aluminum resulted in layers that were too high for plasmons to inform the sensor surface. The film build recorded at around 6 nm were obtained with a PVD chamber pressure of 5×10^{-5} mbar and a deposition rate of 10 \AA/s . After removing the sensors from the PVD chamber the metal with a thickness of only a few nanometers immediately oxidized to aluminum oxide or zinc oxide. The oxide surface of the sensor imitates surface conditions of the hot dipped galvanized steel. The exact film build of the sensors was calculated by fitting the resulting SPR spectra using WinSpall Software V3.02, which is also provided by the manufacturer of the SPR apparatus. The thickness of the layers of the prepared sensors as used in section 3.4 for the polymer adsorption studies are gathered in Tab. 2.1.

Tab. 2.1: Sensor film build as used for the SPR adsorption studies. Layer thickness is measured with SPR and with calculated WinSpall V3.02, Res-Tec.

Layer	Layer thickness [nm]	
	ZnO	Al ₂ O ₃
Chromium	0.5	0.46
Gold	45.73	45.22
Metaloxide	6.21	6.80

2.7 References

- [1] S. J. B. Reed, *Electron Microprobe Analysis*, Cambridge Univ. Press, Cambridge, England (1975)
- [2] D.O. Flamini, S.B. Saidman, *J. Appl. Electrochem* 38 (2008) 663
- [3] K. Tsuji, K. Nakano, H. Hayashi, K. Hayashi, C.-U. Ro, *Anal. Chem.* 80 (2008) 4421
- [4] T. Suter, H. Bohni, *Electrochim. Acta* 42 (1997) 3275
- [5] M.M. Lohrengel, *Electrochim. Acta* 42 (1997) 3265
- [6] C.J. Park, M.M. Lohrengel, T. Hammelmann, M. Pilaski, H.S. Kwon, *Electrochim. Acta* 47 (2002) 3395
- [7] M.M. Lohrengel, A. Moehring, M. Pilaski, *Electrochim. Acta* 47 (2001) 137
- [8] M.D. Henry, M.J. Shearn, B. Chhim, *Nanotechn.* 21 (2010) 245303
- [9] A. Shahmoon, O. Limon, O. Gishavitz, *Microelectronic Engineering* 87 (2010) 1363
- [10] J. Homola, *Chem. Rev.* 108 (2008) 462
- [11] W. Knoll, *Annu. Rev. Phys. Chem.* 49 (1998) 569
- [12] K. S. Phillips, Q. Cheng, *Anal. Bioanal. Chem.* 387 (2007) 1831
- [13] S. Heyse, O. P. Ernst, Z. Dienes, K. P. Hofmann, H. Vogel, *Biochemistry* 37 (1998) 507
- [14] E. Jaehne, S. Oberoi, H.-J. Adler, *Prog. Org. Coat.* 61 (2008) 211
- [15] S. Oberoi, E. Jaehne, H.-J. Adler, *Macromol. Symp.* 254 (2007) 284
- [16] D. Kuckling, M.E. Harmon, C.W. Frank, *Macromolecules* 35 (2002) 6377

Chapter 3 – Results and Discussion

3.1 Substrate characterization

3.1.1 Fundamentals

3.1.1.1 Aluminum in HDG coating alloys

In the process of hot dip galvanizing a steel strip runs through a bath of molten zinc-aluminum alloy. There are in general, three main galvanized steel products distinguishable by their aluminum content: HDG Al 0.5 w.-%, Galfan Al 5 % w.-%, and Galvalume Al 55 w.-% [1]. This study will focus on the most prominent, HDG Al 0.5 w.-% steel. The addition of Aluminum to the zinc bath in the galvanizing process is known to result in zinc-coatings with improved ductility, brightness and uniformity. Aluminum retards the surface oxidation of the molten zinc during the coating application process [2]. Due to the low electrochemical potential of aluminum at -1.66 V (electrochemical potential of zinc -0.76 V) it is highly reactive towards oxygen and oxide formation. In addition, the density of aluminum oxide (3.75 g/cm³) is less than the density of zinc (7.14 g/cm³) or zinc oxide (5.61 g/cm³) which leads to the formation of a fine aluminum oxide layer on the surface of the molten zinc alloy bath and prevents the zinc alloy further oxidizing beneath. All of these characteristics result in a smooth flow of the molten zinc alloy and therefore a final smooth surface of the zinc coated steel sheet [3]. The high

reactivity of aluminum that prevents the zinc molten bath from oxidation is also beneficial when the molten zinc alloy is applied onto the steel substrate. Aluminum reacts preferably with the ferrous steel surface and creates a thin layer of a FeAl-alloy. This reaction in turn disables the zinc iron reaction and the formation of brittle FeZn-alloys. Therefore, aluminum acts as an adhesion promoter between the steel and the zinc phases [4]. G. A. Lopez investigated the solid solubility of aluminum in zinc [5]. He found that the solubility of aluminum is negligible at room temperature and that during solidification of the zinc coating, aluminum segregates towards the outermost surfaces of a solidifying single zinc grain. The poor solubility of aluminum in zinc can be attributed to the different atom radii (Zn 135 pm; Al 125 pm) and their different metal crystal lattice structures. The incorporation of smaller aluminum atoms into the zinc crystal lattice (hexagonal close-packed) results in the distortion of the crystal lattice and a rise in lattice energy. In order to minimize the systems energy, aluminum atoms are sorted out from the zinc lattice and are replaced by zinc atoms during the solidification process. Therefore when aluminum atoms accumulate, they solidify in the aluminum crystal lattice, face-centered cubic [6]. Weinberg et al. made similar observations with Galfan hot-dipped galvanized steel. In their results aluminum segregates to the surface of the zinc coating and provides a passive aluminum oxide/hydroxide layer of a few nanometers thickness [7]. Surface aluminum segregation was assumed as a reason for the enhanced corrosion resistance of Galfan steel. Similar segregation could also be observed in HDG steel with aluminum contents lower than 5 w.-% [8-11]. Selected images of aluminum segregation in HDG steel are shown in *Fig. 3.1*.

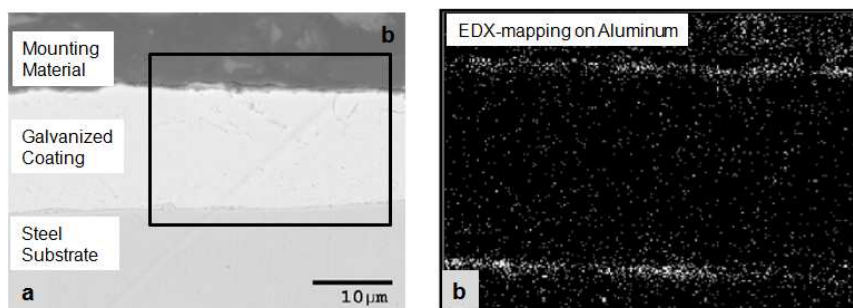


Fig. 3.1: a) SEM image of a cross section of a HDG steel Al < 0.5 w.-%. b) EDX mapping on Aluminum of the cross section. (bright color high Aluminum content) [12].

Nevertheless in these papers the segregation effect of aluminum to the surface is observed and described as equally distributed on the surface. (see Fig. 3.2)

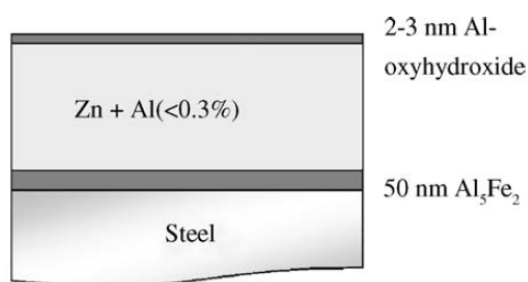


Fig. 3.2: Schematic illustration of the aluminum segregation in HDG coating [8].

Within this study, HDG steel with a zinc aluminum alloy of Al 0.5 w.-% will also be characterized. The focus within this section will be on aluminum segregation towards grain boundaries and their activity in the corrosion process, whereas the following section will deal with inhibiting these electrochemically active spots. However in those publications, the improved corrosion resistivity of HDG steel was also attributed to the aluminum rich surface. Aluminum is very reactive due to its negative electrochemical potential, as discussed earlier in this section. The oxidation reaction of aluminum is rather fast, but due to its auto-passivation ability of a short period; the oxidation of the surface top layer stops when a dense passive aluminum oxide layer has been formed. The volume ratio of aluminum and aluminum oxide can be calculated as 1:1. This ratio is most important so that the oxide layer is stable and not brittle [13]. Therefore the aluminum oxide layer seals the substrate surface and the oxidizing process stops. In comparison with iron and its oxide, the volume ratio is 1:2. The oxide layer needs two times more space on the substrate surface. Subsequently it succumbs to stress induced cracks within the oxide layer. The brittle oxide layer uncovers a new iron surface which reacts with oxygen.

The passive aluminum layer becomes distracting when phosphating is applied on HDG steel. Phosphating is the current technology of surface conversion chemistry and broadly processed in industry. The passive aluminum layer

protects zinc from corrosion and dissolution. At the same time, it is predominant to dissolve the outermost zinc layer from the substrate in order to precipitate a phosphate layer. [14-17]. Fundamentals of phosphating will be discussed in section 3.2: Material Survey for Grain Boundary Application. In order to remove aluminum from the substrate surface alkaline cleaning procedures have been established. These procedures are carried out through simple dipping of the substrate into an alkaline solution with a pH of 12. While aluminum and its oxides dissolve at pH values above 10.5, zinc remains insoluble up to a pH of 13.5. This etching process uncovers the zinc and therefore activates the surface for the phosphating process [18,19]. Berger et al. have investigated the industrial alkaline cleaning process [20] and found that the cleaning procedure does not remove all of the aluminum. Even after a prolonged cleaning procedure, aluminum can be found in some segregated islands and in grain boundaries of the HDG steel surface. Similar observations will be made in the experimental results of this section. It is postulated however on the one hand that the aluminum oxide layer on HDG steel is passivating the substrate surface and improving the corrosion resistance. On the other hand, current technology is making an effort to remove this passive layer in order to apply a phosphate conversion layer. A true benefit of the process would be the direct application of the conversion chemistry on the passivated HDG surface. Following along the lines of this study within this section, the passivated HDG steel surfaces will be characterized towards their surface chemistry. The weak spots, in terms of electrochemical corrosion activity, will be localized and discussed.

3.1.1.2 Grain boundaries and weak zones

Industrial surfaces are heterogeneous, as shown in some obvious cases such as inter-granular corrosion, which is known from metal engineering (see *Fig. 3.3*). For coated substrates it is postulated that corrosion starts mostly at weak spots, which are typically edges and vertices [21]. To date no one in open literature has investigated this assumption for substrates such as HDG steel. It is also possible that segregation spots could generate galvanic cell and contact corrosion. Accumulated alloy elements are in electrochemical contact with the surrounding alloy. In the case of aluminum alloys in near-neutral bulk solutions, it is well

established that pitting is influenced by intermetallic particles that exhibit different surface characteristics to the matrix and may be either anodic or cathodic in relation to the matrix [22-30]. Often in grain boundaries, both segregation of intermetallics and some amorphous metallic structures with edges and vertices on the interphase to air can be observed. Therefore, grain boundaries are known to be electrochemically active species that can also function as transport channels for small molecules and ions [31]. The phenomenon of intergranular corrosion has been soundly investigated [32,33].

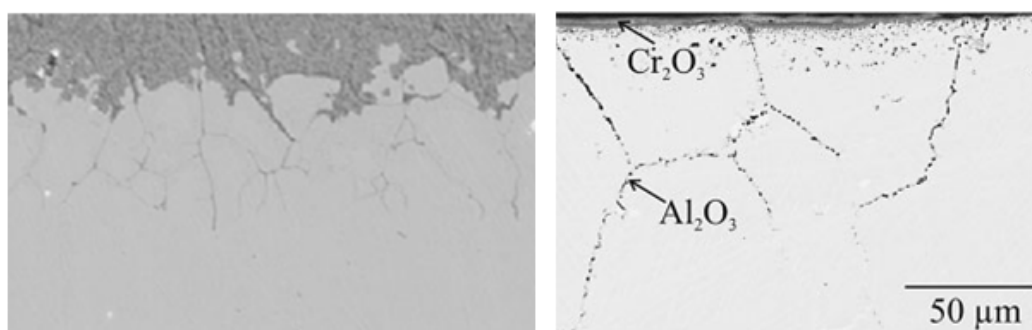


Fig. 3.3: Cross section of Ni-base superalloy after exposure to air at 550°C for 90h. The segregated elements within the grain boundaries oxidize and cause the intergranular corrosion [34].

A prominent example of where intergranular corrosion occurs is in stainless steel. Selected images of intergranular corrosion are shown in *Fig. 3.3*. Chromium rich carbides accumulate in the grain boundaries of the steel during welding or general service leading to corrosion susceptibility. Chromium oxidation, starting from the surface and moving inward, leads to de-adhesion of the grains and intergranular corrosion thus occurs [35-37]. Trinidade et al. describe the role of alloy grain boundaries as short-circuit diffusion paths for inward oxygen transport [34]. Bredesen and Hussey et al. describe high diffusivity for molecular oxygen through micro cracks occurring in the oxidizing grain boundaries [38,39]. However all this knowledge is based on engineering granular materials such as steel where grain boundary reactions lead to embrittlement. But open literature provides no information on how grain boundaries on non-brittle substrate surfaces behave when coated with an organic coating. From observations in

industry it was reported that aluminum in HDG steel was migrating along grain boundaries from the zinc/iron interface to the zinc/coating interface during the baking of the organic coating [40]. In any case grain boundaries are very active sites. Findings from the literature survey show that the grain boundaries also found on HDG steel surfaces could have potential as weak spots. Within this section, surface heterogeneities of HDG steel Al 0.5 w.-% will be investigated in order to determine weak areas with high electrochemical activity.

3.1.2 Experimental procedures

3.1.2.1 Substrate

The HDG-Steel sheets (DX 53D + Z 100 NA 0.6 mm) were provided by voestalpine AG, Austria. The aluminum content in the zinc alloy coating is quantified by the manufacturer at < 0.5 w.-%. For surface characterization and polymer application the steel samples were solvent cleaned in a three step process (see Fig. 3.4). The first step, a thorough rinsing for 10 min in an ultrasonicated bath of Tetrahydrofuran (THF) was followed by drying in a nitrogen gas stream. Step one was repeated twice, once with iso-propanol and then with ethanol, followed by nitrogen drying.

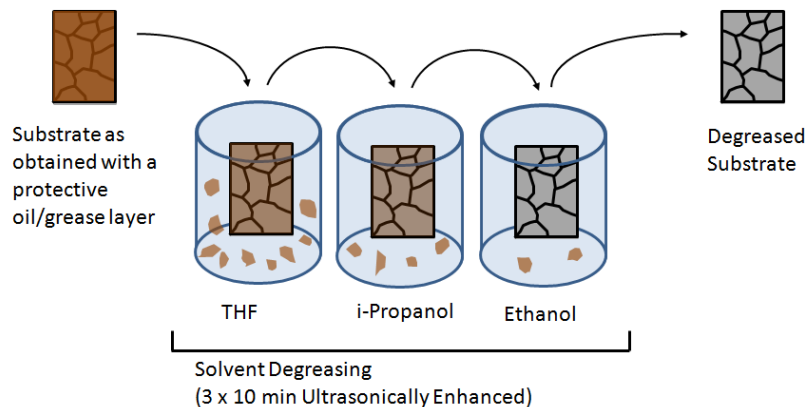


Fig. 3.4: Schematic illustration of substrate cleaning procedure.

3.1.3 Experimental results

3.1.3.1 Surface structure and element distribution on HDG Steel Al 0.5 w.-%

In order to characterize the surface structure and chemistry of the HDG Steel substrate high resolution SEM images and element mappings were obtained. *Fig.3.5.* shows the typical surface structure of HDG steel. The texture arose from the solidification of the molten zinc and is visible as grains, so called spangles, with a diameter of approximately 100 to 200 μm . Where ever two grains are in contact with each other, the grain boundaries are visible. At a higher magnification the grain boundaries can be seen as a grid of connected micro trenches all over the substrate surface. These trenches vary in their cross section dimensions of width and depth from a few nanometers to a micrometer.

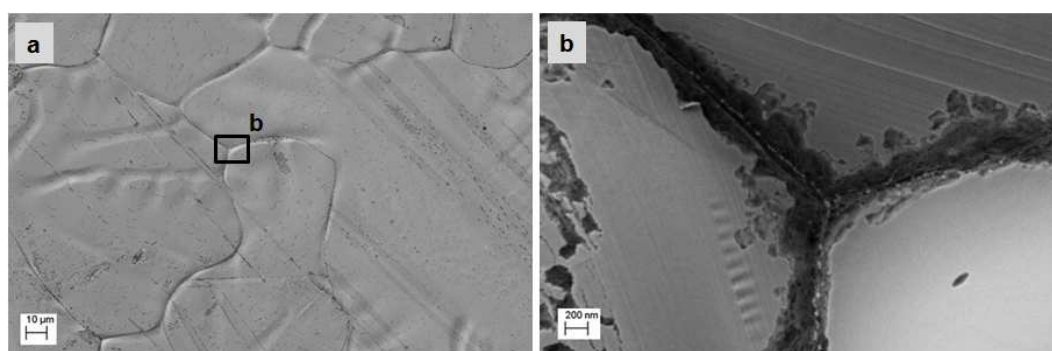


Fig. 3.5: a) Grain (spangle) structure at the surface of HDG steel Al <0.5 w.-%. Grain boundaries can be seen as a grid of connected trenches. b) High resolution image of a triple point of three grain boundaries.

In Fig. 3.5 the dimensions of the grain boundaries at the triple point have an estimated width of 300 to 400 nm. The surface of a single grain can be seen as rather smooth and flat but also with some micro distortions and scratches. The scratches are probably due to the rolling transportation of the steel strip during the zinc coating process. Grain boundaries occur as edges and vertices on the substrate surface, which in literature, as discussed in the fundamentals of this section, are described as the weak zones where the corrosion processes start. In order to characterize the surface element composition EDX mappings were obtained.

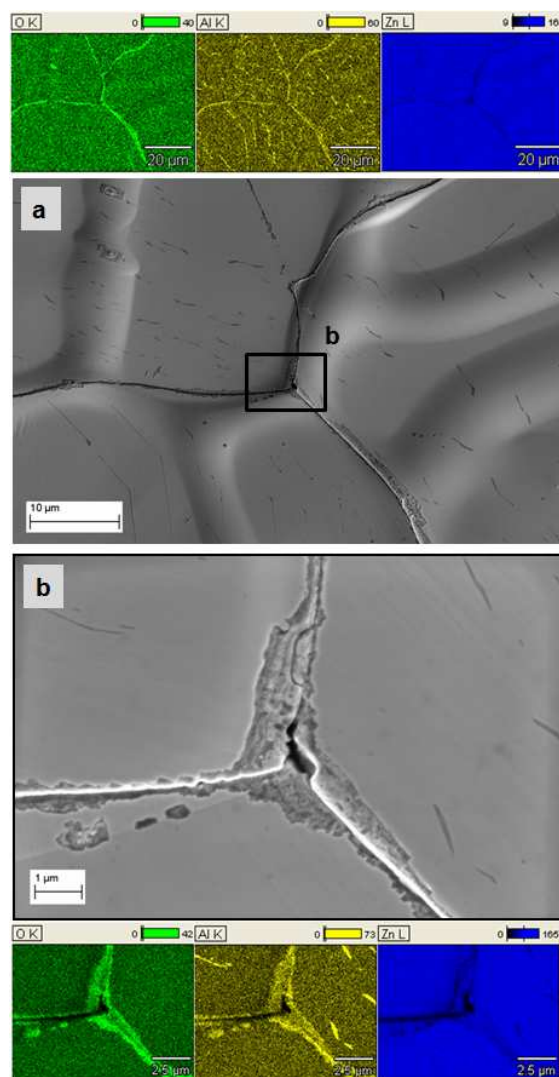


Fig. 3.6: a) SEM image and corresponding EDX element mapping of the HDG steel surface. b) High resolution SEM image and corresponding EDX element mapping focusing a triple point of three grains and its grain boundaries. The mapping was obtained with an accelerating voltage of 5.0 keV and a working distance of 5.0 mm.

Segregation effects of aluminum on HDG steel are most often described to the surface and to the interface of zinc coating and steel. There are also a few observations that have been made where aluminum was found enriched in the grain boundaries of the zinc grains at aluminum concentrations higher than 5.0 w.-% [41,42]. In Fig. 3.6 high resolution EDX mappings clearly show aluminum enriched in the surface grain boundaries, with aluminum concentrations of 0.5 w.-% aluminum in the HDG coating alloy. Most of the surface analytics dealing with coating development use homogeneous averaged element compositions in order to determine the surface characteristics and select the right adhesion promoters for such surfaces. One of the most common arguments stated for not focusing on these heterogeneities is the application of the alkaline cleaning process. As discussed in the fundamentals of this section, alkaline cleaning is used to remove the passive aluminum layer so that the conventional pretreatment procedures can be applied. Literature dealing with alkaline cleaning processes finds only negligible amounts of aluminum on the HDG steel surface after the alkaline cleaning. Therefore in the following, the alkaline cleaning process was investigated with concern to its homogenization of the HDG steel surface.

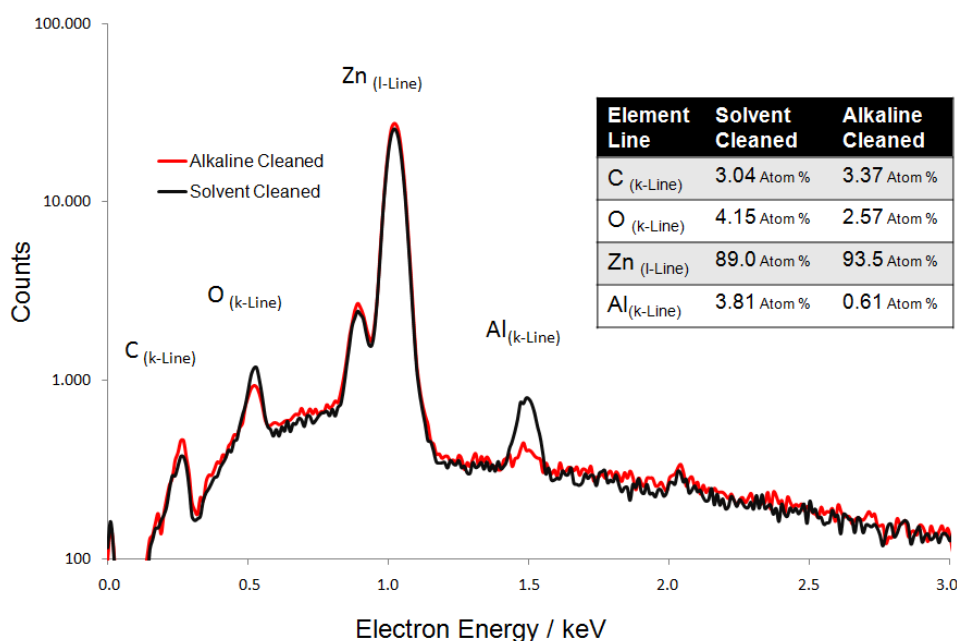


Fig. 3.7: EDX analysis of HDG steel surface 200 x 200 μm before (black line) and after (red line) alkaline cleaning. The measurements were obtained with an accelerating voltage of 5.0 keV and a working distance of 5.0 mm.

Fig. 3.7 provides element spectra of the solvent cleaned HDG steel surface before and after alkaline cleaning as used in industry. The measurements were taken from an area of 500 x 500 μm . This area contains some grains and also some grain boundaries. In analogy to literature the aluminum content of the outermost substrate surface could be reduced from 3.8 Atom-% to an insignificant amount of 0.6 Atom-%. However, before undertaking the alkaline cleaning, most of the aluminum was found in the grain boundaries. It is therefore also important to investigate the element distribution after the alkaline cleaning procedure. Fig. 3.8 shows a high resolution EDX element mapping of a partly alkaline cleaned HDG substrate. In the top of the SEM image (solvent cleaned) a smooth surface is visible.

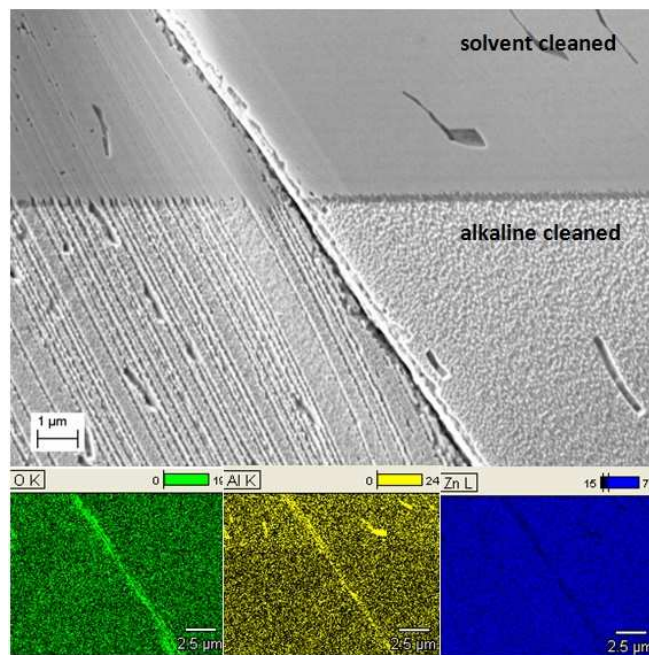


Fig. 3.8: SEM image and EDX mapping of a solvent and partly alkaline cleaned HDG steel substrate. Top of the substrate is solvent cleaned, bottom is alkaline cleaned.

In the lower part of the image (alkaline cleaned) the native oxide surface was removed through alkaline etching. Similar to findings discussed in literature, the rough morphology of grain surfaces is visible. The different morphologies of the two grains imply that grains may have a different main crystallographic

orientation. Most importantly, by scoping the EDX mappings it can be seen that there is little change in the oxygen intensity along the grain boundary. The aluminum intensity decreases along the grain boundary on the bottom where the alkaline has cleaned but does not disappear in total. These findings lead to the conclusion that alkaline cleaning does not create a homogeneous surface on the HDG steel as often stated by industry and in literature. The topography of the grain boundary also does not change much through the procedure of alkaline cleaning. This would imply that if grain boundaries on the HDG steel surface are the weak zones of interest, they probably remain as the weak zones after the alkaline cleaning procedure. Before alkaline etching, only the edges of grains (grain boundaries) may be active while the mean surface of the grain is naturally passivated by a compact aluminum oxide layer. After the alkaline cleaning, the grain surfaces, in addition to the grain boundaries also become activated. The aim of this study is to localize the weak zones of the HDG substrate and create coating material that treats only those weak zones active in the corrosion process. All these findings address the grain boundaries as possible weak zones susceptible for corrosion. The alkaline cleaning process makes sense as an activation process for the corrosive application of conventional pretreatments, e.g. the phosphate layer. Alkaline cleaning does not create a homogeneous surface. However it would be easier and more efficient to use the substrate as produced by steel manufacturing. A coating process could be applied without additional etching and activation of the steel surface that would also lead to economic advantages in the process chain.

3.1.3.2 Surface potential

Scanning Kelvin probe force microscopy (SKP-FM) allows mapping of the topography and Volta potential distribution on surfaces [43]. It combines the classical Kelvin probe technique [44] with atomic force microscopy [45-47]. SKP-FM operates at much smaller distances to the probe surface and uses the cantilever tip as the electrode. This technique allows a higher lateral resolution than the classical Kelvin probe technique. The lateral resolution of SKP-FM is reported to be better than $0,1\mu\text{m}$ [48-50], compared to $\sim 100\mu\text{m}$ for the standard Kelvin probe technique [51,52]. This technique will be applied in order to

determine the weak zones on the HDG Steel. A surface potential mapping of a surface area of 20 x 20 μm containing a grain boundary and some scratches is shown in Fig. 3.9. Results of the SKP-FM measurements show surface potential mappings in an atmosphere with 50% relative humidity at 20°C. Along the grain boundaries and on some of the scratches the potential could be determined as significantly lower than on the smooth surface of the grains. The existence of a negative Volta potential between the grain boundary and the main grain surface implies that the grain boundaries have anodic behavior relative to the surrounding grains [53]. In other words, grain boundaries have a higher affinity to oxidation reactions.

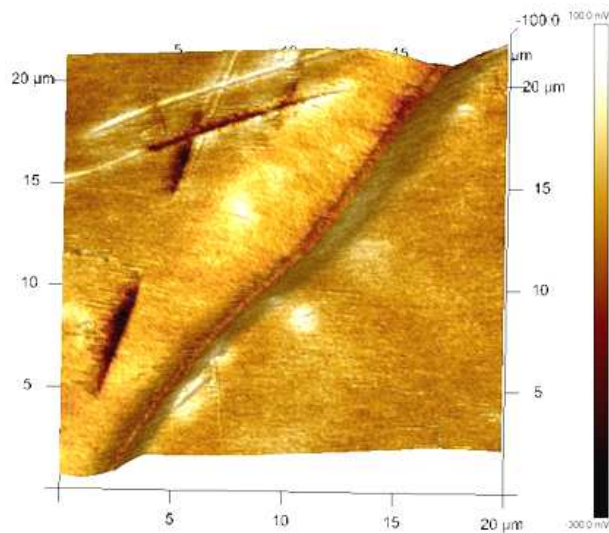


Fig. 3.9: SKP-FM potential mapping over grain boundaries, scratches, and grains.

Andreatta and Terryn et al. find such behavior in intermetallic particles responsible for pitting corrosion [54,55]. In that case SKP-FM was used to measure the Volta potential between intermetallics, the matrix and the air. In the measurements of the HDG steel surface two major effects for the lower surface potential can be considered. The first one is the presence of aluminum in the grain boundaries. According to the fundamentals of this section metallic aluminum is less noble than zinc due to its lower standard potential which would result in lower potentials measured by SKP-FM. The second effect could be

topography. A grain boundary is an edge with a rough nano-structure. Metal atoms from edges are more readily available to chemical reactions. This implies that grain boundaries may be highly reactive species in terms of metal oxidation and dissolution resulting in corrosion also because of their geometry.

3.1.3.3 Dissolution activity of grain boundaries vs. grains

In the following part of this section, the corrosive ability of grain boundaries will be investigated by measuring their susceptibility to electrochemical dissolution. A higher dissolution activity would be an indication of higher corrosion activity. The dissolution activity of grain boundaries in comparison to the flat area of the grains could thus be observed using the micro capillary cell technique. Since the establishment of this technique, many applications in corrosion research, especially in intermetallic particles or single grains of some metallic texture, have been reported [56,57]. Investigations on the dissolution behavior of single grains on polycrystalline zinc have been shown to have different crystallographic orientation of grains resulting in different reactivity in terms of metal dissolution, oxidation and passivation [58]. Similar results could be obtained on ferritic steel [59]. Schreiber et al. observed that grain boundaries of ferritic steel between grains of different crystallographic orientation would also have different dissolution kinetics [60]. However there is no information available on the behavior of grain boundaries in the HDG steel surface. In order to investigate the electrochemical behavior of grain boundaries in the HDG steel substrate, a capillary with a diameter of 20 μm was prepared and set up as described in Chapter 2 of this thesis. The capillary was filled with an acetate buffer of pH 6. *Fig.3.10* shows targeting of the specific surface area and how the target was approached for measurement.

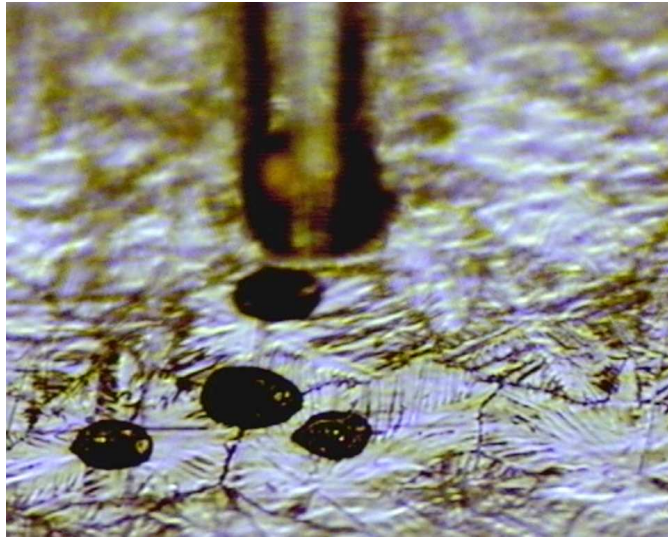


Fig. 3.10: Targeting the micro capillary on the grains and grain boundaries on the HDG Steel substrate surface.

Grain boundary measurements were taken on spots in a triple point of three grains. After touchdown of the capillary on the surface, a potential sweep was run starting from -1.0 V up to + 1.5 V and the current density resulting from the metal dissolution was obtained. Each spot was measured once only because of the changing surface during the measurement. After each measurement the capillary was rinsed with electrolyte before targeting the next spot. *Fig. 3.11* shows a large number of current density – potential curves obtained from measurements on the grains and grain boundaries. The dashed lines always indicate current activity of the grain boundaries and solid lines indicate the grains.

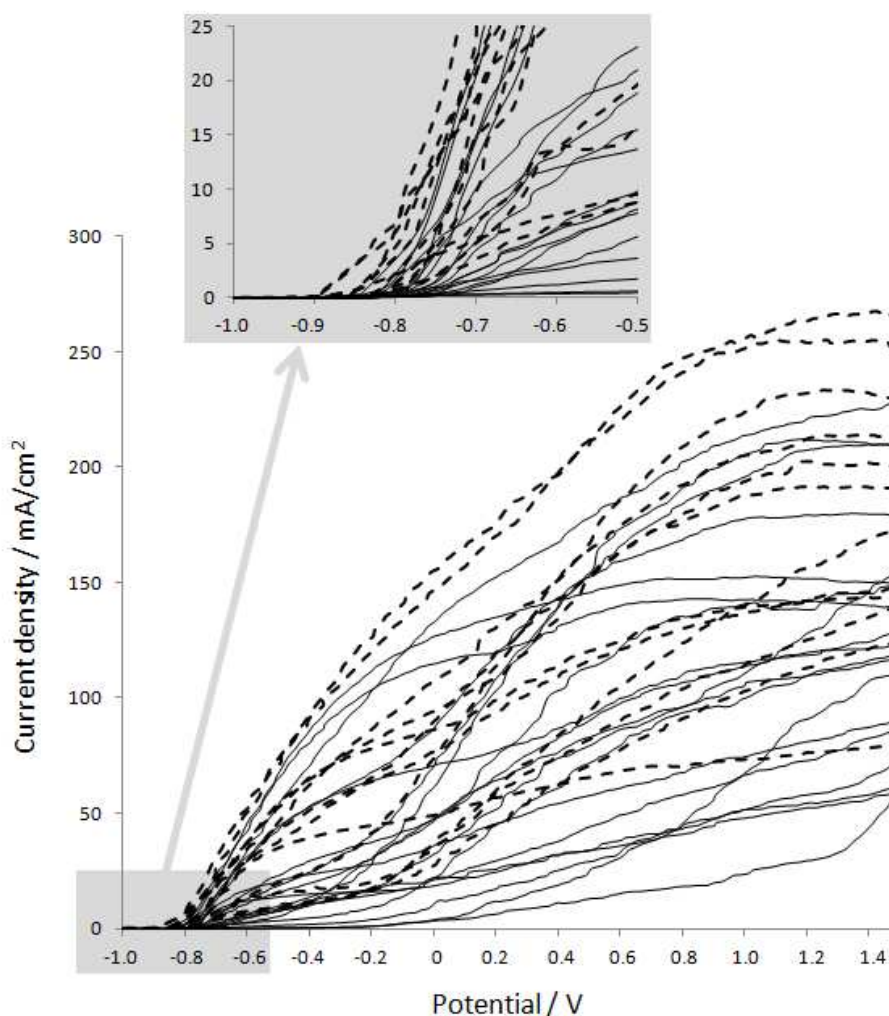


Fig. 3.11: Current density-Potential curves obtained from micro capillary measurements on grain boundaries (dashed line) and on grains (solid line).

On the first view, a broad scattering of the obtained data from the specific spots of the HDG steel surface can be observed. Starting from low potential first current activities can be detected at potentials of around -900 to -800 mV. Due to the oxidation and dissolution of the metal, the current density rises with the higher anodization of the working electrode. In the range between 0 and 1.5 V the slopes of the current density or the potential curves are decreasing. This effect may be attributed to the fall out of metal oxides/hydroxides in the rather small capillary volume. In the backward sweep current density immediately breaks down due to the metal oxides/hydroxides and thus choking the capillary the capillary mouth and interrupt the current flow. All of these observations however

lead to scoping the very beginning of the measurable current activity where the substrate is negatively polarized. Looking closely at *Fig. 3.11* one could assume that the dashed lines indicating grain boundary measurements start a little earlier than the solid lines indicating the flat grains. This observation becomes more visible when applying statistics to the obtained curves (see *Fig. 3.12*).

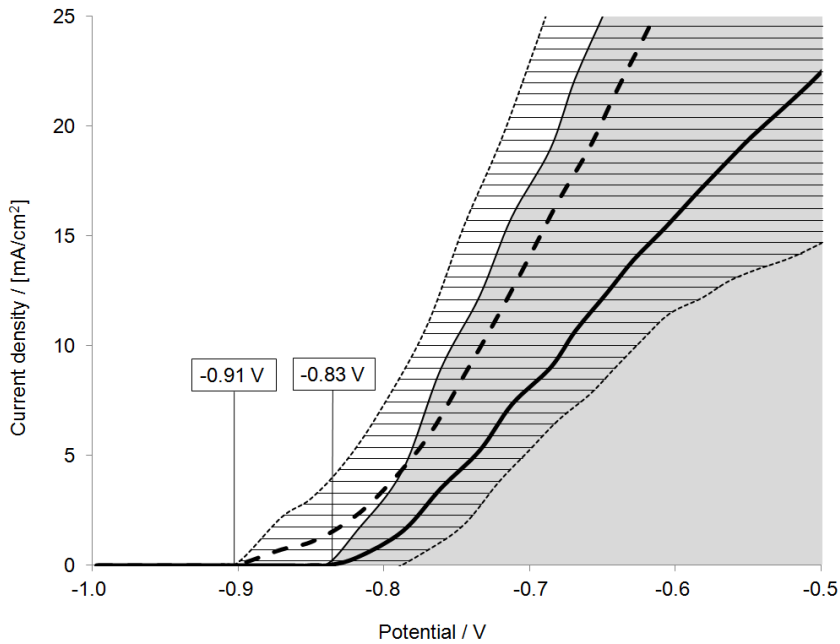


Fig. 3.12: Averaged Current density/Potential plots measured on grain boundaries (bold, dashed line), with the standard deviation (hatched area) and on grains (bold, solid line), with the standard deviation (grey area).

Fig. 3.12 represents the average curves from the measurements taken. The chart shows only a small range of the potential sweep where the starting point of measurable current activity is of interest in order to distinguish the susceptibility to metal dissolution or corrosion processes. In this survey it was found that the starting point of measurable current activity on grain boundary spots is on a lower potential than that of flat grain spots, where the difference can be accounted to approximately 80 mV. These findings indicate that anodic dissolution and oxidation occur more easily on grain boundaries. It should also be considered that grain boundaries with an estimated width of 1 μ m and measuring on a triple point would contribute 30 μ m² to the measured surface of 314 μ m² when

calculated by the capillary geometry (see Fig. 3.13). The grain boundary contribution can be calculated to a maximum of 10 % because of the rather large measured surface area of the micro capillary with an inner diameter of 20 μm .

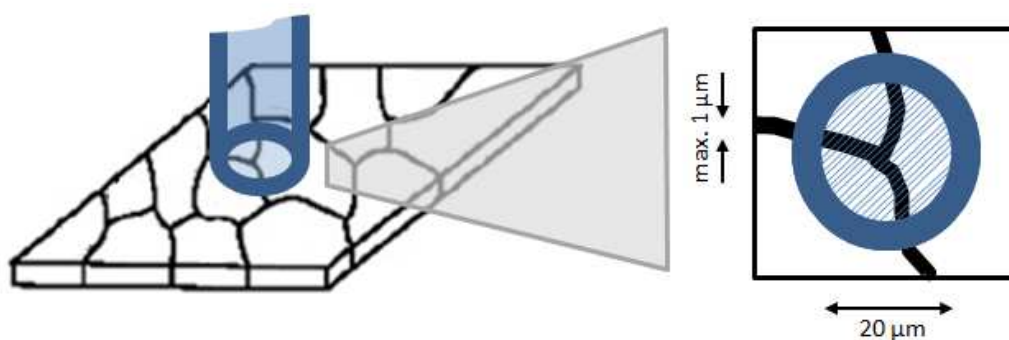


Fig. 3.13: Illustration of grain boundary contribution to the measured area by capillary diameter of 20 μm .

It is assumable that the potential difference when measuring just the grain boundaries could be even higher, however due to capillary limitations it was not possible to provide more precise measurements in this survey. From this point of view the results obtained by the micro capillary cell again provide strong evidence that grain boundaries are highly corrosive active species. One has to consider that this activity can be due to the edge geometry, the alloy composition and the crystallographic stability of the grain boundary area. This anodic dissolution activity of grain boundaries is in analogy to the lower electrochemical potential of the grain boundaries obtained from the SKP-FM measurements. In the following section 3.2: Material Survey for Grain Boundary Application, this dissolution activity of grain boundaries will be investigated in order to control the selective material creation and deposition on grain boundaries for selective inhibition of these corrosive sites. But before focusing on the material for grain boundary corrosion inhibition, the last part of this section will investigate the corrosion behavior of grain boundaries in HDG steel substrate when coated and exposed to a corrosive environment.

3.1.3.4 Corrosion behavior of grain boundaries on coated substrates

Strong evidence was obtained in the previous experiments that grain boundaries are the weak zones susceptible to corrosive reactions. In the following, the question of whether it can be proved that grain boundaries are the preferred pathways for corrosion will be answered. For this reason, the behavior of grain boundaries on coated substrate under corrosive conditions will be investigated. To this end, a HDG steel substrate was coated with a commercial coil coating primer. A defect in the coating was created through a scratch and the sample was exposed in a salt spray chamber for 504 h. After exposure, the delaminated coating was peeled off and the corrosion front was investigated by focusing on the corrosion front (Fig.3.14). The obtained images always showed that corrosion products could be found along the grain boundaries as a forefront of the corroded area.

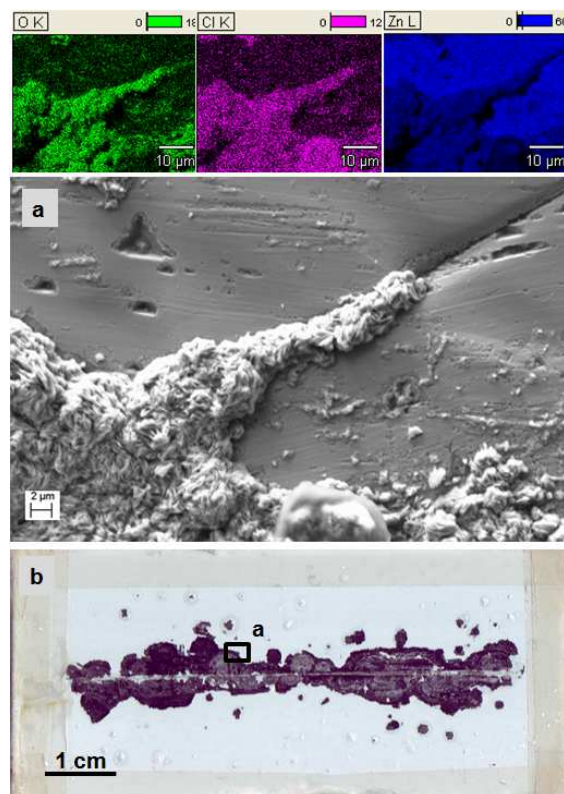


Fig. 3.14: a) SEM images and corresponding EDX mappings of the corrosion front of coated HDG steel substrate. It shows the corrosion propagation along the grain boundaries. b) Scratched sample after exposure in a salt spray chamber for 504 h indicating the area where the SEM image was obtained.

The EDX mappings of *Fig. 3.14* identify oxygen, chlorine and zinc, all of which identify that corrosion products along the grain boundary consist of zinc oxides and zinc chloride. This type of prolongation of corrosion in the interface grain boundary/coating could be found on all grain boundaries and ranged between 50 and 200 μm along the grain boundary when measured from the main corrosion front. These findings correlate closely with the assumptions made in the fundamentals of this chapter and the results obtained from the surface analytics.

At this point, some additional thinking would enable the influence of mechanical adhesion between coating and substrate in terms of corrosion protection to be evaluated. Whilst flat grain surfaces do not provide the appropriate geometry for mechanical adhesion, the porous topography of grain boundaries provides the appropriate geometry for force-fit interlock adhesion. The fast corrosion propagation along the grain boundaries shows that mechanical adhesion is less relevant when the substrate is electrochemically active. The interlocks established from the coating lose their basis when the substrate electrochemically dissolves. However from these observations a model for corrosion pathways on this particular substrate will be derived and discussed in the following part of this chapter.

3.1.3.5 Corrosion pathways as a model development

The general cross-sectional view of corrosive delamination (see chapter 1) becomes more complicated on heterogeneous surfaces. Therefore to visualize the corrosive delamination process based on different corrosion pathways, a top view of the corrosion front of the substrate surface is more appropriate. *Fig. 3.15* illustrates the basic mechanisms that can be derived from experimental findings within this section. The SEM image shows a corroded grain boundary in the forefront of the corrosion front. The detailed explanation of this postulated corrosion process is described based on the schematic illustration of *Fig. 3.16*.

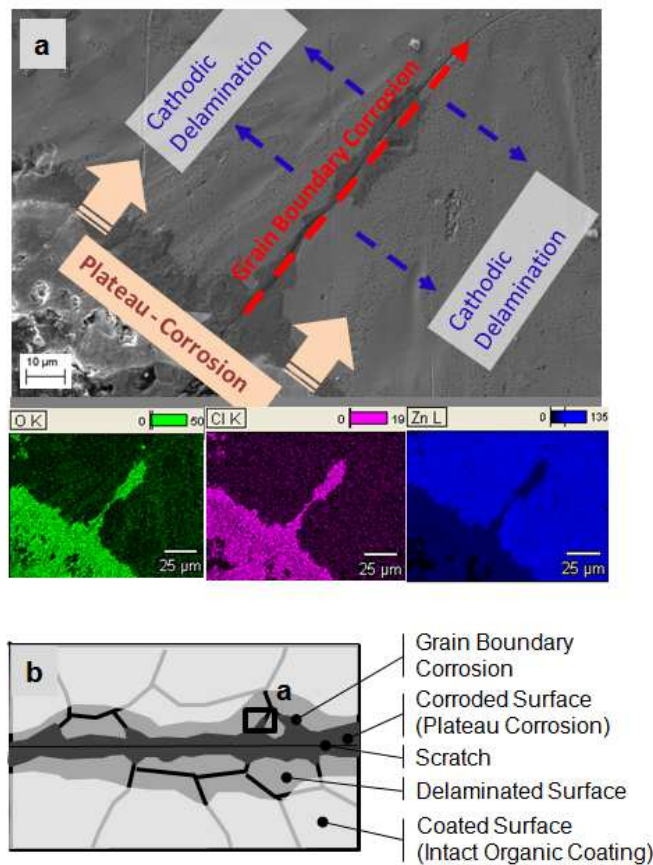


Fig. 3.15: a) SEM image and EDX mapping of the corrosion front and grain boundary. The sample was coated with a conventional coil coating, scratched and exposed for 504 h in a salt spray chamber. After corrosion exposure the coating was removed with THF. The sketches in the image indicate the corrosion pathways on the HDG steel sample. b) Schematically illustrates the tested sample.

Single steps more or less simultaneously occur, but in order to understand the single parts of the process it is necessary to divide the corrosion process into sequential steps as shown in *Fig. 3.16*.

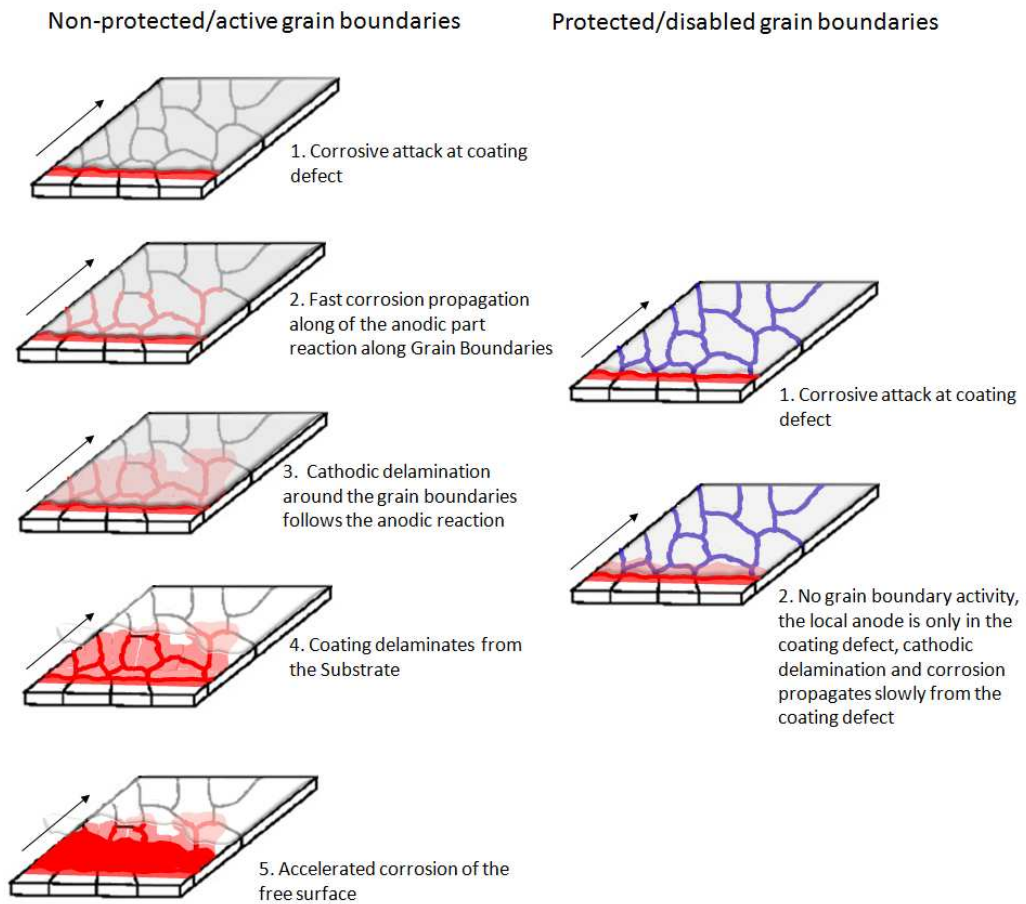


Fig. 3.16: A model for delamination and corrosion propagation on HDG steel with active/non-protected grain boundaries and protected/disabled grain boundaries.

Grain boundaries of HDG steel were found to be electrochemically very active and connected to each other as a grid of trenches in the surface of the substrate. It was also found that grain boundaries preferably undergo anodical dissolution. When a defect in the coating induces a corrosive attack to the substrate, it is assumed that the grain boundaries will propagate at a higher rate, the corrosion process under the intact regions of the coating. The anodic corrosion reaction along the grain boundaries would create local cathodes in the surrounding of the grain boundary area whilst moving forward. Oxygen would be reduced to some

radical species in that area and within water molecules to hydroxyl ions. As described in the general introduction, both species are known to migrate along the substrate/coating interface and delaminate the coating from the substrate. Herein the corrosive delamination would occur on flat areas of the grains. The free and unprotected substrate surface now excessively corrodes as indicated by the plateau corrosion. In summary, there may be two corrosion pathways, a fast one along the grain boundaries and a slower one as represented by the main plateau corrosion. The corrosion rate of the second one, the plateau corrosion, should be influenced by the first one, the grain boundary corrosion. According to these assumptions further investigation should highlight the existence of two time constants for the two corrosion pathways. Rohwerder et al. have applied the SKP-FM technique to investigate the electrochemical aspects of delamination on a model gold substrate [61]. Even though the propagation of corrosion activity along the grain boundary was not discussed in their paper, the obtained images clearly showed corrosive activity in the grain boundaries of the gold substrate. However SKP-FM could provide the appropriate tool to investigate the different corrosion rates of the two assumed corrosion pathway models on HDG steel substrate as postulated within this work. One must consider that the preparation of appropriate samples as well as the experimental set up is very advanced and that the measurement is very time consuming.

In the general introduction to this study it is postulated that corrosion starts at some weak spots, which can be edges or vertices. Based on the results obtained, corrosion can also propagate along these weak zones, when they are grain boundaries and connected with each other all over the substrate surface. Learning from this model, one would assume that disabling grain boundary activity would lead to a slow-down of the corrosion propagation, known as plateau corrosion. The following sections of this study will therefore investigate the possibility of inhibiting grain boundary corrosion activity through the application of inhibiting material exclusively to the grain boundaries.

3.1.4 Conclusion

Investigations with high lateral resolution on surface element composition and electrochemical micro probe techniques lead to the identification of the weak zones of the HDG steel substrate. It could be found that aluminum even at low concentrations of 0.5 w.-% segregates not only to the zinc/iron and iron/air interface but also to the grain boundaries of the zinc grains. It was found that the conventional alkaline cleaning process contrarily to most literature does not remove all of the aluminum from the substrate surface. Even where the overall aluminum content becomes negligible, it still remains within the grain boundaries. Surface potential mappings with the high resolution of the SKP-FM technique discovered the lower potential of the grain boundaries when compared to the surrounding grain surfaces. Spots with lower potential than the surrounding matrix are known to be more corrosively more active. The application of the micro capillary cell showed that the grain boundaries tend to dissolve more easily due to the corrosive currents that could be measured at a lower potential than on the single grains. The final corrosion test in a salt spray chamber on a coil coated and scratched sample showed the higher corrosion activity of the grain boundary. Corrosion products along the grain boundaries beneath the intact coating material could be observed after removing the coating. Collectively these findings led to the development of a corrosion model for heterogeneous surfaces; where the anodic part reaction is quickly propagated forward along the grain boundaries and escorted by the local cathode which delaminates the grains. The plateau corrosion can follow more easily along the delaminated grains. The derivation from this model would be a slowdown of the corrosion propagation through disablement of the grain boundary activity. The proof of this model would lead to new smart coating materials that treated only the weak zones of the substrate which are susceptible to corrosion. The current practice of pretreating the entire substrate surface with the same material would become obsolete and thus save the pretreatment material. This will be the focus in the following chapters.

3.1.5 References

- [1] P.Thissen, J.Wielant, M.Köyer, S.Toews, G. Grundmeier, Surf. Coatings Tech., submitted
- [1] A.Rodnyansky, Y.J. Warburton, L. D. Hanke, Surf. Interface Anal. 29 (2000) 215
- [3] A.R. Marder, *Prog. Mat. Sci.* 45 (2000) 191
- [4] V. Furdanowicz, C.R. Shastry, Metall. Trans. A 30 (12) (1999) 3031
- [5] G.A. Lopez, Dissertation „Segregation and Phase Transformations at Interfaces“ Universität Stuttgart, Max-Planck-Institut für Metallforschung Stuttgart (2004)
- [6] A. F. Holleman, E. Wieberg, Lehrbuch der Anorganischen Chemie, 101 Auflage, deGruyter, Berlin, (1995)
- [7] F. Weinberg, M.Mager, L.Frederick, Can. Met. Quart. 29 (1990)163
- [8] N. Fink, B. Wilson, G. Grundmeier, Electrochim. Acta 51 (2006) 2956
- [9] J. Strutzenberger, J. Faderl, Metall. Trans. A 29 (2) (1998) 631
- [10] S. Feliu Jr., V. Barranco, Acta Mater. 51 (2003) 5413
- [11] L.A. Rocha, M.A. Barbosa, Corrosion 47 (7) (1991) 536
- [12] A.Rodnyansky, Y.J. Warburton, L. D. Hanke, Surf. Interface Anal. 29 (2000) 215
- [13] J. Ruf, „Organischer Metallschutz“ Vincentz, Hannover (1993)
- [14] U. Koenig, J.W. Schultze, Galvanotechnik 98 (2007)1834
- [15] D. Zimmermann, A.G. Munoz, J.W. Schultze, Surf. Coat. Tech. 197(2005) 260
- [16] A.G. Munoz, J.W. Schultze, Electrochim. Acta 49 (2004) 293
- [17] E. Klusmann, J.W. Schultze, Electrochim. Acta 48 (2003) 3325
- [18] D. Zimmermann, A.G. Munoz, J.W. Schultze, Electrochim. Acta 48 (2003) 3267
- [19] A. Losch, J.W. Schultze, J. Electroanal. Chem. 359 (1993) 39
- [20] R. Berger, U. Bexell, N. Stavlid, T.M. Grehk, Surf. Interf. Anal. 38 (2006) 1130
- [21] E. Almeida, I. Alves, C. Brites, L. Fedrizzi, Prog. Org. Coat. 46 (2003) 8
- [22] N. Birbilis, R. G. Buchheit, *J. Electrochem. Soc.*, 152 (2005) B140

- [23] G. O. Ilevbare, O. Schneider, R. G. Kelly, J. R. Scully, *J. Electrochem. Soc.* 151 (2004) B453
- [24] M. Büchler, T. Watari, W. H. Smyrl, *Corros. Sci.* 42 (2000) 1661
- [25] O. Schneider, G. O. Ilevbare, R. G. Kelly, J. R. Scully, *J. Electrochem. Soc.*, 151 (2004) B465
- [26] G. O. Ilevbare, J. R. Scully, *J. Electrochem. Soc.*, 148 (2001) B196
- [27] J. R. Scully, T. O. Knight, R. G. Buchheit, D. E. Peebles, *Corros. Sci.*, 35 (1993) 185
- [28] R. G. Buchheit, *J. Electrochem. Soc.*, 142 (1995) 3994
- [29] R. P. Wei, C.-M. Liao, M. Gao, *Metall. Mater. Trans. A*, 29 (1998) 1153
- [30] N. Birbilis, R.G. Buchheit, *J. Electrochem. Soc.* 155 (2008) C117
- [31] G. Ibe, K. Lucke, *Am. Soc. Met.* (1966) 434
- [32] M. Shimada, H. Kokawa, Z.J. Wang, Y.S. Sato, I. Karibe, *Acta Mater.* 50 (2002) 2331
- [33] H. Liu, M. Gao, D. Harlow, R. Wei, *J. Scr. Metall. Mater.* 32 (1995) 1807
- [34] V.B. Trinidade, U. Krupp, Ph. E.-G. Wagenhuner, H.-J. Christ, *Mater. Corr.* 56 (2005) 785
- [35] E. Trillo, L. Murr, *J. Mater. Sci.*, 33 (1998) 1263
- [36] E.P. Bulter, M.G. Burke, *Acta. Metal.*, 34 (1986) 557
- [37] M.S. Laws, P.J. Goodhew, *Acta Metal. Mater.* 39 (1991) 1525
- [38] R. Bredesen, P. Kofstad, *Oxidation of Metals* 34 (1990) 361
- [39] R. J. Hussey, M. Cohen, *Corrosion Science* 11 (1971) 713
- [40] Interview R&D Group, BASF Coatings GmbH, Münster
- [41] G.A. Lopez, E.J. Mittemeijer, B.B. Straumal, *Acta Mater.* 52 (2004) 4537
- [42] B. Straumal, R. Valiev, O. Kogtenkova, P. Zieba, T. Czeppe, E. Bielanska, M. Faryna, *Acta Mater.* 56 (2008) 6123
- [43] F.M. Ferry, K. Kjoller, J.T. Thornton, R.J. Tench, D. Cook, *Electric Force Microscopy, Surface Potential Imaging, and Surface Electric Modofocation with Atomic Force Microscopy (AFM)*, Digital Instrument, Veeco Metrology Group, Application Note 27 (1999)
- [44] M. Stratmann, H. Streckel, *Corr. Sci.* 30 (1990) 681
- [45] G. Binning, C.F. Quate, C. Gerber, *Phys. Rev. Lett.* 56 (1986) 930
- [46] Q. Zhong, D. Inniss, K. Kjoller, V.B. Ellings, *Surf. Sci.* 290 (1993) L688
- [47] A.P. Quist, J. Ahlbom, C.T. Reimann, B.U.R. Sandqvist, *Nucl. Instr. Meth.* B88 (1994) 164

- [48] P. Schmutz, G. Frankel, J. Electrochem. Soc. 145 (1998) 2285
- [49] H.O. Jacobs, H.F. Knapp, S. Müller, A. Stemmer, Ultramicroscopy 69 (1997) 39
- [50] M. Nonnenmacher, M.P. O'Boyle, H.K. Wickramasinghe, Appl. Phys. Lett. 58 (1991) 2921
- [51] S. Yee, A. Oriani, M. Stratmann, J. Electrochem. Soc. 138 (1991) 55
- [52] M. Rohwerder, F. Turcu, Electrochim. Acta. 53 (2007) 290
- [53] B.S. Tanem, O. Lunder, A. Borg, J. Mardalen, Int. J. Adhes. Adhes. 29 (2009) 471
- [54] F. Andreatta, M.M. Lohrengel, H. Terryn, J.H.W. de Wit, Electrochim. Acta 48 (2003) 3239
- [55] F. Andreatta, A. Turco, I. de Graeve, H. Terryn, J.H.W de Wit, L. Fedrizzi, Surf. Coat. Tech. 201 (2007) 7668
- [56] A. Schreiber, C. Rosenkranz, M.M. Lohrengel, Electrochim. Acta 52 (2007) 7738
- [57] K. Fushimi, S. Yamamoto, R. Ozaki, H. Habazaki, Electrochim. Acta 53 (2008) 2529
- [58] C.J. Park, M.M. Lohrengel, T. Hamelmann, M. Pilaski, H.S. Kwon, Electrochim. Acta 47 (2002) 3395
- [59] K.A. Lill, A.W. Hassel, G. Frommeyer, M. Stratmann, Electrochim. Acta 51 (2005) 978
- [60] A. Schreiber, C. Rosenkranz, M.M. Lohrengel Electrochim. Acta 52 (2007) 7738
- [61] M. Rohwerder, E. Hornung, M. Stratmann, Electrochim. Acta 48 (2003) 1235

3.2 Material survey for grain boundary application

3.2.1 Fundamentals

The following section of this work will deal with the major question of what material is appropriate to disable the corrosion activity of grain boundaries and how to focus it on the identified weak zones. In section 3.1 the substrate surface was characterized and it was found that grain boundaries are electrochemically very active. As could be seen in the micro capillary cell measurements, they have a strong drive towards anodical dissolution. It is assumed that the same strong drive of grain boundaries to corrosion can be used as a trigger for the selective application of inhibiting materials on grain boundaries. Promising known materials from literature and industrial use with the potential for adaptation to an exclusively grain boundary application were investigated and are discussed within this chapter. Phosphating, surface polymerization and polymer deposition were found to be the most promising for further evaluation. All three of these techniques deposit or create the corrosion inhibiting material on the substrate surface by partly dissolving metal ions from the substrate surface. However all of these techniques cover the entire substrate surface as applied. This survey will evaluate the controllability of addressing the material deposition or creation on grain boundaries of:

- Phosphating;
- surface spontaneous polymerization; and
- polymer deposition.

3.2.1.1 Phosphating

The phosphating of metals for corrosion protection has been an established technique since the 1960s [1-5]. This technique uses the anodic dissolution of the surface metal e.g. zinc and the subsequent phosphate crystal growth on the substrate surface controlled by the pH. The main components of phosphating solutions are diluted phosphoric acid and zinc cations. State of the art phosphating technology also uses nickel and manganese cations [6]. In a first step, a pickling attack from the phosphoric acid (pH 2.5 – 3.5) on the substrate metal consumes protons and zinc cations are released. This leads to a pH-gradient and zinc cation gradient build up. The increased cation concentration and the higher pH on the substrate surface shift the protolytic equilibrium of the phosphoric acid to the phosphate anion which results in precipitation of hopeite caused by its extremely low solubility. The precipitation of hopeite is basically controlled by the amount of phosphate anions in the phosphating solution [7]. However this technique is always applied on the entire substrate surface. When applying to HDG steel, the substrate surface has to first be activated by an alkaline etching process (see section 3.1). Alkaline etching removes the native aluminum oxide / hydroxide passive layer [8,9]. The remaining bare zinc surface can be easily dissolved as it is needed in order to create a phosphate layer. In the experimental results of this chapter it will be shown that exposure of HDG steel to acidic solutions in the pH range of 3.6 to 4.0 dissolve only the grain boundaries. The flat grain areas remain non-etched. This can be attributed to the passive aluminum oxide / hydroxide layer and the flat topography of the grains. The topography of grain boundaries is very rough with vertices and edges. The high solubility of grain boundaries can be attributed to the high accessibility and loose structure of the metal atoms. In this part of the study, the high solubility of grain boundaries will be used to create phosphate crystals selectively on the grain boundaries. Aside from phosphoric acid, vinylphosphonic acid (VPA) will also be investigated in the phosphating process modified for the grain boundary. VPA is attractive for such processes due to its polymerizable double bond. Shannon et al. have investigated copper and zinc precipitates of VPA and its radical polymerization. Their purpose was to immobilize the catalytically metal atoms in order to use the newly created material as a heterogeneous catalyst

[10-12]. In this study the aim will be to use the reactive double bond in order to react it with the UV coating system applied on top. The main idea is to establish a covalent bond between the grain boundary applied phosphonate layer and the top coating material.

3.2.1.2 Surface spontaneous polymerization

In the late 1990s Zhang, Agarwal and Bell developed an environmentally friendly polymeric coating process for aluminum [13,14] and steel [15-17] substrates through a surface spontaneous polymerization. The coating is directly synthesized on the metal surface by simply dipping the metal sample into the solution of monomers for a few seconds. The mechanism of spontaneous polymerization is based on the high copolymerization reactivity of donor acceptor monomers and has been studied by several researchers [18,19]. A monomer with a negatively polarized double bond (donor) is able to combine to a donor-acceptor complex with a positive polarized double bond of a monomer (acceptor) under certain conditions [20,21]. Therefore spontaneous copolymerization can take place only if there is a substantial polarity difference between the reacting monomers. An addition of Lewis acids to the system then destabilizes the donor-acceptor complex and spontaneous polymer chain propagation starts. Bell et al. have investigated the surface spontaneous polymerization in a simple system of styrene (St) and n-phenylmaleimide (NPMI). The electron donating character of styrene comes from the presence of the phenyl ring next to the C=C bond while the two carbonyl groups withdraw electrons from the double bond of NPMI. The driving force for spontaneous polymerization in that system comes from the aluminum surface, where Lewis acids such as Al^{3+} -cations are generated when a sample of aluminum is immersed in an acidic solution. The aluminum cation is classified as a hard Lewis acid and therefore has a strong affinity to electron pair acceptance (see section 1.4). Learning gained from the literature survey makes the surface spontaneous polymerization very interesting when applying selectively to grain boundaries. In section 3.1: Substrate Characterization, it was shown that grain boundaries are enriched with aluminum. Therefore the controlled release of aluminum cations and their ability to initiate the spontaneous

polymerization directly on grain boundaries of HDG steel will be investigated within this chapter.

3.2.1.3 Polymer deposition

Among a broad variety of application methods for polymers, dip coating is the most promising process for selective application on micro structures such as grain boundaries. The two major dip coating applications for water based polymer dispersions are driven by electrophoresis and autophoresis. Electrophoretic coatings were introduced to the automotive industry in the 1960s. Nowadays these primer systems are applied on almost all automotive bodies due to the improved corrosion protection offered [22]. Autophoretic coatings were initially invented by Amchem Products Inc. and became available in the US in the 1980s [23-25]. Due to constant development throughout the last decades, these coating systems found a broad application for corrosion protection on industrial goods with less surface quality [26-33]. After Henkel AG & Co. KGaA acquired Amchem Products Inc. in the late 1990s, autophoretic coatings also became available in Europe [34-40]. In 2009 Henkel re-launched the autophoretic coating system under the brand of Aquence© [41] Henkel's coating system is environmentally friendly due to its water based system containing no volatile organic compounds (VOC). It reduces the application process steps because special substrate pretreatment such as phosphating becomes redundant. There is also finally, no electric current required in order to apply the polymeric coating material to a steel part as it is in the electrophoretic coating system. The clear focus of Henkel is entry into the automotive industry with its advanced technology. BASF Coatings GmbH also recently patented some variations of autophoretic coatings systems [42-47]. However, the principle of the autodeposition of the polymeric coating material is based on the ability of the substrate to corrode. In this process, the substrate to be coated is immersed in a stabilized latex bath containing a hydrofluoric acid, oxygenated water and various other additives [48,49]. When the substrate is immersed in the coating bath, the major chemical reaction that takes place is the dissolution of the metal substrate surface. Subsequently the metal cations generated on the substrate surface coagulate and precipitate the polymer latex. The aggressive oxidants in the coating bath continue to penetrate the

deposited but still porous polymer particles and the metal oxidation and polymer precipitation continues. The final coating thickness depends on the immersion time, the solid content and the pH of the Bath [50,51]. The mechanism of the autophoretic polymer deposition will be investigated for the exclusive application to grain boundaries of HDG steel surfaces. Therefore the controlled release of cation from the grain boundaries might also be of importance for the selective application of polymer particles. A screening of a variety of water based polymer dispersions will be provided within the following experiments.

3.2.2 Experimental procedure

3.2.2.1 Grain boundary dissolution

Grain boundary dissolution experiments were carried out by dipping the HDG substrate in phosphoric acid solutions of different pH values and by varying the dipping time.

3.2.2.2 Phosphating

Phosphoric Acid

The phosphating experiments were carried out in a 100 mL beaker. The starting formulation and parameters for the phosphating bath were derived from Müller et al [52]. A standard 100 mL phosphating bath contained 25 mmol phosphoric acid, 1.6 mmol zincoxide, and 100 mL of distilled water. The phosphating experiments were carried out by varying the bath temperature, the pH and the dipping time of the substrate.

Vinylphosphonic Acid

The phosphonating experiments with vinylphosphonic acid were carried out following the same procedure of the experiments from phosphoric acid. A

standard formulation for the phosphating bath was derived from the phosphating experiments with phosphoric acid and contained 14.7 mmol/100 mL of VPA, 9.2 mmol/100 mL of ZnO and 100 mL water.

3.2.2.3 Surface spontaneous polymerization

The formulation of the monomer solution and the conditions for carrying out the surface spontaneous polymerization experiments were derived from Bell et al. The experiments were carried out in a 100 mL flask. The following monomer composition was dissolved in 21.5 g of water and 28.5 g n-methylpyrrolidone (NMP).

Monomer composition

n-phenylmaleimide (NMPI)	0.866 g (0.1 mol)	<i>acceptor</i>
Styrol (St)	1.042 g (0.2 mol)	<i>donor</i>
2-Methacryloxy-Ethylacetat (MEA)	1.071 g (0.1 mol)	<i>acceptor, adhesion promoter</i>
Bis-N-Methylmaleimid (BMI)	0.09 g (0.005 mol)	<i>acceptor, cross-linker</i>

The polymerization experiments were carried out under an inert atmosphere. The pH was varied within a range of 2.5 and 4.0.

3.2.2.4 Polymer deposition

A variety of exemplaric polymer dispersions were investigated in terms of their selective deposition on grain boundaries of the HDG steel. The applications were carried out by varying the dipping time and the pH.

3.2.3 Experimental results

3.2.3.1 Grain boundary dissolution

Grain boundaries were found to preferably undergo anodical dissolution (see section 3.1). The ability of grain boundaries to corrode will be investigated in the use of the selective application of corrosion inhibiting material onto grain boundaries. It was shown that grain boundaries do not preferably dissolve when exposed to alkaline solution of high pH values. Therefore the dissolution of grain boundaries was investigated in acidic conditions as shown in *Fig. 3.17*.

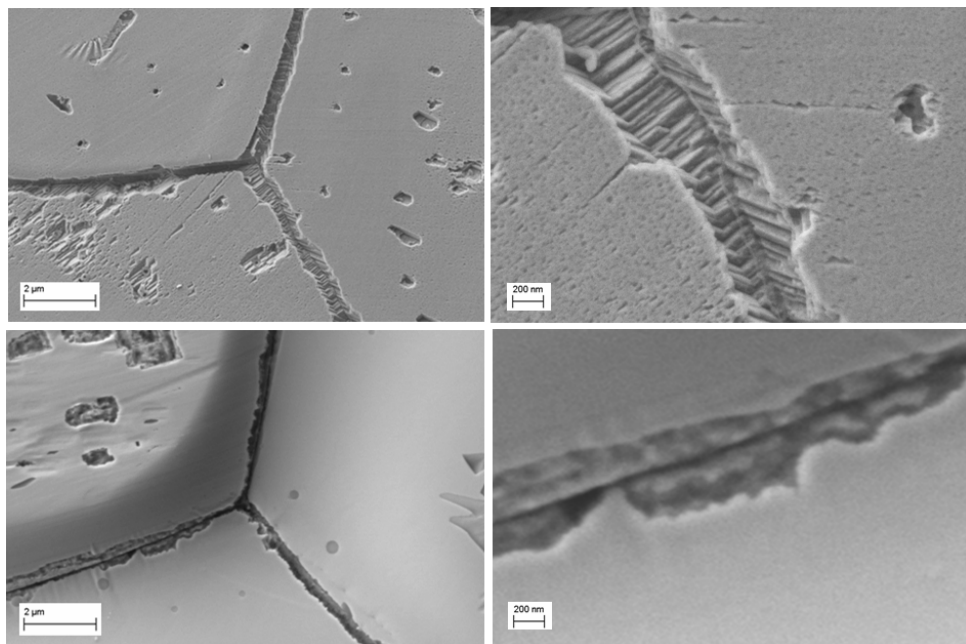


Fig. 3.17: SEM images of grain boundaries. Top) grain boundaries selectively etched with diluted phosphoric acid pH 3.6 for 30s. Bottom) natural grain boundaries on HDG steel surface.

SEM images in *Fig. 3.17* show dissolved grain boundaries in comparison to natural grain boundaries of HDG steel. The substrate after etching in phosphoric

acid at pH 3.6 is shown in the top images. Selective grain boundary dissolution of the grain boundaries could only be observed in the pH range of 3.6 to 4.0. Above a pH of 4.0, no dissolution activity of the substrate was observed. When the pH was lower than the value of 3.6, dissolution of grain surfaces also became visible where the material is removed from the grain boundaries and they appear excavated. Therefore the grain boundaries as shown in the bottom SEM images of *Fig. 3.17* should consist of an amorphous structure. The dissolution of the grain boundaries releases cations that will be used for selective material deposition on grain boundaries in the following part of this chapter.

3.2.3.2 Phosphating

Phosphoric Acid

In order to find the right parameters for grain boundary selective phosphating, the precipitation parameter of the phosphating solution had to be investigated. Therefore zinc phosphate precipitation was reviewed in relation to a dependency of the pH and the temperature for different ion concentrations in the phosphating bath (see *Fig. 3.18*).

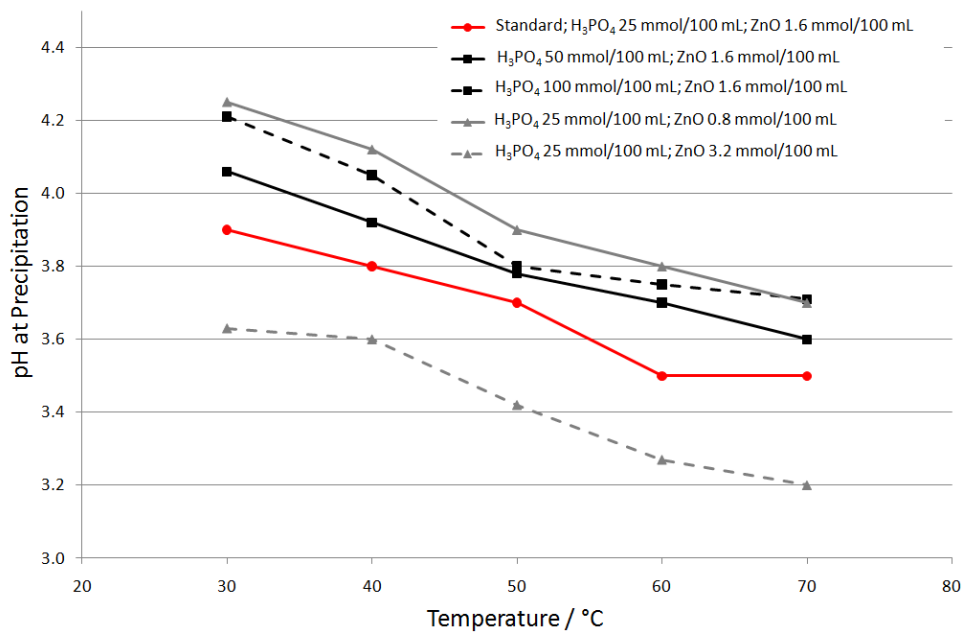


Fig. 3.18: pH-Temperature dependency for zinc phosphate precipitation for a variety of phosphating bath formulations.

Each of the phosphating bath formulations has an initial pH lower than 3.0, where the phosphating solution appears as a clear liquid. At the specific temperature the pH was raised slowly by the addition of 0.1 n sodium hydroxide solutions. The pH value was transferred to the chart in *Fig. 3.18* when visible precipitation occurred. Overall the higher temperature resulted in a lower pH where precipitation occurs, which can be attributed to the endothermic crystallization behavior of zinc phosphate. A rise in the phosphate ion concentration from 25 mmol/100 mL to 50 mmol/100 mL to 100 mmol/100 mL results in a slightly parallel shift of precipitating pH values to higher numbers. This is not surprising because the phosphating bath is formulated with an excess of phosphate ions for this very reason the zinc ion concentration can be used to control the crystallization process. When varying the amount of zinc ions in the phosphating bath, lower zinc ion concentration leads to more stability in the bath and a parallel shift to higher pH values for precipitation. Higher zinc ion concentration led to lower pH values for precipitation of zinc phosphate. These results are in line with the phosphating process, where the dissolution of the outermost metal atoms of the substrate consumes H^+ ions and releases Zn^{2+} ions, resulting in a rise in the pH and zinc. Within this section however it was observed that selective dissolution of grain boundaries occurred in the pH range of 3.6 to 4.0.

The appropriate pH range for selective phosphating is assumed to also be in this range. The release of cations from the grain boundaries should raise the ion concentration locally. The pH would also rise in the grain boundary area due to the reduction of protons. Both should lead to zinc phosphate crystal growth.

The experiments were carried out within these parameters. In addition, the substrate exposure time in the phosphating bath varied from 10 to 240 s. The pH of each phosphating bath was adjusted to 0.2 pH lower than the precipitation pH value in *Fig. 3.18*. In phosphating experiments at pH values above 3.5, very few crystals could be obtained on the substrate surface. These few crystals also provided no specific selectivity to grain boundaries. In industrial applications, bath parameters are adjusted to 65°C and pH 3.4. Under these conditions the substrate surfaces are covered with zinc phosphate crystals within 60 s but this is also very rare. This example is shown in *Fig. 3.19*.



Fig. 3.19: SEM image of zinc phosphated HDG steel in a standard zinc phosphating bath (H_3PO_4 25 mmol/100 mL; ZnO 1.6 mmol/100 mL) at 60°C and p hosphating time of 60 s.

According to *Fig. 3.19* there is no specific selectivity that can be observed towards grain boundaries. The reason for these poor phosphating results can be attributed to the aluminum passive layer that is inhibiting the pickling process (see section 3.1). In addition dissolved aluminum is inhibiting the zinc phosphate formation and precipitation due to the higher solubility product of aluminum phosphates [23]. Therefore aside from removing the aluminum layer from the substrate surface, in industrial application fluorine salts are always added in order to capture remaining aluminum ions from the substrate. The high aluminum content of the grain boundaries would therefore be counterproductive to the selective grain boundary phosphating approach. The next step towards the aim of selective inhibition of the corrosion active grain boundaries was to first etch the grain boundaries and then apply the phosphating procedure as the second step. The HDG steel substrate was first therefore exposed to an acidic solution of pH 3.6 for 30 s. This procedure resulted in almost aluminum free grain boundaries (see *Fig. 3.17*). Because in the phosphating results there was still no improvement in grain boundary selectivity, an activator (Fixodine from Henkel AG

& Co. KGaA) was introduced to the phosphating process to act as seed crystals. The size of the crystals is less than 5 nm and could not be resolved with scanning electron microscopy. After etching the grain boundaries a Fixodine solution of 5 g/L as recommended from Henkel was rinsed over the substrate followed by a rinse with distilled water. The aim of this procedure was to deposit the seed crystals within the grain boundaries. The following phosphating process led to enhanced crystal growth starting from grain boundaries. *Fig. 3.20* shows a zinc phosphate HDG steel surface when etching the grain boundaries, depositing seed crystals and choosing the application parameter in the pH range of 3.6 to 4.0. Similar results could be obtained for different concentrations and temperatures.

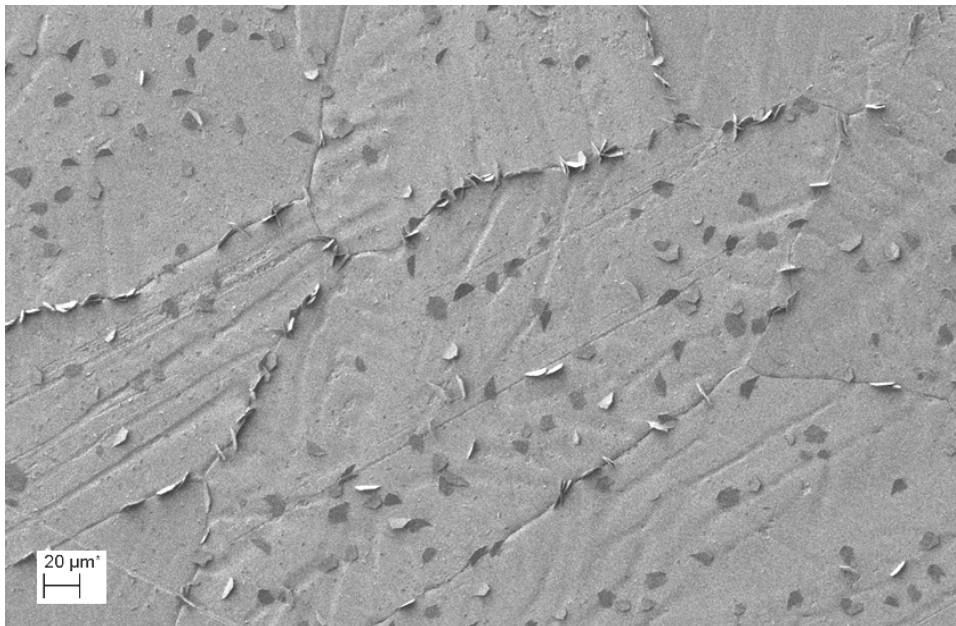


Fig. 3.20: SEM image of zinc phosphated HDG steel in a standard zinc phosphating bath (H_3PO_4 25 mmol/100 mL; ZnO 1.6 mmol/100 mL) at 30°C and p hosphating time of 70 s after etching the grain boundaries rinsing with seed crystals.

However zinc phosphate crystals were obtained on grain boundaries as well as on the grains. Not all grain boundaries were covered with crystals and the crystal density along the grain boundaries was poor. Satisfactory selectivity towards grain boundaries could thus not be achieved. When reducing the dipping time,

the dipping tendency for grain boundary selective phosphating also dropped. The higher the exposure time of the substrate to the phosphate bath, the more crystals were found on the grains.

Vinylphosphonic Acid

Grain boundary selective phosphating experiments with VPA were carried out in analogy to the experiments with phosphoric acid. The best results could be obtained with a phosphating bath formulation of 14.7 mmol/100 mL VPA, 9.2 mmol/100 mL ZnO and 100 mL water at pH of 3.5, temperature of 60°C and a dipping time of 60s. To achieve this result the substrate was cleaned and grain boundaries were etched and then rinsed with seed crystals as found in the previously discussed phosphating experiment. The best result is shown in *Fig. 3.21*.

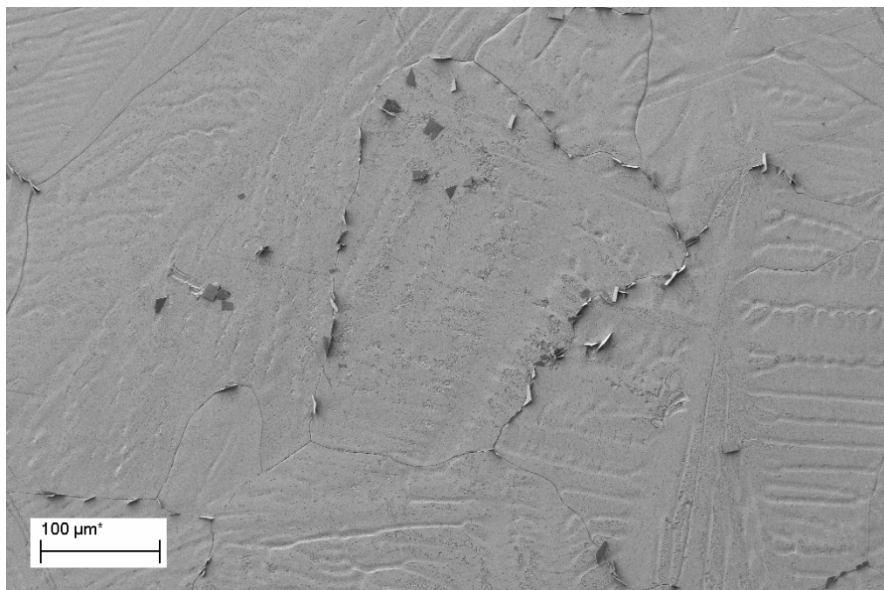


Fig. 3.21: SEM image of zinc phosphonated HDG steel in a standard zinc phosphonating bath (VPA 14.7 mmol/100 mL; ZnO 9.2 mmol/100 mL) at 40°C and phosphating time of 60 s after etching the grain boundaries rinsing with seed crystals.

Replacing phosphoric acid by vinylphosphonic acid led to similar results in terms of the selective deposition of corrosion inhibiting materials on grain boundaries. The crystal density on the grain boundaries was again found to be rather poor. Driving the bath parameters towards higher phosphating activity always led to crystal growth all over the grain surface and thus not improving the crystal density in the grain boundaries. In summary, selectivity towards grain boundaries could only be partly achieved with the support of the activating seed crystals. The process of etching and depositing seed crystals is inconvenient for industrial applications. A truly innovative process should be applicable through a one-step dipping process that takes only a few seconds.

3.2.3.3 Surface spontaneous polymerization

Spontaneous polymerization was attempted in order to adapt the grain boundaries of HDG steel. For this reason the high aluminum presence in the grain boundaries of the HDG steel surface was most promising. The procedure and monomer composition was derived from Bell et al. By varying the pH of the monomer solution the study tried to control the polymerization towards the grain boundaries. Results on surface spontaneous polymerization on HDG steel are shown in *Fig. 3.22*.

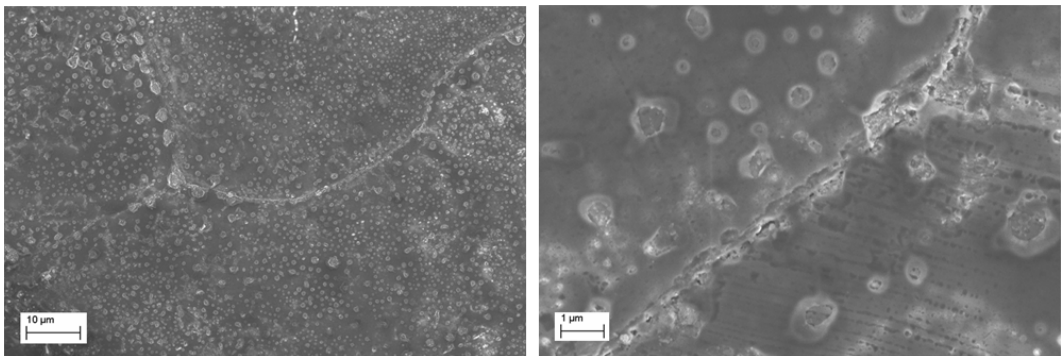


Fig. 3.22: SEM images of polymer on HDG steel surface obtained through spontaneous polymerization at a pH value of 3.0 and polymerization time of 10 min.

Within the pH range of 3.6 to 4.0, where grain boundaries selectively dissolve, polymerization on the HDG steel surface could not be observed; only when the

pH was lowered to the value of 3.0 for an exposure time of 10 minutes, could a polymer be found on the substrate surface as is shown in *Fig. 3.22*. The high resolution SEM image shows that along grain boundaries especially, the polymer is less visible than on the flat grain surface. Within these experiments the spontaneous surface polymerization could be observed on HDG steel substrates. The polymer creation on HDG was very slow in comparison to the polymerization on aluminum substrates as observed by Bell et al. However selective polymerization on grain boundaries failed in the provided experiments.

3.2.3.4 Polymer deposition

A number of exemplaric water borne polymers were investigated in terms of their applicability to grain boundaries of HDG steel. In order to apply the polymer dispersion they were diluted to a solid content of 1.0 w.-%. It was considered for the polymer application that a simple dip process would be the most convenient in an industrial application process on fast moving steel strips in coil production. Due to the very specific and small structure of the grain boundaries, only an autophoretic coating process can provide a selective deposition of the polymer on the desired substrate areas. The application process was carried out by varying the pH and the dipping time. These most satisfying results could be obtained from the primary anionically stabilized dispersions. Acronal 250D was found to be stable in the entire pH range from 1.0 to 14. The best application results could be obtained with a pH of 2.0 and a dipping time of 15 s (see *Fig. 3.23*).

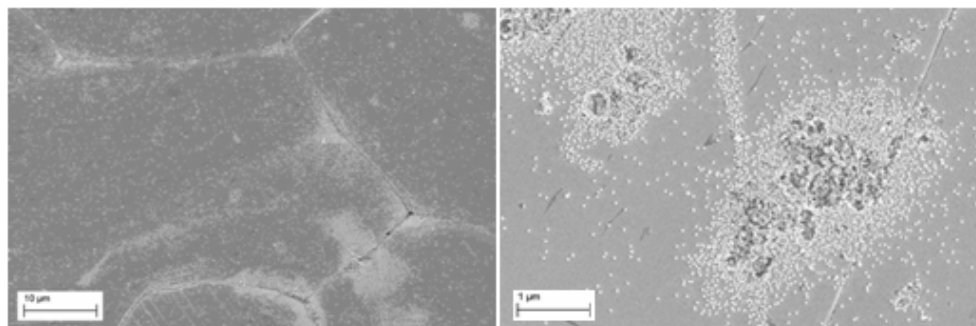


Fig. 3.23: SEM image of Acronal 250D a primary anionically stabilized dispersion from BASF SE applied to HDG steel substrate at the pH of 2.0 and a dipping time of 15 s. (Polymer particles appear bright in the images.)

At lower pH levels or higher dipping times, the selectivity to the grain boundaries was decreasing and more of the polymer was found on the entire substrate surface. At a higher pH, fewer polymers could be deposited on the grain boundaries even at a longer dipping time.

The next dispersion of interest to this study was Aquence from Henkel AG & Co. KGaA which is developed especially for the autophoretic coating processes and is based on an anionic stabilized primary dispersion. In the commercial formulation Aquence contains highly oxidizing acids, fluorides and peroxides in order to dissolve the outermost metallic layer so that the metal cations coagulate and precipitate the polymer on the surface. However this commercially available product was diluted to 1.0 w.-% prior to the experiments. In the corresponding image, the surface coverage with the polymer after just one second of dipping is shown in *Fig. 3.24*. Unfortunately, the polymer can be found on the entire surface which can be attributed to the high reactivity of the oxidizing ingredients in the commercial formulation. A longer dipping process resulted in coverage of the entire surface with a film build up to 20 μm (30 s). Therefore Aquence as it is commercially formulated cannot be selectively applied on grain boundaries in line with the aim of this study.

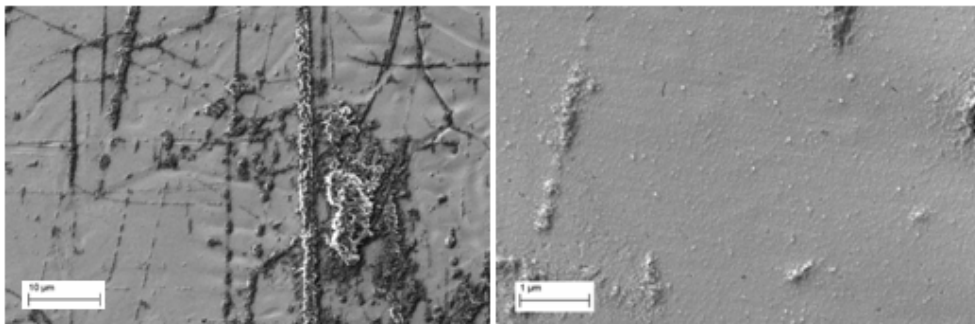


Fig. 3.24: SEM image of Aquence from Henkel AG & Co. KGaA. A primary anionically stabilized dispersion specifically developed and formulated for autophoretic coating deposition. Applied to HDG steel substrate at the pH of 3.0 (as obtained through diluting to 1.0 w.-%) and a dipping time of 1 s. (Polymer particles appear dark in the left image)

In the next experiment, a cationic secondary dispersion which can be found in a typical electro coat binder was investigated. This dispersion was found to be stable only in a small pH range from 4.0 to 8.0. Within this pH range no polymer

could be autophoretically applied to the substrate. The results shown in the corresponding image (*Fig. 3.25*) were obtained at a pH of 4.0 with a dipping time of 30s. The polymer on the substrate is applied non-selectively all over the substrate. The coagulated polymer particles were obviously precipitated due to the disability of the dispersion at a low pH. There is no evidence that the cation release from the substrate surface triggered the precipitation. This experiment shows that the dispersion must be stable in the pH range of the controlled release of cations from the surface.

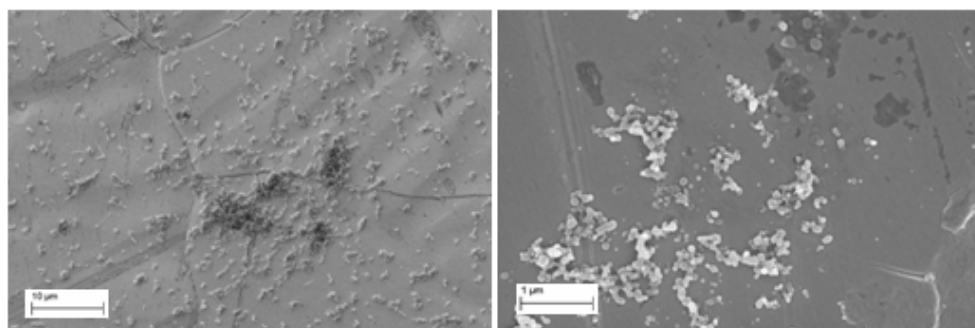


Fig. 3.25: SEM image of E-Coat Binder a secondary cationically stabilized dispersion from BASF Coatings GmbH. Applied to HDG steel substrate at the pH of 4.0 and a dipping time of 30 s. (Polymer particles appear dark in the left image and bright in the right image)

The following polymer is a polyurethane dispersion which is a typical anionic stabilized secondary dispersion and behaves in a similar way to the E-Coat binder. The pH range where the dispersion is stable was found to be very narrow between the pH of 5.0 to 8.0. Aside from this pH range, similar observations to that of the image of the E-Coat binder can be made. The corresponding image for the polyurethane dispersion in *Fig. 3.26* shows the polymer application experiment at a pH of 5.5 and a dipping time of 30 s. The image was taken at a higher magnification to demonstrate that only very few polymer particles are randomly distributed on the substrate surface with no specific selectivity for grain boundaries.

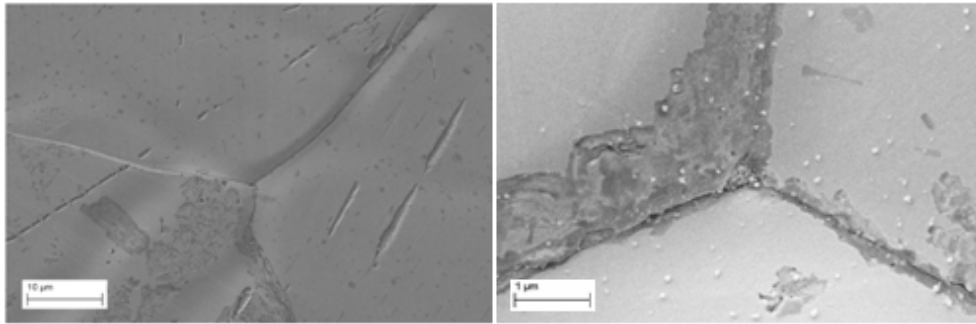


Fig. 3.26: SEM image of Polyurethane Dispersion a secondary dispersion developed for Coil Coating applications. Applied to HDG steel substrate at the pH of 5.5 and a dipping time of 30 s. (Polymer particles appear bright in the right image)

The last polymer considered for the application screening process was a block-co-polymer that is semi soluble in water. An explanation for the semi solubility of the polymer in water may be derived from its highly hydrophilic block which dominates the solubility in water. The polymer was synthesized by the RAFT technique in solvent and dissolved afterwards in water. It shows some particle structure but also a dominant behavior of a solubilized polymer e.g. viscosity. The stability of this polymer could be observed on a broad pH range from 2.0 to 10. But the application in a dipping process always showed smudgy covered surface areas without any selectivity to the specific HDG surface characteristics (see Fig. 3.27).

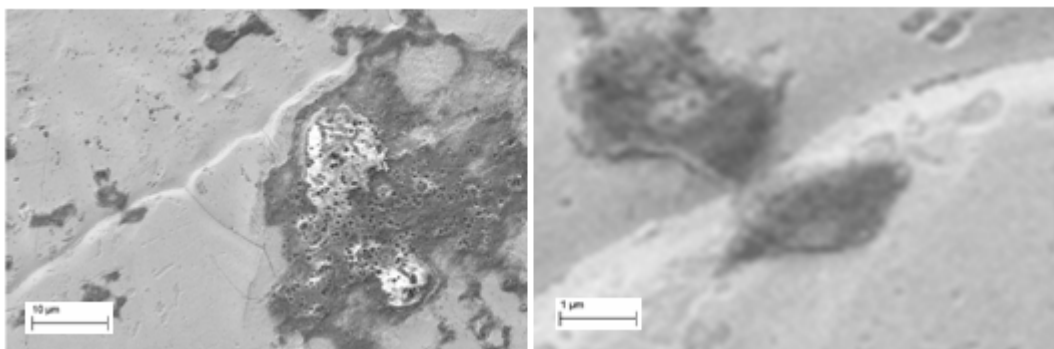


Fig. 3.27: SEM image of a Block-co-Polymer semi soluble in water from Rhodia Co. Developed for anti-corrosion primer application. Applied to HDG steel substrate at the pH of 3.0 and a dipping time of 30 s. (Polymer appears dark images)

These results may be attributed to the high solubility of the polymer in water. For this reason, the polymers in this dispersion exist as particles as well as solute polymer chains. When some of the particles become destabilized during application, the precipitating polymer particles drag more polymers with them. This results in more polymers being deposited on the surrounding substrate area but with less precision. Therefore sharply dispersed polymer particles provide more precise deposition on grain boundaries, on which the focus should be when considering the polymer design for grain boundary application.

3.2.4 Conclusion

The experiments within this section were dealing with two major questions, how to apply corrosion inhibiting material exclusively on the grain boundaries and what that material should be. In section 3.1 it was found that grain boundaries are the weak spots of the HDG steel substrate and that they are highly electrochemically active, which is attributed to their high aluminum content and to their rough topography. It was also found that grain boundaries can be dissolved in acidic solutions. Therefore the application of choice would be to use the anodical solubility of grain boundaries for the application of the corrosion inhibiting material. The material investigated for grain boundary selective deposition was either inorganic precipitates (phosphates) or polymeric material. Phosphating with phosphoric acid and then right away with vinylphosphonic acid on the grain boundaries was not successful. It is assumed that the aluminum is inhibiting the phosphate crystal growth. This is one of the major reasons that aluminum is removed from the substrate surface in industrial phosphating applications through alkaline etching. Only when selectively etching the grain boundaries and applying the seed crystals (Fixodine) first, could some crystal growth along grain boundaries be achieved. But the poor selectivity and crystal density along grain boundaries excluded this approach from further investigations.

Spontaneous surface polymerization can be triggered by strong Lewis acids such as aluminum cations. It was assumed that the aluminum cations released from the grain boundaries could initiate the spontaneous polymerization at the grain boundaries. Unfortunately the polymerization was not very selective. One could

observe even fewer polymers on grain boundaries than on the grains themselves. From these findings, spontaneous polymerization was evaluated as a technique with low potential for grain boundary polymerization on the specific substrate.

The best results could be obtained from the autophoretic deposition of dispersions. Among the screened dispersions, the primary anionically stabilized ones were the most stable at low pH values which they need for the release of cations from the grain boundaries. Acronal 250 D was found to especially provide some initial selectivity towards the grain boundaries. Henkel's Aquence is based on similarly polymer particles but is formulated for application on the entire surface and can therefore not be used for selective grain boundary application. As a result of this survey, the approach towards inhibited grain boundary of HDG steel will be focused on local autophoresis of water borne polymer particles. In the following section polymer dispersion with specific functionalities will be synthesized and selectively deposited on grain boundaries.

3.2.5 References

- [1] E.L. Ghali and R.J.A. Potvin, *Corros. Sci.*, **12** (1972) 583 594.
- [2] G.D. Cheever, *J. Paint Technol.*, **39** (1967) 1 13.
- [3] G. Lorin, *Galvano-organo, Trait. Surf.*, **4** (1985) 385 387.
- [4] J.B. Lakeman, D.R. Gabe and N.O.W. Richardson, *Trans. Inst. Met. Finish.*, **55** (1976) 47 53.
- [5] B. Ptacek, F. Dalard, J.J. Rameau, *Surf. Coat. Tech.* **82** (1996) 277
- [6] D. Zimmermann, A.G. Munoz, J.W. Schultze, *Surf. Coat. Tech.* **197** (2005) 260
- [7] E. Klusmann, J.W. Schultze / *Electrochimica Acta* **48** (2003) 3325
- [8] D. Zimmermann, A.G. Munoz, J.W. Schultze, *Electrochim. Acta* **48** (2003) 3267
- [9] A. Losch, J.W. Schultze, *J. Electroanal. Chem.* **359** (1993) 39
- [10] I.J. Shannon, *New J. Chem.*, **26** (2002) 906
- [11] A.D. Knight, *J. Chem. Soc. Dalt. Trans.*, **6** (2002) 824

- [12] I.J. Shannon, *J. Mat. Chem.*, **12** (2002) 350
- [13] R. Agarwal, J.P. Bell, *Polym. Eng. Sci.* 38 (1998) 299
- [14] X. Zhang, R. Agarwal, J.P. Bell, *Pat.:* US 2003/0153704 A1 (2003)
- [15] X. Zhang, J.P. Bell, *J. Appl. Polym. Sci.* 66 (1997) 1667
- [16] X. Zhang, J.P. Bell, *Mater. Sci. Eng. A*, A257 (1998) 273
- [17] X. Zhang, J.P. Bell, *Polym. Eng. Sci.* 39 (1999) 119
- [18] Y. Shirota, H.J. Mikawa, *Macromol. Sci. Rev. Macromol. Chem.* C17 (1977) 129
- [19] D.J.T. Hill, J.T. O'Donnell, P.W. O'Sullivan, *Prog. Polym. Sci.* 8 (1982) 215
- [20] J. R Ebdon, *Macromol. Chem. Macromol. Symp.* 10 (1987) 441
- [21] A.Saito, D. A. Tirrel, *European Polym J.* 29 (1993) 343
- [22] E. Almeida, *Guide on anticorrosive protection in automotive industry*, INETI, Lisbon (200) 79
- [23] W.S. Hall, H.M. Leister, *US Patent* 4,243,704 (6 January 1981), to Amchem Products Inc.
- [24] M. Chaker, *US Patent* 4,313,983 (2 February 1982), to Amchem Products Inc.
- [25] W.S. Hall, *US Patent* 4,318,944 (9 March 1982), to Amchem Products Inc.
- [26] H.M. Leister, J.C. Donovan, W.S. Hall, *US Patent* 4,357,372 (2 November 1982), to Amchem Products Inc.
- [27] W.S. Hall, *US Patent* 4,366,195 (28 December 1982), to Amchem Products Inc.
- [28] W.S. Hall, *US Patent* 4,414,350 (8 November 1983), to Amchem Products Inc.
- [29] K. Park, *US Patent* 4,457,956 (3 June 1984), to Union Carbide Co.
- [30] B.M. Ahmed, *US Patent* 4,562,098 (31 December 1985), to Amchem Products Inc.
- [31] R.W. Broadbent, E.A. Stockbower, *US Patent* 4,632,851 (30 December 1986), to Amchem Products Inc.
- [32] W.S. Hall, *US Patent* 4,637,839 (20 January 1987), to Amchem Products Inc.
- [33] K.C. Benton, Weinert Jr., J. Raymond, *US Patent* 4,657,788 (14 April 1987), the Standard Oil Co.
- [34] N. Shachat, *US Patent* 5,061,523 (29 October 1991), to Henkel Co.
- [35] R.W. Broadbent, *US Patent* 5,080,937 (14 January 1992), to Henkel Co.

- [36] B.M. Ahmed, R.W. Broadbent, US Patent 5,342,694 (30 August 1994), to Henkel Co.
- [37] W.S. Hall, US Patent 5,352,726 (4 October 1994), to Henkel Co.
- [38] B.M. Ahmed, US Patent 5,385,758 (31 January 1995), to Henkel Co.
- [39] O.E. Roberto, M.A. Maxim, US Patent 5,486,414 (23 January 1996), to Henkel Co.
- [40] B.M. Ahmed, R.M. Jayasuriya, T.R. Hopkins, US Patent 5,500,460 (19 March 1996), to Henkel Co.
- [41] Henkel AG & Co. KGaA, Dürr AG, *Metal Finishing* 2 (2009) 67
- [42] M. Dornbusch, DE 10 2005 023 728 A1 (23 May 2005) to BASF Coating GmbH
- [43] M. Dornbusch, A. Wiesmann, R. Wegner, DE 10 2005 023 729 A1 (23 May 2005) to BASF Coating GmbH
- [44] M. Dornbusch, E. Austrup, H. Hintze-Bruening, DE 10 2006 053 291 A1 (13 November 2006) to BASF Coating GmbH
- [45] M. Dornbusch, A. Wiesmann, DE 10 2006 053 292 A1 (13 November 2006) to BASF Coating GmbH
- [46] M. Dornbusch, A. Wiesmann, H. Hintze-Bruening, WO 2008/058586 A2 (22 May 2008) to BASF Coating GmbH
- [47] M. Dornbusch, A. Wiesmann, WO 2008/058587 A1 (22 May 2008) to BASF Coating GmbH
- [48] E. Almeida, I. Alves, C. Brites, L. Fedrizzi, *Prog. Org. Coat.* 46 (2003) 8
- [49] B. Pfeiffer, J.W. Schultze, *J. Appl. Electrochem.* 21 (1991) 877
- [50] Zh. I. Bepalova, L.G. Miroshnichenko, Yu.A. Lovpache, Yu.D. Kudryavtsev, *Russ. J. Appl. Chem.* 77 (2004) 1888
- [51] S. Balova, M. Christov, *Corr. Sci.* 41 (1999) 1633
- [52] N. Müller, Einfluss von Bad- und Substratkomponenten auf die Bildung von Phosphatschichten, Dissertation, Universität Düsseldorf (2000)
- [53] Interview BASF Coatings GmbH, Münster

3.3 Polymer design for grain boundary application

3.3.1 Fundamentals

3.3.1.1 Requirements and characteristics of the polymer of choice

In the previous section a survey on materials for selective application on grain boundaries was provided. It was found that among different techniques polymer particle deposition was the most promising in terms of disablement of the corrosion activity of natural substrate defects such as grain boundaries and alloy segregations. Therefore the need to find a polymeric coating material which is highly selective for such surface heterogeneities is present. Considering the use of this polymeric material as an environmentally friendly pretreatment, it must be water borne without any volatile organic compounds (VOC) and it must in the first instance, easily produced on an industrial scale. Polymers based in water can exist in two main physical systems; in a molecular solution where the entire hydrophilic polymer molecule is dissolved in water and in a physical system where water borne polymers is a dispersion obtained either by emulsion polymerization or by dispersing a solvent borne polymer solution into the water. In the first case the monomers are emulsified with a surfactant in water into small droplets. The polymerization then occurs within the droplets and the resulting dispersion is stabilized by the amphiphilic surfactant. In this case the terminology "latex" is frequently used, the most relevant of which are the styrene-co-polymers established since the 1950s for use in coatings and adhesives. In the second case, the polymer is synthesized in organic solvents and has preferably integrated functionalities able to make the ionic solubilizing such as carboxylic acids or amines. In the stripping process the organic solvent is removed from the

system and the simultaneous addition of water and the counterpart for the ionic solubilizing results in a water dispersed polymer. Nevertheless in terms of corrosion protection it seems to be a double play of the appropriate balance of hydrophilic and hydrophobic properties within one polymeric molecule [1,2]. While the hydrophilic part of the polymer chain is interacting with the metal/oxide surface, the hydrophobic part is establishing a barrier for oxygen, water and electrolytes. Bringing in more hydrophilic functionality than is necessary for covering and adhesion to the metal/oxide surface will lead to a higher hydrophilicity within the polymer layer and therefore decrease the barrier properties. The amphiphilic surfactant in dispersions also behaves in the same way and can be counterproductive to corrosion protection.

In the material survey of the last chapter it was found that dispersions are more precise in selective depositions on small structures such as grain boundaries rather than soluble polymer systems. Primary anionically stabilized dispersions also showed a better stability over a broad pH range, where the low pH regions are especially of importance as the anodic dissolution of the grain boundaries on HDG at a low pH will be used to precipitate the polymer particles. The mechanism of the local autophoretical precipitation of polymer particles on grain boundaries will be discussed in section 3.4. For the selective deposition the synthesis of the polymer should allow the incorporation of functional groups that strongly react with the dissolved cations from the grain boundaries and with the specific surface chemistry of the substrate when deposited.

Based on these requirements and characteristics of the polymer of choice as outlined in some literature, discussed synthetic approaches for the synthesis of block-co-polymers will be evaluated towards primary, anionically stabilized and surfactant free polymer dispersion in the following part of this section. This synthesis route should allow a broad variation of functional monomers to be incorporated in a fast and easy manufacturing process.

3.3.1.2 Synthesis of block-co-polymers

Functional block-co-polymers, due to the development of new polymerization techniques and the preparation of a wide range of new polymeric materials have

found in the last decade a broad field of applications such as surfactants, lubricants, adhesives, additives, thermoplastic elastomers, as well as biomedical and electronic applications [3-7]. When considering polymerization techniques there are two major routes to such multifunctional polymers; the living anionic polymerization and the controlled radical polymerization which in corresponding literature is often described as the controlled living radical polymerization (CLRP) [8]. Living anionic polymerization offers high levels of control in terms of well-defined polymers and precise molecular architectures, but the process is much less flexible than radical polymerization as it is very sensitive to monomer functionalities and impurities [9]. The difficulties in handling the anionic polymerization process make it unusable for industrial production processes. Radical polymerization on the other hand is of enormous industrial importance. It is easy to handle, tolerant to impurities, compatible with water and a huge variety of functional monomers and thus it can be implemented in an industrial plant. Approximately 50% of all commercial polymers are produced by radical polymerization. The major drawback of radical polymerization is that it is not possible to prepare block-co-polymers or polymers of narrow molecular weight distributions due to the high reactivity of the propagating radicals and their affinity to undergo bimolecular termination, transfer and other side reactions. The lifetime of a propagating radical is typically less than one second and chains are continuously initiated throughout the polymerization [10]. The combination of the robustness of the radical polymerization with the controllability offered by living ionic polymerization was found in controlled radical polymerization (CRP). The three most important ways to apply CRP as discussed in literature are the nitroxide mediated radical polymerization (NMP) [11-13], the atom transfer radical polymerization (ATRP) [15-17] and the reversible addition fragmentation chain transfer polymerization (RAFT) [18-22]. Evaluating these techniques for the stated anti-corrosion application purpose in the requirements and characteristics for the polymer of choice these major three techniques fail due to provide different reasons. The ideal block-co-polymer would be non-conventional, water borne, easy to functionalize, surfactant free and it would be obtained through a straight forward polymerization.

One of the major disadvantages of all three of these polymerization techniques is their poor applicability in a straight forward polymerization in water. In all cases, as known from classical emulsion polymerization, surfactants have to be used.

RAFT and ATRP agents are also sensitive to aqueous solution. RAFT is one of the CRP techniques most described in literature and the number of papers describing RAFT in aqueous dispersed systems is increasing rapidly. The stability of the RAFT agent 'dithiocarbonyl derivatives' in water is however poor [23,24]. Depending on the experimental conditions the hydrolysis of the dithiocarbonyl species may be significant as the rate of hydrolysis is dependent on the pH parameters and temperature when in the aqueous phase [25,26]. In the ATRP process, transition metal compounds mostly based on copper are used as the control reagent. Most of the Cu-complex ligands are employed in bulk or solution and are highly water soluble which leads to partitioning and deactivation of the controlling agent [27-30]. Even though a series of hydrophobic ATRP agents have been developed Cu(I) and Cu(II), reaction with water would occur only with the loss of their controlling functionality [31].

However, a multitude of other CRP techniques exist, Bremser et al. for example developed the DPE method using 1,1-diphenylethene as a control agent [32-34]. It was found that conventional radical polymerizations become controllable when a small amount of 1,1-diphenylethene (DPE) is added. Even though the DPE route does not provide the high control and livingness known from the typical controlled radical polymerizations as stated above, it allows a build up of block-co-polymers in the water phase without the use of any surfactants [35]. This makes the DPE method a very interesting alternative to the other methods if the block co-polymer formation only has the goal of controlling free radical polymerizations. In this sense it is the only technique based entirely on hydrocarbons, where no other ingredients such as halides, nitroxides or metal ions are needed. Moreover, it can be easily adapted on an industrial scale [36,37]. The mechanistic investigation of the block-co-polymer formation in the presence of DPE was thoroughly investigated by Viala et al [38-40]. It was found that the DPE route is basically a two-step procedure requiring in the first step, the preparation of a precursor polymer in the presence of DPE. This precursor polymer is then used as the active species in a second polymerization, where block co-polymer formation takes place. The activity of the precursor polymer is based on its unique semiquinoid structure where the α,p -dimer is formed by the combined termination of two DPE-ended radical chains. The two-step procedure can be carried out either as a one-pot reaction with consecutive monomer

additions or spatially and timely separated. The two-step, one-pot procedure is especially interesting from an economic perspective as it allows the adaptation of the widely used semi-batch feeding procedures and it is practical for the requirements of this study. So far the DPE route to functional block-co-polymers is described only for a small variety of monomers such as Methyl Methacrylate (MMA), Acrylic Acid (AA), Styrene (St) [38] and Vinyl Acetate (VAc) [41]. In this chapter the DPE technique will be introduced to a broader variety of functional monomers such as Vinylphosphonic Acid (VPA), Triethoxyvilsilane (TEVS) and Maleic Acid (MA) which are suited to all requested characteristics of the block-co-polymer and its polymerization process as stated in section 3.3.1.1: Requirements and Characteristics to the Polymer of Choice.

3.3.1.3 Mechanistic understanding of the block-co-polymer formation in the presence of DPE

The mechanism for the DPE route to functional block-co-polymers in the following is derived from Viala et al. As proposed, the synthesis is undergoing a two-step process in a one-pot synthesis. In the first step the hydrophilic monomers polymerize until the active end of a growing chain runs into the 1,1-diphenylethylene molecule which then stabilizes the radical and stops the growth of a chain while the radical remains alive as shown in *Fig. 3.28*.

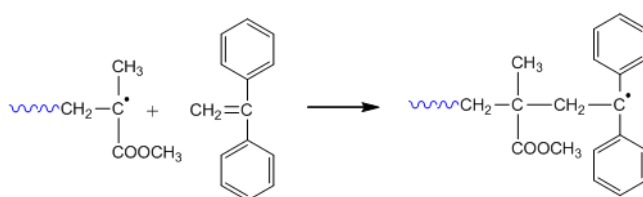


Fig. 3.28: Trapping of a growing polymer chain by DPE.

The stabilized radical is inactive to participate in further polymerization reactions and recombines with a second species of itself into a semiquinoid structure as shown in *Fig. 3.29*. The pre-polymer consisting of two hydrophilic blocks is forming a hetero phase system in the water. It can be isolated and reaches a molecular weight of 1.000 g/mol to 3.000 g/mol.

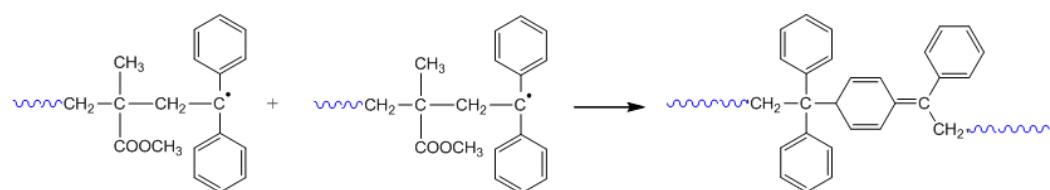


Fig. 3.29: Stabilizing the radical by recombination of two DPE ended chains to a semiquinoid structure.

For the one-pot synthesis the pre-polymer will be left in the reactor. After raising the temperature to 90°C the monomers for the second, hydrophobic block are added to the batch and then get polymerized by the residual initiator. The rise in temperature destabilizes the semiquinoid structure of the pre-polymer. The newly created and propagating hydrophobic polymer chain runs into the destabilized semiquinoid structure of the pre-polymer and forms the block-co-polymer as shown in Fig. 3.30.

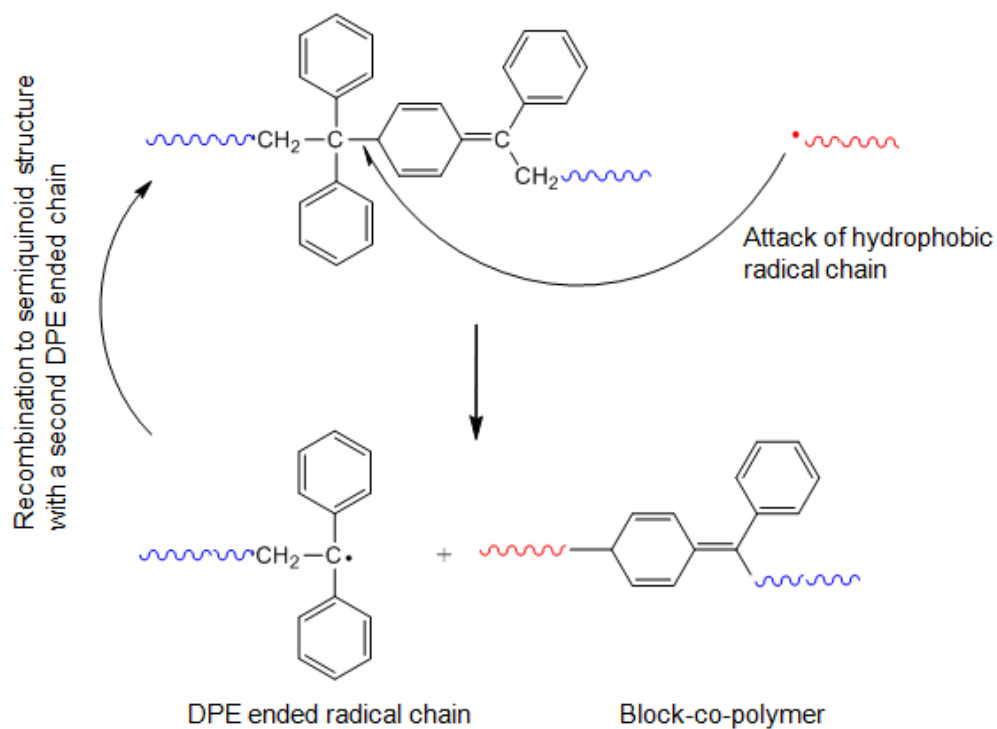


Fig. 3.30: Formation of the block-co-polymer.

Throughout the whole process there is no need for external emulsifiers. The hydrophilic blocks of the block-co-polymers are intrinsically stabilizing the dispersion particles in the water. An example of a resulting block-co-polymer dispersion is shown by a SEM image in *Fig. 3.31*. The typical particle sizes obtained ranged between 40 and 200 nm by varying the monomer compositions.

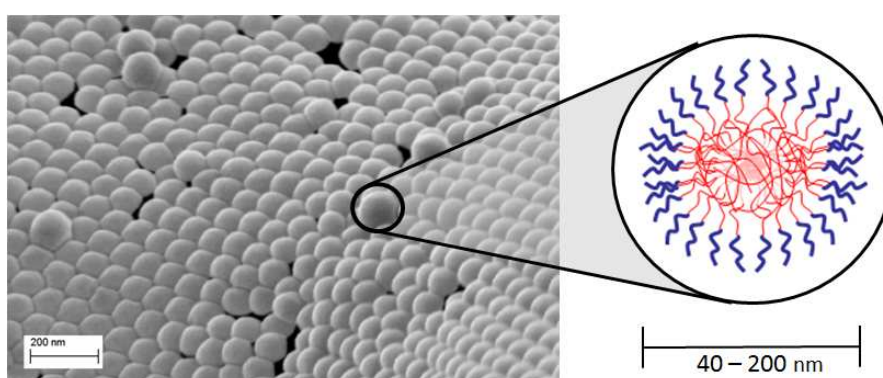


Fig. 3.31: SEM image of the block-co-polymer dispersion obtained via the DPE route containing Vinylphosphonic Acid (VPA) and a scheme of the block-co-polymer aggregated particle.

In this study the use of a broad variety of functional monomers such as Vinylphosphonic Acid (VPA), Triethoxyvinylsilane (TEVS) and Maleic Acid (MA) were successfully introduced to the block-co-polymer synthesis via the DPE method. The monomers in this study were chosen as a result of their specific and well known functionality to interact with inorganic surfaces such as zinc/zinc oxide and aluminum/aluminum oxide. The screening of the adequate monomers in terms of adhesion to these specific surfaces was carried out and reported in a previous publication [42]. Molecules with anchoring groups such as phosphonic acid, carboxylic acid or silane were found to be very good at adsorbing to metal oxide surfaces. It is also very well-known through literature that these functionalities form strong bonds with metal oxides and are used for example, to produce self-assembled monolayers that protect steel from corrosion and

increase adherence of coatings or adhesive bonding [43]. Below, the results obtained by the incorporation of these functionalities into block-co-polymers in the aqueous phase will be reported.

3.3.2 Experimental procedures

3.3.2.1 Materials

All reagents were used without further purification. Methyl Methacrylic Acid (MMA, 99%), Butylmethacrylate (BMA, 99%), Hydroxyethylmethacrylate (HEMA, 98%), 1,1-diphenylethylene (DPE, 97%), Ammonium Persulfate ($(\text{NH}_4)_2\text{S}_2\text{O}_8$, 98%), Maleic Acid (MA, 99%) and Triethoxyvinylsilane (TEVS, 97%) were purchased from the Aldrich Chemical Co. Vinylphosphonic Acid (VPA, 97%) was donated by BASF SE.

3.3.2.2 Synthesis of functional block-co-polymers in a hetero phase system

A two liter glass reactor equipped with an anchor stirrer was filled with 770g of deionized water, 2.1g DPE and the monomers for the hydrophilic block of the block-co-polymer 25g MMA and 25g of one of the anchoring groups containing monomers MA or VPA. Under a flow of nitrogen the reactor was heated to 70°C and held at that temperature for 60 minutes at which point the initiator solution of 3.1g $(\text{NH}_4)_2\text{S}_2\text{O}_8$ in 67g H_2O was dropped into the reactor for further 30 minutes. The reactor temperature was maintained at 70°C and raised to 90°C after 2 hours when the addition of the monomers for the hydrophobic block of the block-co-polymer started. The solution of 250g BMA and 12.5g HEMA and in the case of DPE-TEVS block-co-polymers Triethoxyvinylsilane was also added into the reactor for a duration of 2 hours and the temperature of 90°C was kept for a further 2 hours in order to complete the conversion of the monomers.

3.3.3 Experimental results

3.3.3.1 Overview of synthesized block-co-polymers

Based on the results of the screening experiments for polymerizable monomers and their ability to adsorb to metal oxide surfaces such as zinc oxide or aluminum oxide in the preliminary of this study, a selection of these monomers were chosen to be incorporated into the block-co-polymer dispersion within this section [42]. Variations of the functionalities in the block-co-polymer chains are shown in *Fig. 3.32*.

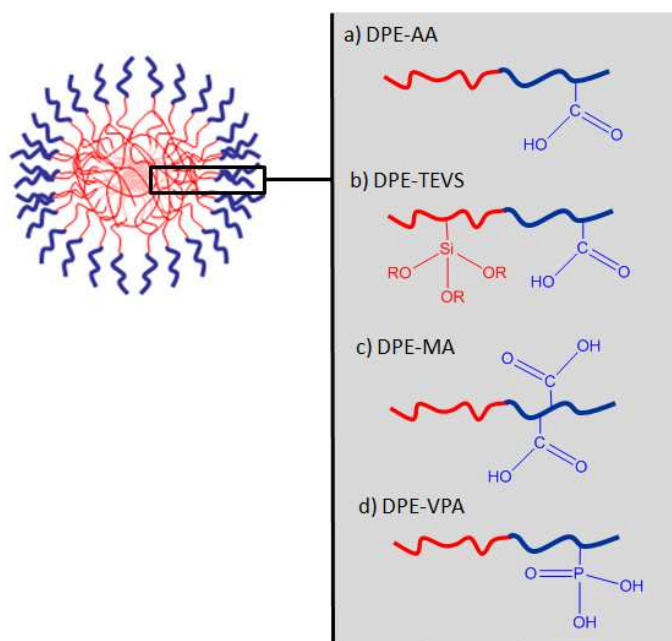


Fig. 3.32: Functionalities incorporated into the hydrophilic and hydrophobic region of the block-co-polymer. Red (left) indicates the hydrophobic block, blue (right) indicates the hydrophilic block.

Carboxylic acid is quite often described as a good adhesion promoter on aluminum oxide surfaces [44,45]. This finding could also be obtained in the previous screening experiments. In this study the carboxylic function will be incorporated into the block-co-polymer by acrylic acid (AA) and maleic acid (MA). It was also found that triethoxyvinylsilane is a good adsorbate. The last monomer of choice with promising adhesion properties, as found in the adsorption experiments is vinylphosphonic acid. Block-co-polymer dispersions with four different functionalities could be obtained via the one-pot-two-step-DPE-route. One must consider that each block of the polymer contains some basic monomer compositions which remain the same through all variations. These are for the hydrophilic block MMA and for the hydrophobic block HEMA and BMA. MMA was copolymerized in the hydrophilic block in order to reduce or adjust the hydrophilicity of the block-co-polymer in the way that the block-co-polymers are able to form stable micelles. Creating the first block out of a hydrophilic monomer such as acrylic acid only, will lead to a polymer solution in water in the first step and to a fall out of the polymer in the second step. With this method no stable micelles could be obtained. Triethoxyvinylsilane is barely soluble in water; it is rather hydrophobic but still remains a good adhesion promoter to polar materials. By establishing chemical bonding to such oxidic surfaces, it cleaves the organic alcohol and obtains a polar anchoring group. Therefore TEVS could only successfully be incorporated into the block-co-polymer in the second step where the hydrophobic block is created. Due to stabilization issues in the first block acrylic acid had to be added.

3.3.3.2 GPC and particle size observations

The molecular weight build up during the one-pot-two-step polymerization routine was detected by GPC. *Fig. 3.33* shows the molecular weight distribution after the first block is created and after the block-co-polymer was formed with the example of DPE-VPA(4.5%).

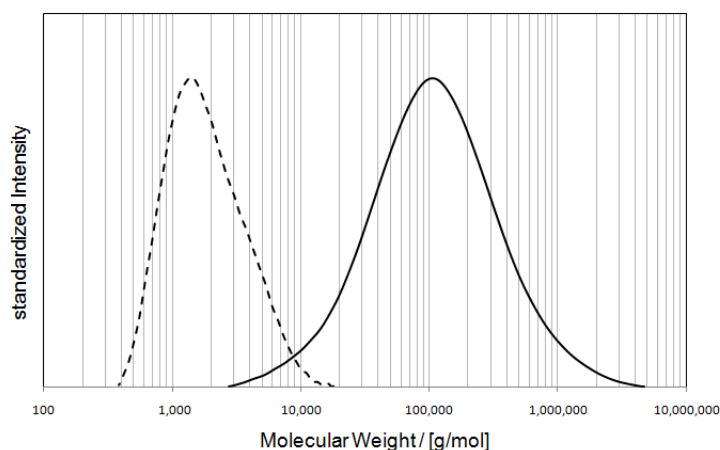


Fig. 3.33: Molecular weight distribution of the hydrophilic di-block (dashed line) and of the block-co-polymer (solid line) on the example of DPE-VPA(4.5%). The measurements were obtained in THF at 25°C. The molecular weight was calculated in respect to narrow polydispersity polystyrene standards.

The stepwise growth of the block-co-polymer was tracked by their molecular weight. The smaller peak in *Fig. 3.33* shows the molecular weight distribution of the hydrophilic di-block obtained after the first step in the polymerization process. According to the mechanism of the reaction process, one hydrophilic block is connected to a second hydrophilic block via two DPE units also known as the semiquinoid structure. This number would thus have to be divided in two in order to estimate the molecular weight distribution for single hydrophilic blocks. The second peak at the higher molecular weight values is obtained through the complete block-co-polymer. Based on this procedure the molecular weights M_n , M_w and its Polydispersity D , as well as the resulted dispersion particle sizes of the synthesized block-co-polymer dispersions were analyzed (see *Tab. 3.1*). The percentage indication in the labels of the polymer dispersions specify them by the solid content of the functional monomer based on the solid polymer. E.g. in DPE-AA(6.2%) from all monomer weights 6.2 % are acrylic acid. In the case of the DPE-VPA the vinylphosphonic content varied from 1.3 to 8.2%.

Tab. 3.1: Molecular weights M_n , M_w , and its polydispersity D resulted from GPC experiments. The measurements were carried out in THF at 25°C and calculated on polystyrene with narrow polydispersity. The particle sizes are obtained via light scattering.

	Molecular Weight				Polydispersity		Particle Size	
	Mn [g/mol] Block AA	Mn [g/mol] Block AB	Mw [g/mol] Block AA	Mw [g/mol] Block AB	D (Block AA)	D (Block AB)	d [nm] (Block AA)	d [nm] (Block AB)
a) DPE-AA (6,2%)	1.6×10^3	2.3×10^4	2.1×10^3	1.1×10^5	1.3	4.8	362	84
b) DPE-TEVS (4,5%)	--	--	--	--	--	--	--	42
c) DPE-MA (4,5%)	1.9×10^3	1.8×10^4	2.9×10^3	1.0×10^5	1.5	5.8	482	63
d ₁) DPE-VPA (1,3%)	1.6×10^3	5.3×10^4	2.1×10^3	3.7×10^5	1.3	6.9	403	229
d ₂) DPE-VPA (4,5%)	1.5×10^3	7.0×10^4	1.9×10^3	3.7×10^5	1.2	5.3	331	101
d ₃) DPE-VPA (8,2%)	1.6×10^3	2.4×10^4	2.0×10^3	1.5×10^5	1.3	6.3	376	150

Based on the results shown in Tab. 3.1, molecular weights (M_n) for the hydrophilic di-block range from 1.5×10^3 to 1.9×10^3 g/mol in all batches. When the block-co-polymer synthesis is finished, molecular weights (M_n) rise to 1.8×10^4 to 7.0×10^4 g/mol. The polydispersities D (M_w/M_n) show rather narrow molecular weight distributions in the pre-polymer obtained in the first step but quite broad molecular weight distributions in the final block-co-polymer. The first block is certainly a very short chain polymer with a high hydrophilicity. The second block due to a great number of monomers must be polymerized and shows more clearly the molecular weight distribution which is typical for the radical polymerization process. These observations support the assumptions on radical polymerization that were made in the literature survey of this chapter. But even though the molecular weight is broadly scattered, the obtained particle sizes are quite narrowly distributed, as shown in Fig. 3.31. At the same time the particle sizes can vary on a wide range along the nanometer scale with different monomer compositions. From Tab. 3.1 there is no correlation that can be derived between the molecular weight and the final particle size of the dispersion. The particle size variation obtained was from 40 to 230 nm. Reproductions of batches always resulted in similar numbers for the particle sizes. These findings imply the monomer composition and its ability to form and stabilize the particle micelle must be responsible for the final particle size. In all cases it can be observed that

the pre-polymer formed in step one has much higher particle sizes than the final block-co-polymer. This is probably due to the high hydrophilicity of the hydrophilic di-block and its less dense agglomerated structure. The hydrophobic core creates the dense particle stabilized by a hydrophilic shell.

3.3.3.3 Conversion ratios of the monomers

Conversion ratios can be easily calculated from solids. The weight ratio of the monomers, DPE and Initiator to water that have been weighed and added into the polymerization reactor, should be equal to the weight ratio of the resulting polymer to its water phase in the dispersion, the solids. All theoretical and experimental solid ratios are shown in *Tab. 3.2*.

Tab. 3.2: Theoretical and experimental solids of the polymer dispersion and their calculated conversion ratios

	Solids		Conversion (based on Solids)
	Theoretical Solids [%]	Experimental Solids [%]	Solid Ratio [%]
a) DPE-AA(6.2%)	26.8	25.4	94.8
b) DPE-TEVS(4.5%)	28.4	26.4	92.9
c) DPE-MA(4.5%)	26.3	25.7	97.7
d ₁) DPE-VPA(1.3%)	26.8	25.9	96.6
d ₂) DPE-VPA(4.5%)	26.8	25.3	94.4
d ₃) DPE-VPA(8.2%)	26.8	24.3	90.6

The weight difference can be attributed to the residual monomers in the polymer dispersion. Across all cases, the calculated conversion ratios have not reached 100%. The best conversions were obtained for c)DPE-MA with the solid ratio of 97.7 % and for d₁)DPE-VPA with the solid ratio of 96.6 %. The worst conversion ratios were obtained for b)DPE-TEVS with the solid ratio of 92.2 % and for d₃)DPE-VPA with the solid ratio of 90.6 %. In any case experimental solids were performed by evaporating water and all volatile compounds from 1 g of the

dispersion at 130°C for 2 hours at atmosphere pressure. However most of the monomers such as TEVS, AA, BMA and HEMA are highly volatile and evaporate, making the experimental solids technique reasonable. The high volatility of such monomers also leads to a loss of these monomers by continuously purging the reactor with a nitrogen flux. Monomers such as VPA with a boiling point of around 200°C would probably remain in the sample even if they had not reacted and falsify the result. On the other hand the DPE-VPA with the highest VPA content shows the lowest conversion ratio. The overall block-co-polymer yields of more than 90% are consistent with experimental findings from Viala et al [38]. Therefore a number of polymer dispersions b)DPE-TEVS, d₁)DPE-VPA, and d₂)DPE-VPA were analyzed for their residual monomers (see *Tab. 3.3*). The experimental procedure was performed with Gas Chromatography (GC) by BASF Coatings GmbH. The most interesting findings can be derived from the residual monomeric VPA content of the corresponding dispersions. This data shows that only small amounts of VPA can be copolymerized by this synthesis route.

Tab. 3.3: Residual monomers in polymer dispersions after block-co-polymer formation. Data obtained with Gas Chromatography by BASF Coatings GmbH.

	Residual Monomers after Polymerization in w.-%					
	TEVS	AA	VPA	BMA	MMA	HEMA
b)DPE-TEVS(4.5%)	not detectable (< 0.03 w.-%)	not detectable (< 0.07 w.-%)	--	0.5	not detectable (< 0.01 w.-%)	< 0.1
d ₁)DPE-VPA(1.3%)	--	--	0.2	0.2	not detectable (< 0.01 w.-%)	not detectable (< 0.03 w.-%)
d ₂)DPE-VPA(4.5%)	--	--	1.0	0.6	< 0.1	not detectable (< 0.03 w.-%)

These observations become clearer when correlating the added VPA monomers to the synthesis of the copolymerized VPA monomer and the residual VPA monomers as illustrated in *Fig. 3.34*.

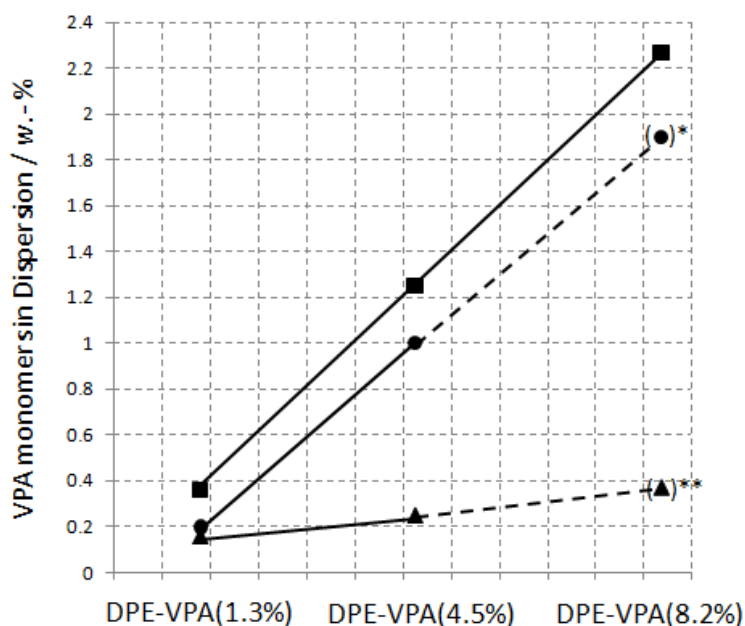


Fig. 3.34: Correlation of VPA residual monomer (●), VPA monomer co-polymerized (▲) on the weigh percentage of VPA monomer added to the synthesis batch (■). *Value for residual monomer estimated from the experimental ratios. ** Calculated from residual monomer.

E.g. in the d₁) DPE-VPA dispersion the residual VPA monomer in the dispersion is 0.2 w.-% from 0.36 w.-% added to the synthesis batch only 0.16 w.-% can be polymerized and incorporated into the block-co-polymer. Calculated on the solid block-co-polymer, the incorporated VPA would only be 0.6 %. For the solid d₂)DPE-VPA(4.5%) the VPA content polymerized into the block-co-polymer can be calculated at 1.0%. For the solid d₃)DPE-VPA(8.2%) the VPA content can be estimated only through the correlation of the two experimental results to 1.5%. The derivation can thus be conclusively made that the polymerization of VPA is limited, even though providing the system with an excess of VPA does not result in significantly higher VPA content in the polymer. Connecting these results with the solid ratios, one could also estimate that the higher VPA content may also inhibit the polymerization of other monomers, as the highest VPA content results gave the lowest overall yield. BMA is the only one of the other monomers that could be detected in the experiment as significantly present. BMA has the highest weight proportion (20% on dispersion) in the synthesis recipes of monomer

compositions. The aim in this section was to incorporate special functionalities such as phosphonic acid into the block-co-polymer. Among other functional monomers VPA was chosen for its ability to establish a strong bond to aluminum oxide surfaces and its strong complexing ability with aluminum cations (chapter 1). However residual monomers in dispersion could be distracting to the selective application of polymer particles on grain boundaries in two different ways. They could and preferably do, adsorb onto the metal oxide surface and terminate it. Because of their small size, monomers should have higher mobility and thus reach these active adsorption points before the polymer particles. The second negative influence of the monomers could occur when they complex the released cations of the grain boundary. These cations would then no longer be available for complexing the phosphonic acid groups incorporated into block-co-polymer chains. This would result in less effective precipitation of polymer particles on the grain boundaries. The precipitation activity on aluminum and zinc oxides as well as on grain boundaries of HDG steel will be investigated in the following section of this study.

3.3.3.4 Dispersion stability

The long-term stability of dispersion was found to be rather high and thus particle sizes were measured over a period of one year as shown in *Tab. 3.4*.

Tab. 3.4: Particle sizes of dispersions over one year period.

	Particle Size d [nm]					
	Initial	2 Weeks	1 Month	3 Month	6 Month	1 Year
a) DPE-AA(6.2%)	84	79	82	84	82	82
b) DPE-TEVS(4.5%)	42	42	43	42	41	42
c) DPE-MA(4.5%)	63	62	62	63	65	64
d ₁) DPE-VPA(1.3%)	229	227	227	230	227	228
d ₂) DPE-VPA(4.5%)	101	101	101	102	102	99
d ₃) DPE-VPA(8.2%)	150	153	152	153	152	152

It was found that particle sizes did not change significantly over time. There was also no significant settling observed during this period. The high stability of dispersion can mainly be attributed to its narrow particle size distribution. As the particle sizes are similar to each other no “Ostwald-Ripening” can occur and dispersion thus remains stable.

3.3.4 Conclusion

The aim of this part of the study was to synthesize water borne block-co-polymer dispersions with specific functionalities. In line with this aim, it was found that the DPE route to obtain such polymers can be provided in water without any use of surfactants. The one-pot-two-step polymerization routine could easily be adapted to new monomer compositions. Co-polymerization of monomers such as maleic acid (MA), triethoxyvinylsilane (TEVS), and vinylphosphonic acid (VPA) could be introduced to the above described block-co-polymerization procedure. The specific functionality of MA, TEVS and VPA in previous experiments was found to provide good adhesion to metal/metal oxide substrates as a result of its ability to establish strong chemical bonds. These functionalities will also be used for their good complexing abilities of aluminum cations. In the case of VPA only small amounts of the monomer could be co-polymerized. Residual VPA monomers could therefore negatively influence the selective deposition of the corresponding block-co-polymer dispersions. The dispersion particle sizes were obtained in a range from 40 to 230 nm. Even though the molecular weight distribution of each batch was found to be significantly broad, the particle sizes showed a narrow size distribution. The long-term stability of the block-co-polymer dispersions can also be attributed to this phenomenon of narrow particle size distribution. The polymer dispersions obtained in this part of the study will be introduced to the selective application on grain boundaries of hot dipped galvanized steel in the next section of this study.

3.3.5 References

- [1] W.J. Soer, W.H. Ming, C.E. Koning, R.A.T.M. van Benthem, *Prog. Org. Coat.* 61 (2008) 224
- [2] W. J. Soer, Dissertation „Bridging adhesion with good barrier properties on function dispersions – Towards waterborne anti-corrosion coatings” Universiteit Eindhoven (2007)
- [3] Braunecker, W. A.; Matyjaszewski, K. *Prog. Polym. Sci.* 2007, 32, 93
- [4] Matyjaszewski, K. *Controlled/Living Radical Polymerization: From Synthesis to Materials*; Matyjaszewski, K., Ed.; ACS Symposium Series 944; American Chemical Society: Washington, DC, 2006
- [5] Matyjaszewski, K. In *Advances in Controlled/Living Radical Polymerization*; Matyjaszewski, K., Ed.; ACS Symposium Series 854; American Chemical Society: Washington, DC, 2003; p 2
- [6] Davis, K. A.; Matyjaszewski, K. *Adv. Polym. Sci.* 2002, 159
- [7] Matyjaszewski, K. *Prog. Polym. Sci.* 2005, 30, 858
- [8] P.B. Zetterlund, Y. Kagawa, M. Okubo, *Chem. Rev.* 108 (2008) 3747
- [9] M. Szwarc, M. Levy, R.J. Milkovich, *J. Am. Chem. Soc.* 78 (1956) 2656.
- [8] A. Goto, T. Fukuda, *Prog. Polym. Sci.* 29 (2004) 329
- [10] C.J. Hawker, A.W. Bosman, E. Harth, *Chem. Rev.* 101 (2001) 3661
- [12] M.K. Georges, R.P.N. Veregin, P.M. Kazmaier, G.K. Hamer, *Macromolecules* 26 (1993) 2987
- [13] D.H. Solomon, E. Rizzardo, P.U.S. Cacioli, U.S. Patent 4, (1986)
- [14] M. Kamigaito, T. Ando, M. Sawamoto, *Chem. Rev.* 101 (2001) 3689
- [15] K. Matyjaszewski, J. Xia, *Chem. Rev.* 101 (2001) 2921
- [16] M. Kato, M. Kamigaito, M. Sawamoto, T. Higashimura, *Macromolecules* 28 (1995) 1721
- [17] J.S. Wang, K. Matyjaszewski, *J. Am. Chem. Soc.* 117 (1995) 5614
- [18] G. Moad, E. Rizzardo, S.H. Thang, *Aust. J. Chem.* 58 (2005) 379
- [19] S. Perrier, P. Takolpuckdee, *J. Polym. Sci., Part A: Polym. Chem.* 43 (2005) 5347
- [20] G. Moad, E. Rizzardo, S.H. Thang, *Aust. J. Chem.* 59 (2006) 669

- [21] C. Barner-Kowollik, M. Buback, B. Charleux, M.L. Coote, M. Drache, T. Fukuda, A. Goto, B. Klumperman, A.B. Lowe, J.B. McLeary, G. Moad, M.J. Monteiro, R.D. Sanderson, M.P. Tonge, P. Vana, J. Polym. Sci., Part A: Polym. Chem. 44 (2006) 5809
- [22] J. Chiefari, Y.K. Chong, F. Ercole, J. Krstina, J. Jeffery, T.P.T. Le, R.T.A. Mayadunne, G.F. Meijs, C.L. Moad, G. Moad, E. Rizzardo, S.H. Thang, Macromolecules 31 (1998) 5559
- [23] J. Loiseau, N. Doerr, J.M. Suau, J.B. Egraz, M.F. Ilauro, C. Ladaviere, J. Claverie, Macromolecules 36 (2003) 3066
- [24] S.W. Prescott, M.J. Ballard, E. Rizzardo, R.G. Gilbert, Macromolecules 35 (2002) 5417
- [25] J.F. Baussard, J.L. Habib-Jiwan, A. Laschewsky, M. Mertoglu, J. Storsberg, Polymer 45 (2004) 3615
- [26] C.L. McCormick, A.B. Lowe, Acc. Chem. Res. 37 (2004) 312
- [27] M. Li, K. Matyjaszewski, Macromolecules 37 (2004) 2106
- [28] S.G. Gaynor, J. Qiu, K. Matyjaszewski, Macromolecules 31 (1998) 5951
- [29] K. Matyjaszewski, J. Qiu, D.A. Shipp, S.G. Gaynor, Macromol. Symp. 155 (2000) 15
- [30] H. Gao, K. Min, K. Matyjaszewski, Macromol. Chem. Phys. 207 (2006) 1709
- [31] J. Qiu, T. Pintauer, S.G. Gaynor, K. Matyjaszewski, B. Charleux, J.-P. Vairon, Macromolecules 33 (2000) 7310
- [32] W. Bremser, F. Strickmann, M. Bendix, W. Paulus, R.B. Raether, D.I. Christie, PAT: WO 2000037507 A1, BASF Coatings AG, 2000
- [33] M. Bendix, R. Clauss, R. Nickolaus, W. Bremser, PAT: WO 2001042310 A2, BASF Coatings AG, 2001
- [34] M. Bendix, W. Bremser, D. Christie, PAT: WO 2001042311 A1, BASF Coatings AG, 2001
- [35] W. Bremser, B. Raether, Prog Org Coat 45 (2002) 95
- [36] R. Clauss, W. Bremser, M. Bendix, M. Antonietti, PAT: WO 2001042379 (2001)
- [37] P.C. Wieland, N. Stoeckel, O. Nuyken, J Macromol Sci, Pure Appl Chem A40 (2003) 11
- [38] S. Viala, K. Tauer, M. Antonietti, R.-P. Krüger, W. Bremser, Polymer 43 (2002) 7231
- [39] S. Viala, M. Antonietti, K. Tauer, W. Bremser, Polymer 44 (2003) 1339

- [40] S. Viala, K. Tauer, M. Antonietti, I. Lacik, W. Bremser, *Polymer* 46 (2005) 7843
- [41] D. Chen, Y. Shi, Z. Fu, *J. Appl. Polym. Sci.* 111 (2009) 1581
- [42] S. Toews, Adsorption funktionaler Monomere an oxidischen Grenzflächen, Master Thesis, Universität Paderborn (2007)
- [43] M.-L. Abel, J.-F. Watts, *J. Adhes.* 80 (2004) 292
- [44] J. Wielant, R. Posner, G. Grundmeier, H. Terryn, *J. Phys. Chem. C* 112 (2008) 12951
- [45] W.J. Soer, W. Ming, C.E. Koning, R.A.T.M. van Benthem, J.M.C. Mol, H. Terryn, *Prog. Org. Coat.* 65 (2009) 94

3.4 Polymer application on grain boundaries

3.4.1 Fundamentals

3.4.1.1 Colloid stability

Within this section all findings from the previously conducted experiments will be combined into the approach of polymer particle dispersion deposition on grain boundaries of HDG steel. Therefore it is important to review the basics of particle or colloid stability. Further, it is even more important to focus on the controlled destabilization of such systems.

Dispersed particles are attracted to and approach one other due to attraction van der Waals and London forces [1,2]. Dispersed particles could coagulate without repulsive stabilization mechanisms. The three stabilization mechanisms one should consider are electrostatic, steric and electrosteric stabilization [3]. Electrostatic stabilization of colloids is described by the DLVO-theory and was developed simultaneously by Derjaguin and Landau as well as Verwey and Overbeek [4,5]. Within the DLVO-theory, dispersed particles can be seen as hard spheres bearing an electric charge. In the case of anionic polymer particles such as those obtained via the DPE dispersions in section 3.3, this charge is negative due to the co-polymerized anionic functionalities such as carboxylic or phosphonic acid. Negatively charged particles attract mobile positive charges from the bulk aqueous matrix resulting in an electrical double layer surrounding the particles. This charge cloud shields the particles from surface charge. The distribution of the positive counter ions in the surroundings of the particle is described by the Stern-Gouy-Chapman-theory in which the potential at the surface is dropped across two layers, a compact inner layer (Stern Layer) and a diffuse outer layer (Gouy Chapman Layer) as illustrated in *Fig. 3.35 [6]*. At the

shear plane between these two layers the ζ -potential is measurable. The shear plane separates the adherent counter ion layer (basically Stern layer) from the loose counter ion cloud which will not stick to the particle when it is in motion.

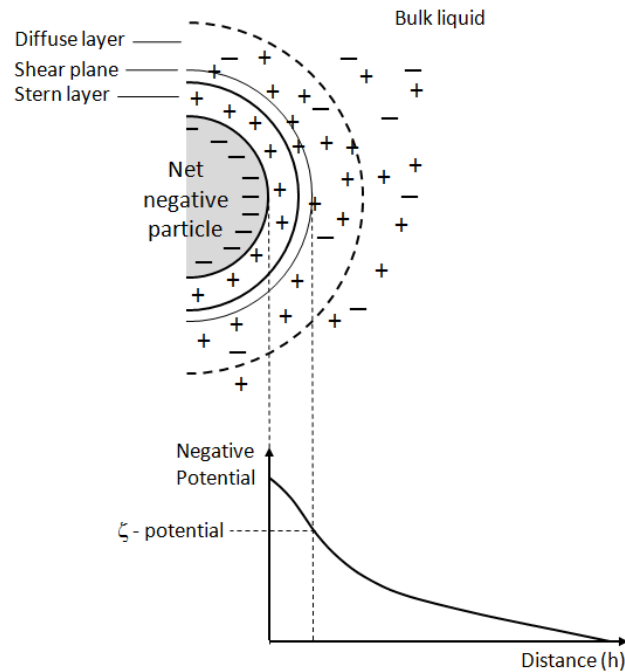


Fig. 3.35: Illustration of the distribution of electrical potential in the double-layer region surrounding a charged particle showing the zeta potential [6].

The DLVO-Theory is basically a linear addition to the total potential (V_T) of attractive and repulsive forces and expresses that dispersed particles are only stable when repulsive potential (V_R) dominates the attractive potential (V_A).

$$V_T = V_A + V_R \quad (3.1)$$

The total interaction potential curve for two electrostatic stabilized particles is illustrated in Fig. 3.36. When two particles approach each other their diffuse charge clouds will overlap and as they have the same charge, the clouds repulsive forces become dominant towards the attractive van der Waals forces hindering any further approach. This repulsion is expressed through the total

potential maximum. One must consider that the shape of the curve with regard to the maxima and minima is always dependent on the system.

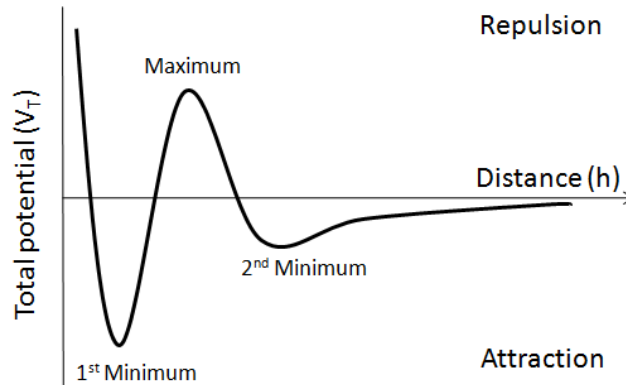


Fig. 3.36: Total interaction potential curve for two charge stabilized particles considering all possible potential maxima and minima in dependency of the distance according to the DLVO-theory [7].

The second minimum which leads to flocculation mostly appears under certain salt concentration only, where dispersions due to the maximum repulsion remain stable. At the same time, the thermodynamic drive of such stabilized systems is always towards the first minimum, where particles coagulate. The height of the total potential maximum determines the time period over which the dispersion remains stable. Addition of multivalent counter ions to the system will eliminate the maximum and drive the system directly into the first minimum where aggregation and coagulation occurs for each collision of two particles.

Electrostatic stabilization is dependent on the chemical environment such as the salt concentration, counter ion type and pH, while the ζ -potential can be used as an indicator for stability [8]. Counter ions are dominant in the Stern and diffuse layer. Their valency is therefore of major importance to particle stability. Multivalent ions can bridge the Stern layer of two particles and cause them to coagulate. (elimination of the total potential maximum), Schultze and Hardy derived an expression for the critical coagulation concentration (ccc) as dependent to the counter ion valency [9-11]:

$$ccc \sim \frac{1}{z^n} \quad (3.2)$$

In this equation z is the counter ion valency and n the exponent ranging between 2 and 6 dependent on the particle potential [8]. For example, aluminum counter ions would be 10 times more efficient in coagulation than sodium ions and 4 times more efficient than zinc ions considering the Schultz-Hardy-Equation with the lowest exponent of 2.

The ζ -potential is characteristic for the measurable charge density of a dispersed particle and can be adjusted by the pH. In general, a system is no longer electrostatically stabilized when the ζ -potential reaches the value of zero. In which case, there is no charge on the particle surface to provide repulsion forces. Experimental observations have shown that absolute values of ζ -potentials smaller than |20| mV can cause instability and coagulation of anionic stabilized dispersions [8]. In general it is suggested to maintain the ζ -potential above the absolute value of |30| mV [12].

In section 3.1 and 3.2 of this study it was found that aluminum ion dissolution from aluminum enriched grain boundaries could be of importance to the selective deposition of polymer particles on grain boundaries. Therefore both the counter ion type and pH required in order to dissolve the counter ions from the grain boundaries will be investigated within the experimental part of this chapter.

From the 1950s onwards, steric stabilization of dispersed particles has been described by a variety of scientists [13-17]. For this type of stabilization, freely moving polymer chains have to be adsorbed by one end to the particle surface [18,19]. The particles result in spherical polymer brushes (see *Fig. 3.37*).

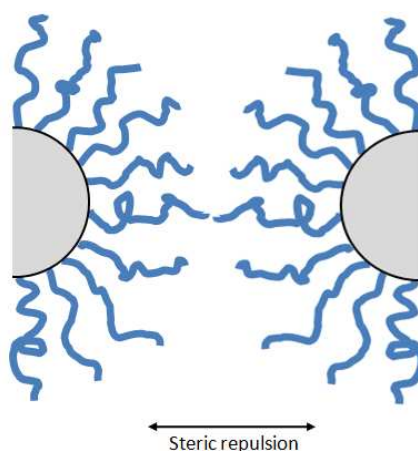


Fig.3.37: Illustration of particles with polymer brushes sterically hindered in their approach.

When two particles approach one another their polymer brushes start to interpenetrate. This interpenetration reduces the degree of freedom of polymer chains and therefore the entropy of the system. According to the Gibbs expression for free energy derived from the second law of thermodynamics ($\Delta G = \Delta H - T\Delta S$), a physicochemical process can only spontaneously follow in a certain direction when the free energy ΔG of that system becomes negative. The decrease of entropy ΔS at constant temperature T and constant free enthalpy ΔH would result in an increase in the free Gibbs energy ΔG . Because entropy is the determining factor of steric stabilization it is also called entropic stabilization. This mechanism of stabilization works only when the polymer brushes are soluble in the surrounding solvent matrix [20]. Therefore Fischer's solvency theory becomes predominant to the stability of steric stabilized dispersions [21]. Fischer characterized the θ -point of dissolved polymers where the polymer chain has undisturbed free mobility and creates a coil conformation. Solubility above the θ -point is provided by good solvents. In this case, the coil conformation is unrolled and the polymer chain is craned towards one direction. A solubility level lower than the θ -point causes the coil formation to collapse and precipitation of the polymer to occur. Therefore steric stabilized dispersions can only be stable above θ -point conditions for the polymer brushes on the particles. Steric

stabilized particles are also less sensitive towards multivalent ions than those that are electrostatically stabilized. The most common polymer types for steric stabilization in aqueous media are polyvinylalcohol and polyethylenoxide. These polymers are most often designed as block-co-polymers with some specific anchoring blocks in order to adsorb on the particle surface following the adsorption mechanisms (see Chapter 1).

Grafted polyelectrolyte chains are also commonly used for particle stabilization in dispersions [22,23], because polyelectrolyte chains are charged, they combine the characteristics of electrostatic and steric stabilization resulting in the so called electrosteric stabilization. An illustration of polyelectrolyte brushes is shown in *Fig. 3.38*

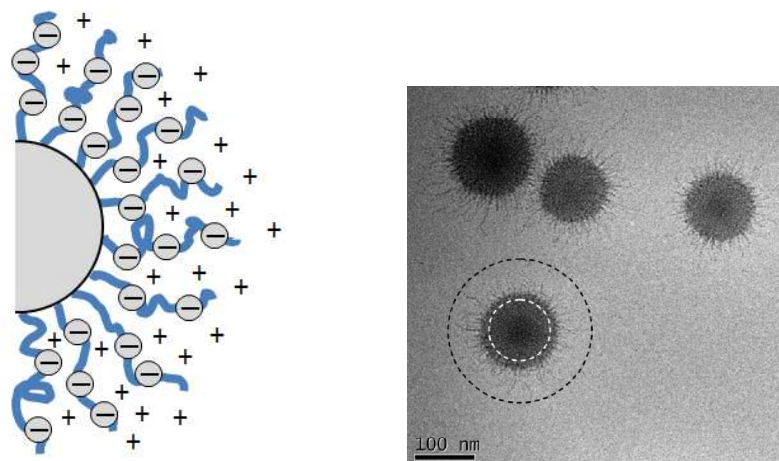


Fig. 3.38: (left) Illustration of grafted polyelectrolyte brushes on a particle. (right) TEM image of polyelectrolyte brushes on a polystyrene particle [24].

Several experiments have shown that stabilizing dispersed particles with adsorbed or grafted polyelectrolyte brushes increases the stability towards multivalent counter ions and pH values in aqueous matrix [25-28].

It is assumed that DPE block-co-polymer dispersions similar to those synthesized within this study are also electrosterically stabilized [29,30]. The creation of stable dispersion particles without any use of surfactants as described in section 3.2 of this study is attributed to this stabilization method. It is therefore assumed that

hydrophilic polyelectrolyte chains are grafting on the surface of the polymer particle during polymerization.

While electrosteric stabilized particles are less dependent on the pH of the surrounding aqueous matrix and have more tolerance towards multivalent counter ions, it can be assumed that the obtained DPE dispersions would be more controllable for the mechanism of selective deposition on grain boundaries.

3.4.2 Experimental procedure

3.4.2.1 Titration on ion selectivity

The influence of aluminum and zinc ions on the coagulation behavior of the dispersion was investigated by titration combined with particle size detection. Therefore the block-co-polymer dispersions were reduced to a solid content of 1.0%. The titration was carried out on 20 ml of the reduced dispersion. Aluminum and zinc chloride solutions of 0.01 mol/L were added in 0.5 mL steps to the dispersions whilst being stirred, using a burette. After each step the particle size of the dispersion was measured with the Zetasizer Nano-ZS from Malvern.

3.4.2.2 SPR measurements

SPR studies were performed as described in Chapter 2: Applied Techniques.

3.4.2.3 Grain boundary selective polymer application

Grain boundary selective polymer application was carried out through a dip coating process. The polymer dispersion was diluted to a solid content of 1.0%. and the pH was adjusted with nitric acid to 2.2 – 2.4. The solvent cleaned substrates were dipped in the prepared dispersion for 30 s. After 30 s no visible difference in the resulted coated substrate surface was found. Within this

application window only the grain boundaries of the hot dipped galvanized steel were covered with the polymer material.

3.4.2.4 Coating application and testing

Within in the salt spray test, HDG steel sheets were spin coated with a coil coating primer, Coiltec Universal P CF. The spin coater P6700 from Specialty Coating Systems was operated at 500 r/min. This setting resulted in a constant coating thickness of 10 μm .

The salt spray tests were carried out in a salt spray chamber for 504 hours in accordance with the German Association for Industrial Testing DIN EN ISO 9227-2006.

3.4.3 Experimental results

In section 3.1: Surface Characterization it was found that grain boundaries are electrochemically more active than the surrounding grain surfaces. They were therefore identified as the weak zones of the HDG steel substrate surface. This corrosive behavior was attributed to both the enriched aluminum content in the grain boundaries and their non-compact structure. Aluminum is more electronegative in its potential than zinc and would therefore preferably electrochemically dissolve. The less compact structure provides a great accessible surface for dissolution activity and seemingly the atomic structure in the grain boundaries is more amorphous.

In section 3.2: Material Survey for Grain Boundary Application it was found that grain boundaries can selectively be dissolved with a dependency on the pH value. It was assumed that the dissolution causes aluminum cations, which could then be used for selective deposition of material on the grain boundaries. The most promising results were obtained by polymer particle deposition.

Within the following experimental part of this section the specifically obtained block-co-polymer dispersions (chapter 3.3) will be investigated in terms of their selective applicability to the grain boundaries of HDG steel.

However in terms of the systematic in this study, the deposition of DPE dispersions on grain boundaries will be described in this section. Historically the first observations of DPE dispersions selectively covering the grain boundaries were nevertheless made in the very beginning of this study and initiated the fundamental investigation around this phenomenon.

3.4.3.1 Polymer ion selectivity

The pH value and multivalent counter ion concentrations were described as the predominant parameter for instability of electrostatic particles. These parameters are also dominant to the stability of electrosteric stabilized particles even though they are less in power. In order to deposit the obtained block-co-polymers selectively on the grain boundaries one has to investigate the coagulation activity towards the specific ions in the system, aluminum and zinc. This was provided by titration of the block-co-polymer dispersions with aluminum and zinc ions (see Fig. 3.39).

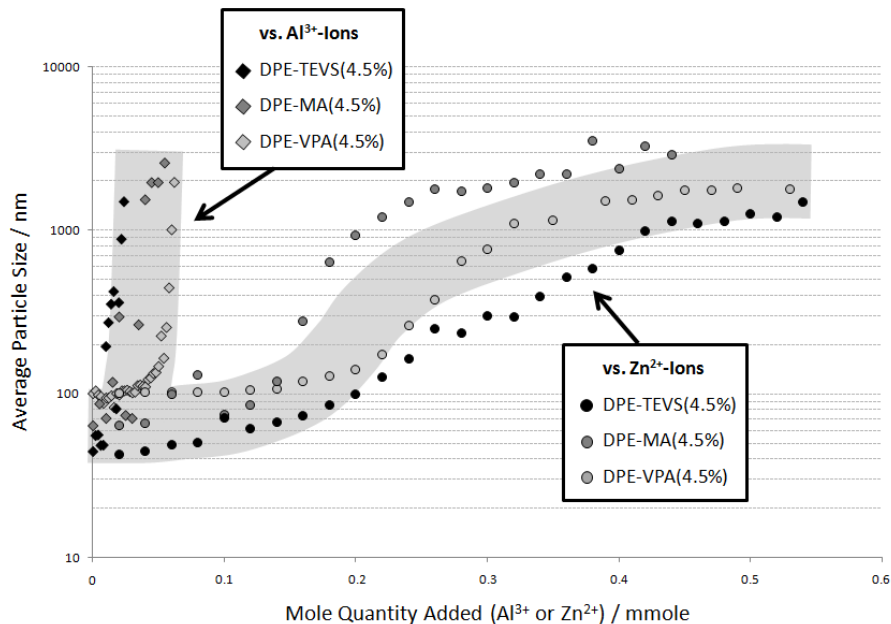


Fig. 3.39: Selectivity of block-co-polymer dispersions to aluminum and zinc ions determined by dispersion particle coagulation in dependency of the ion content.

Whilst as part of the process the step of adding multivalent counter ions to the diluted polymer dispersions included tracking of the particle size, it was found

that dispersions quickly coagulate in the presence of small amounts of aluminum ions. Less than 0.05 mmol of aluminum ions raise the particle size from around one hundred nm (single particles) up to thousands of nm as detected until the entire dispersion precipitates. At the same time these dispersions are more tolerant to the presence of zinc ions. The particle size starts to significantly rise between 0.1 and 0.2 mmol of zinc ions added to the batch of 20 mL dispersion. After 0.2 mmol the dispersion precipitates. The different coagulation behavior of the dispersion particles can be attributed to different charge densities of aluminum and zinc ions. Aluminum cations are triple charged on a rather small ion radius which makes them highly charged atoms, able to attract the anionic polymer particles and act as a bridging charge between the polymer particles. This quickly leads to agglomeration and destabilization of the block-co-polymer particles. Zinc ions on the other hand are positively double charged on a rather large ion radius which results in a lower charge per radius relation. The anionic stabilized polymer particles can tolerate more of the zinc ions before charge quantity is reached and the stabilization of the polymer particles collapse. This aligns with the Schulze-Hardy theory for critical coagulation concentration of multivalent counter ions.

According to the assumptions of electrosteric stabilization of block-co-polymer particle dispersions, the polyelectrolyte brushes due to their spatial extension into the water matrix would also very quickly form a complex between the functional group and the cation. There are basically two possible scenarios that could occur. The first would be that polymer brushes from one particle catch out the cation from the surrounding water matrix and create a complex within the brushes. This particle then remains stable until the polyelectrolyte brushes become saturated with the multivalent counter ions. In the second scenario the complex would be created between one counter ion and different polymer chains from different particles. In this case the counter ion would bridge the two particles and they would destabilize and coagulate. In both scenarios aluminum cations would also provide a stronger complex with the hard Lewis bases such as phosphonic and carboxylic acid (see Chapter 1).

However these results open a window of individual cation quantities that must be locally present for a selective coagulation and deposition of polymer particles on the grain boundaries. In the next step it is important to investigate the stability of

these polymer dispersions in relation to dependency of the pH values, as this is also an important factor and the selective release of aluminum cations from the grain boundaries was found to occur under acidic conditions.

3.4.3.2 Polymer particle stability in dependency of pH values

The stability of polymer dispersions in regions of low pH values is of importance considering the desired application mechanism on the grain boundaries. Whilst the creation of cations locally in the grain boundary region should precipitate the polymeric material selectively, the dispersion should remain stable where no aluminum cations are present but the pH value is low. Fig. 3.40 shows the obtained results for particle size and ζ -potential in dependency of the pH value.

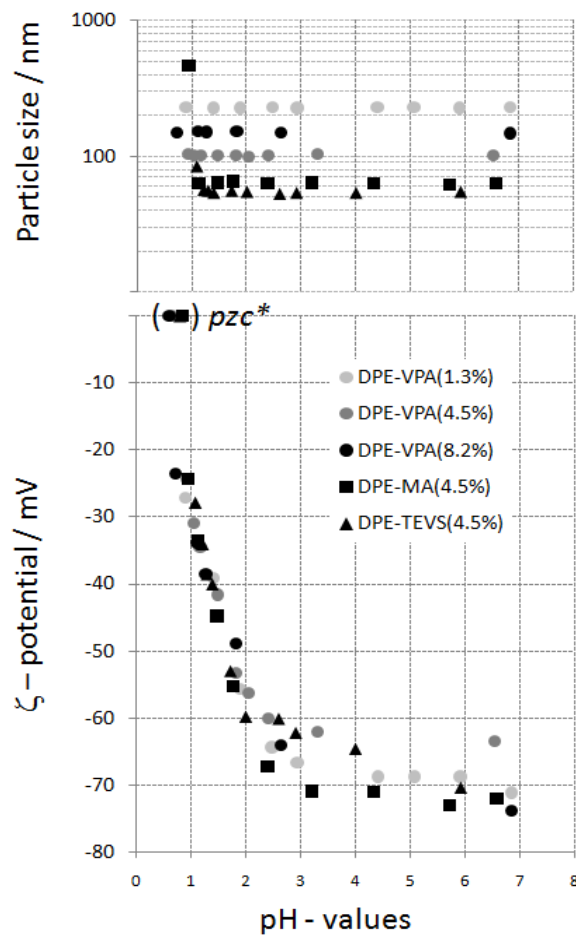


Fig. 3.40: Particle size and ζ -potential in dependency of pH values. *(pzc) point of zero charge theoretically correlated from experimental data.

All dispersions remain stable down to the pH value of 1.0. When crossing the pH 1.0 value, particle sizes from DPE-MA and DPE-TEVS significantly rise, whereas the DPE-VPA dispersions remain stable.

At this point particle size may be of significant importance. Cosgrove derives calculations from the DLVO theory where the maximum of the total potential (V_T) (Fig. 3.33) has a different relation to the particle size [8]. For particles below 100 nm the radius of the particle is directly proportional to V_T . For particles sizes above 100 nm the relationship is more complicated but less dependent on the radius. This means that down to particle sizes of 100 nm the repulsion maximum decreases slower than the particle size. Below the particle size of 100 nm the decrease of the repulsion maximum is steeper which results in a smaller barrier to be overcome for the coagulation of smaller particles. This may be the reason why DPE-TEVS and DPE-MA particles start to aggregate even though the ζ -potential indicates a stabilized system.

A significant change towards smaller absolute values in the ζ -potential starts below the pH value of 2.0. This behavior aligns with the theory discussed in the fundamental part of this chapter. The point of zero charge can be estimated by correlation functions of the obtained data to a range between 0.5 and 1.0 pH for the individual dispersions. However down to pH values of 1.0 all dispersions remain stable. This may be of importance when it comes to the selective application process on grain boundaries at low pH values.

3.4.3.3 Polymer particle adsorption to aluminum and zinc oxide surfaces

Within the following experiments polymer particle adsorption to aluminum and zinc oxide will be investigated. These experiments aim to provide specific application characteristics and to find the appropriate parameter window for the selective grain boundary deposition of polymer particles. The trigger for aluminum release from grain boundaries was found to be the pH value. Therefore the variation parameter will be the pH value using the surface plasmon resonance spectroscopy as a surface sensitive detector for polymer adsorption. The resulting spectra are shown *Fig. 3.41* with the example of the DPE-VPA(4.5%) on an aluminum oxide SPR sensor. The gathered spectra highlight

the shift of the reflection minima to higher angles. This indicates an adsorption of polymer particles on the surface of the sensor. The greater the shift of the minima towards higher angles, the higher the thickness of the adsorbed layer on the sensor. In all of these measurement cases only the relative shift will be considered and evaluated. The information about the reflectivity index of the adsorbed polymer particle layer will remain unknown in this study. But considering that different polymer dispersions have a reflectivity index in the same range, the relative angle shift will be comparable and provide information on the adsorption process of the particles to each of the substrates.

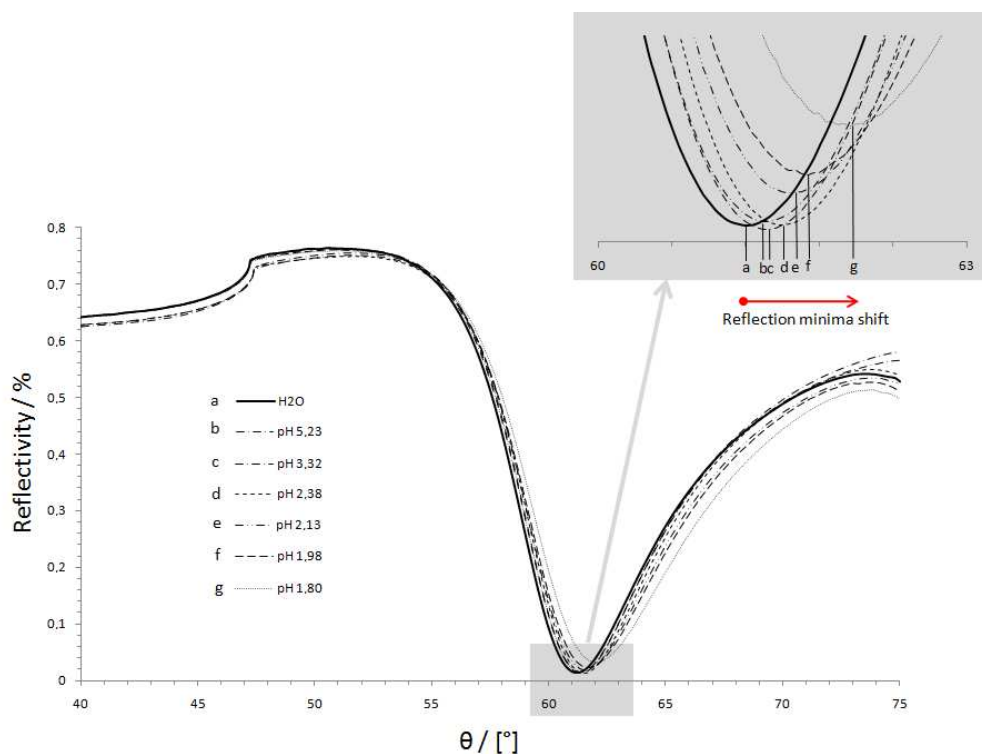


Fig. 3.41: Step scan spectra of DPE-VPA(4.5%) on aluminum oxide at different pH values. The reflection minima shift is indicated by character from a) deionized water to g) polymer dispersion DPE-VPA(4.5%) adjusted to the pH of 1.80.

The reflectivity minimum measured in water before each measurement with the varied pH is the scaling point in order to calculate the angle shift. In the case of DPE-VPA(4.5%) the angle has shifted from water 61.18° to 62.03°. At the angle of 61.18°, no adsorption occurred while at the angle of 62.03° (pH 1.80) a dense polymer film was adsorbed to the sensor surface. The adsorption of the polymer

could be controlled by SEM imaging and the SPR sensor after each adsorption measurement was run. *Fig. 3.42* shows high resolution SEM images of the surface of a bare aluminum oxide sensor after measurement in the water, the polymer DPE-VPA(4.5%) adsorbed on the sensor at the pH of 2.38, and at the pH of 1.80.

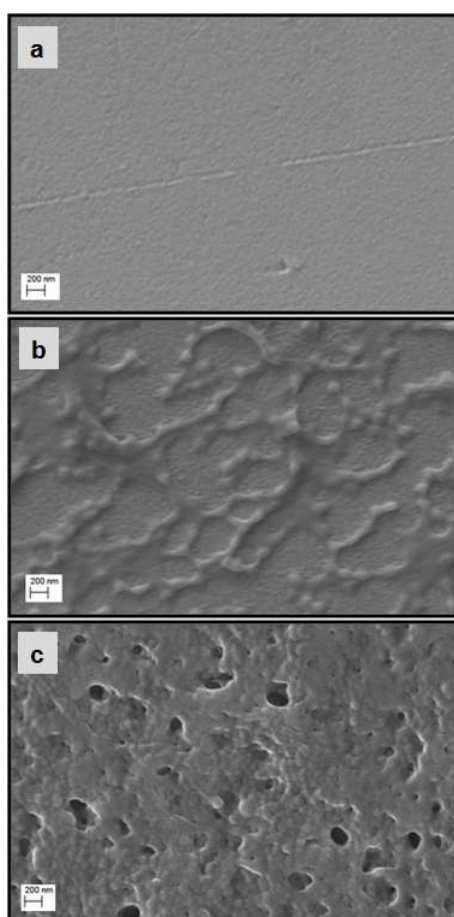


Fig. 3.42: High resolution SEM images of sensor surfaces: a) aluminum oxide sensor after measured in distilled water, b) aluminum oxide sensor after measured the adsorption of DPE-VPA(4.5%) at the pH of 2.38 and c) at the pH of 1.80.

One must consider that the detection area on the sensor is the same as the diameter of the laser beam, which is a few 100 μm . The area where the reflectivity information can be gathered is around the size of one of the SEM

images as shown in *Fig. 3.42*. The minimum shift is dependent on the adsorbed layer thickness. When this area is not homogeneously covered with the polymer the obtained information has to be considered as an averaged thickness of the adsorbed particles over the sensor surface. A good example for such a heterogeneously covered sensor surface is provided in *Fig. 3.40b*, with the SEM image of the adsorbed polymer dispersion DPE-VPA(4.5%) at the pH of 2.38. It shows that the entire surface is not covered with polymer particles. The sensor surface remains visible all over the image but the SPR spectra shows a minimum shift towards higher angles as shown in *Fig. 3.41*. The image obtained after the adsorption at the lowest pH of 1.80 shows an entirely covered sensor surface with partly coagulated polymer particles. One must consider that coagulation of these particles occurs also whilst the SEM image is obtained as initiated through the energy from the electron beam.

The reflection minima shifts of all the investigated polymer dispersions on the aluminum oxide and zinc oxide sensors by variation of the pH are provided in *Tab. 3.4*. From this data it is apparent that all polymer dispersions roughly follow the same trend. While on the aluminum oxide surface a minimum shift occurs at the highest pH levels, there are no adsorption events that occur on the zinc oxide surface. Only for pH values of around 2.0 does some adsorption of polymer particles to the zinc oxide surface occur and the reflectivity minimum shifts towards higher angles.

Tab. 3.4: SPR reflectivity minima shifts of investigated dispersions at different pH values on aluminum oxide and zinc oxide sensors.

Dispersion	pH	$\Delta\theta_{\text{Al}_2\text{O}_3}$ [°]	$\Delta\theta_{\text{ZnO}}$ [°]
DPE-VPA(8.2%)	1.76	0.3219	0.1649
	1.90	0.0698	0
	2.05	0.0537	0
	2.31	0.0549	0
	3.36	0.0269	-
	5.53	0.057	-
DPE-VPA(4.5%)	1.80	0.8539	0.7241
	1.98	0.5069	0.1902
	2.13	0.3853	0
	2.38	0.122	0
	3.58	0.0548	-
	5.23	0.0479	-
DPE-VPA(1.3%)	1.89	1.1318	0.126
	2.10	0.1927	0.0082
	2.27	0.1043	0
	2.62	0.0604	0
	3.32	0.0819	-
	5.24	0.1107	-
DPE-TEVS(4.5%)	1.89	-	0.2296
	2.10	1.7203	0.0875
	2.38	0.6538	0
	2.68	0.1776	-
	3.13	0.0353	-
	5.50	0.0217	-
DPE-MA(4.5%)	1.89	0.3252	0
	2.09	0.1113	0
	2.32	0.1597	0
	3.08	0.119	0

The numbers from the minima shifts provide a potential application window for selective deposition of polymer particles on grain boundaries when using the pH as a trigger. Fig. 3.43 shows the correlation between the minima shift to higher angles when lowering the pH. Overlaying the charts for aluminum oxide and zinc

oxide visualize the pH range window where adsorption on the aluminum oxide surface occurs but not for the zinc oxide surface.

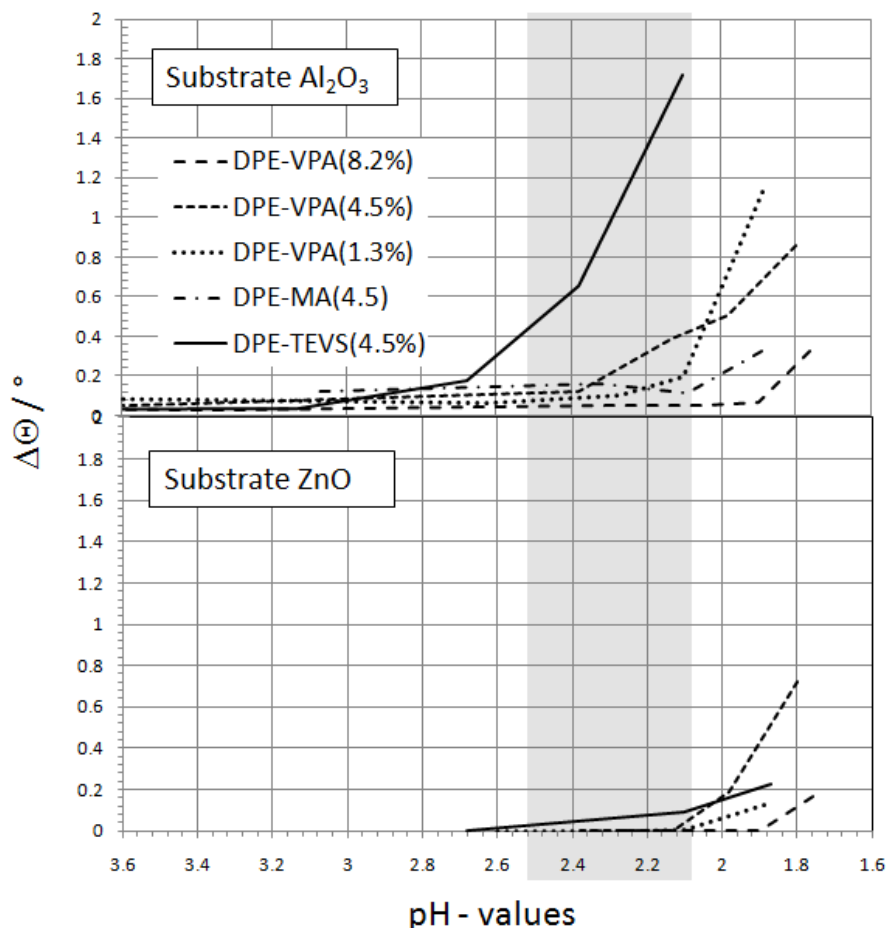


Fig. 3.43: SPR reflectivity minima shift in dependency of the pH on aluminum oxide (top) and on zinc oxide (bottom).

In Chapter 3.2: Material Survey for Grain Boundary Application, the best pH range for grain boundary dissolution and therefore the release of cations from the grain boundary was found to be 3.6 to 4.0. SPR measurements found the best application range to be in the pH region of 2.1 and 2.5. This difference may arise from the different topography of the sensor (aluminum oxide or zinc oxide) compared to the grain boundaries (see section 3.1). The porous structure with edges and vertices may expose the metal atoms and their oxidic species in a manner more accessible for anodic dissolution into the surrounding acidic water.

The sensor is rather flat and therefore it may remain stable towards dissolution of the outermost ions at lower pH values. The selective deposition on grain boundaries will most probably be found in the pH region between 2 and 4 pH.

However one interesting observation that can be made is that aside from DPE-VPA(8.2%), all dispersions provide different adsorption behavior towards the two different oxide surfaces. Only DPE-VPA(8.2%) shows significant polymer particle adsorption at the same pH value of 1.78 for both substrates. This dispersion obviously does not distinguish between the surface types.

An explanation for this observation may come from the findings in Chapter 3.3 where VPA was found to be limited in copolymerization in block-co-polymer synthesis. In DPE-VPA(8.2%) the residual VPA monomer content can be estimated at 1.9 w.-%. As discussed in the previous chapter one can assume that the small VPA monomer preferably complex the released cations from the sensor surface. In this scenario polymer particles would not access the amount of counter ions they need to coagulate at mild conditions. One could imagine that only when counter ions are released excessively would polymer particles also coagulate and precipitate, and because the zinc dissolution at a lower pH is higher than aluminum, there is a loss of selectivity towards the different surfaces.

Another explanation in terms of the residual VPA monomers would also be the surface stabilizing effect of VPA. As described in Chapter 1, phosphonic acid derivatives are able to anchor on aluminum/aluminum oxide surfaces and assemble into a stable monolayer. This monolayer would protect the substrate for dissolution at moderate pH levels. Thissen et al. investigated the stability of long chain (C_{18}) phosphonic acid SAMs on different aluminum oxide surfaces [31]. Besides the polar $Al_2O_3(0001)$ surface the adsorbed monolayer remained stable when it was exposed to water. This was also the case on aluminum oxide surfaces created through physical vapor deposition, in the same way the SPR sensors were prepared for the experiment in this section. Liakos et al. found that C_{18} – alcylic phosphonic acid self-assembled monolayers remain stable down to the pH value of 1.0 on aluminum oxide surfaces [32]. It was also discussed that the stability of SAM is most stable at a pH of 3.0. In the same paper it was found that short chain (C_4) phosphonic acid SAMs could be washed off the surface with pure water after several rinsing cycles. However, VPA is a C_3 phosphonic acid.

Since in the system of SPR experiments of this study there was no rinsing, one could assume that some adsorption of VPA to the surface occurred. However by evaluating the literature survey one would assume that the adsorbed monolayer would desorb above the value of 1.0 pH. Nevertheless both scenarios could explain the lack of selectivity of dispersions bearing a high amount of residual functional monomers such as vinylphosphonic acid. In the next step the findings from these model substrates will be transferred to the real technical substrate, the HDG steel.

3.4.3.4 Selective deposition on grain boundaries of HDG steel

In the following experiments all understanding gained in terms of the substrate characteristics, polymer design and polymer-substrate interaction, as generated in the previous investigations will be transferred to the selective deposition of polymers on grain boundaries of the technical substrate of interest, hot dipped galvanized steel. The application process is illustrated in *Fig. 3.44*.

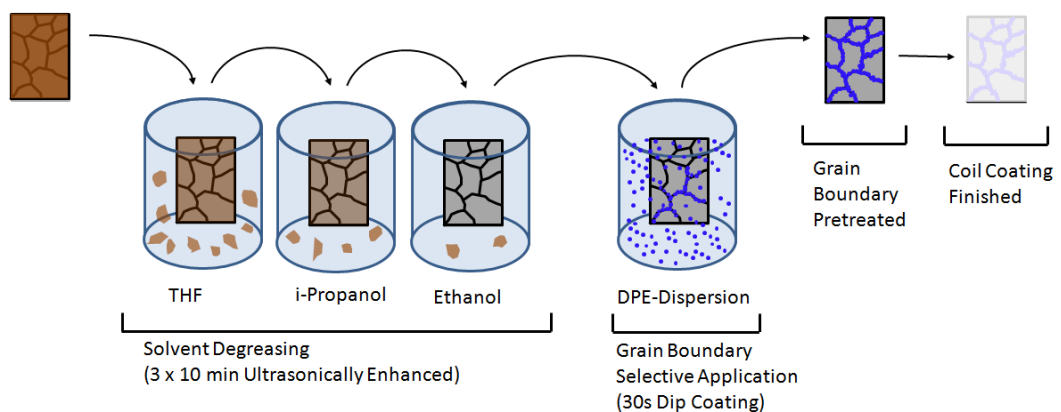


Fig.3.44: Illustration of the selective polymer application process on grain boundaries of HDG steel.

Running through the application process the substrate has to first be degreased. It was therefore dipped in a cascade of each solvent bath for 10 minutes and

ultrasonically enhanced. This procedure was found to be very effective in removing all organic compounds from the surface and leaving an analytically clean substrate [33]. However for industrial application the cleaning process could probably be optimized in terms of time and solvent type. One could assume that washing with aqueous detergent solutions could be introduced into a fast cleaning process. After cleaning, the selective polymer deposition on the grain boundaries occurs. Therefore the polymer dispersions were diluted to the solid content of 1.0 w.-% and adjusted to the pH with a step-wise variation in accordance with the most promising application window for selective polymer deposition on the grain boundaries. The application is carried out through a dipping of the substrate into the adjusted polymer dispersion. After dipping for 30 s the sample is rinsed with pure water and dried in a nitrogen stream. At this stage of the process the grain boundary selective pretreatment is completed. For end finishing the samples were coil coated. The resulting surface of the grain boundary pretreated substrate was monitored via SEM imaging. An example of a result obtained from selective deposition on the grain boundaries of DPE-VPA(4.5%) is provided in *Fig.3.45*.

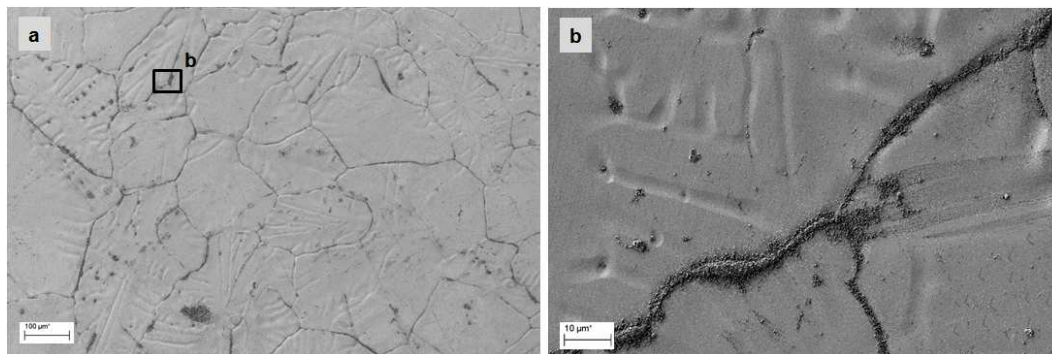


Fig. 3.45: SEM images of HDG steel substrate with the polymer dispersion DPE-VPA(4.5%) selectively applied to the grain boundaries of the substrate. a) overview, b) grain boundary triple point. The polymer dispersion was adjusted to solid content of 1.0 w.-% and the pH of 2.4. The dipping time was 30 s.

The SEM images in *Fig. 3.45* visualize how polymer particles are concentrated on the grain boundaries whilst almost no polymer can be found on the

grains/spangles. Such results could be obtained with all of the tested DPE polymer dispersions besides DPE-VPA(8.2%). For all polymer dispersions a good window in the application process on the real HDG substrate was also found with pH values of 3.0 to 2.2. The results of dip coating for 30 s within this application window always led to similar images as shown in *Fig. 3.45*. The dispersion DPE-VPA(8.2%) was the only one not able to be applied selectively on the grain boundaries. Down to the pH value of 2.2 there was almost no dispersion found on the HDG steel substrate. Therefore at the pH value 2.0 the entire substrate was covered with a monolayer of polymer dispersion particles. These findings are consistent with the adsorption results obtained via the SPR technique and discussed in the earlier part of this chapter. These results show that DPE-VPA(8.2%) has similar adsorption behavior on both aluminum oxide and zinc oxide sensors.

It was assumed that either residual VPA monomers were stabilizing the substrate surface by creating a self-assembled monolayer or that the small VPA molecules complex the released cations from grain boundaries and deactivate these cations from the destabilization of the polymer particles. With regard to the theory of SAM formation as discussed in Chapter 1 of this thesis and the topography of grain boundaries as found in section 3.1: Surface Characterization, it is most likely that the loose structure of edges and vertices of grain boundaries would not be stabilized by any type of self-assembled monolayer. Recent studies have also shown that phosphonic acid derivatives precipitate to zinc phosphonates on HDG steel with an aluminum content of 0.5 w.-% rather than create a self-assembled monolayer [34]. Stable SAM of organophosphonic acids could be obtained only on galvanized steel with aluminum contents above 5 w.-%. Zinc phosphonates on HDG steel could easily be washed off from the substrate surface with pure water. It is therefore most likely that residual monomers catch the released cations so they cannot destabilize the polymer particles of the dispersion. In addition, the co-polymerized ratio of VPA in DPE-VPA(8.2%) must be greater than that for the other dispersions as discussed in section 3.3, even though the residual monomer values are at the highest. The higher the amount of VPA incorporated into the block-co-polymer, the higher the negative charge of the particle and rise in the repulsion maximum according to the DLVO theory, which makes the dispersion more stable towards counter ions. This goes along with the slightly higher ζ -

potential and point of zero charge that was found for DPE-VPE(8.2%). This factor may enhance the lack of counter ions due to residual monomers and both factors cause very poor selectivity in the application process. For all other polymer dispersion applied to the HDG substrate *Fig. 3.44* summarizes the selective application of the polymer dispersion on the grain boundaries.

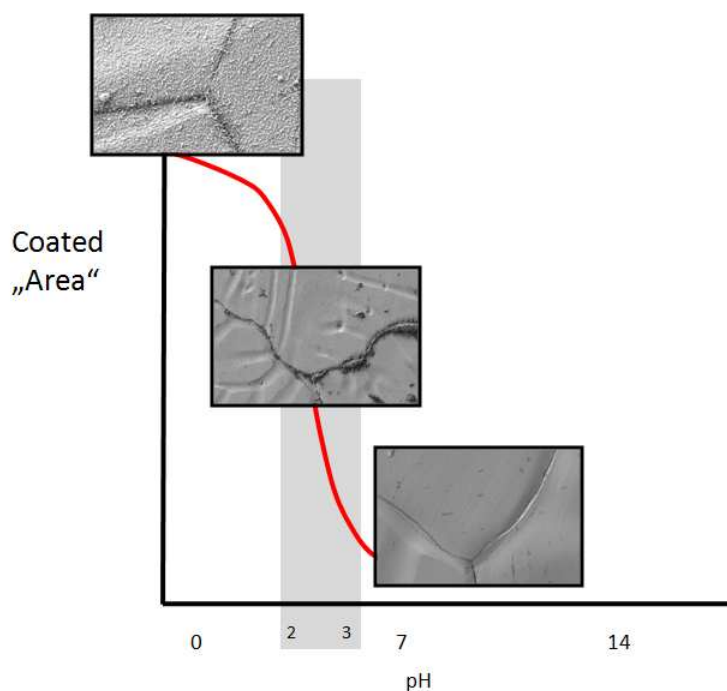


Fig. 3.44: Scheme of the polymer application results on HDG steel substrates by dip coating in dependency of the pH value.

When coming from higher pH value regions down to 3.0, there is no autophoretic polymer application possible for the investigated dispersions. Between the pH values of 2.0 and 3.0 the grain boundaries are selectively coated with the block-co-polymer particles. Below the pH value of 2.0 polymer particles cover the entire substrate surface. The selective polymer deposition on the grain boundaries could be achieved due to their different electrochemical behavior. The high aluminum concentration within the grain boundaries and their topography led them in turn to have higher electrochemical activity. While the surface of grains is

rather flat and smooth the structure of grain boundaries is rough and consists of multiple edges and some sort of amorphous sponge like surface within the tranches. The higher susceptibility of the grain boundaries to the corrosion process leads to a faster dissolution of the metal of the grain boundary material and the release of multivalent metal cations. Aside from aluminum cations it is most likely that zinc cations will also be dissolved as zinc/zinc oxide (theoretical dissolution at pH of 5.8) is less stable under acidic conditions than aluminum/aluminum oxide (theoretical dissolution at pH of 3.8) [35]. As discussed in section 3.1: Surface Characterization grain surfaces are also terminated with a layer of aluminum oxide that is a few nano-meters thick. In addition to the flat geometry, this layer may also provide the grain surface with more stability towards electrochemical dissolution in acidic environments; even though the aluminum surface density on grains is too low to create a stable SAM out of phosphonic acid derivates. A scheme illustrating this process is shown in *Fig. 3.45* where a local release of cations drives the coagulation and precipitation of the polymer particles directly to the grain boundaries in the second step. The entire process can be described as a local autophoresis.

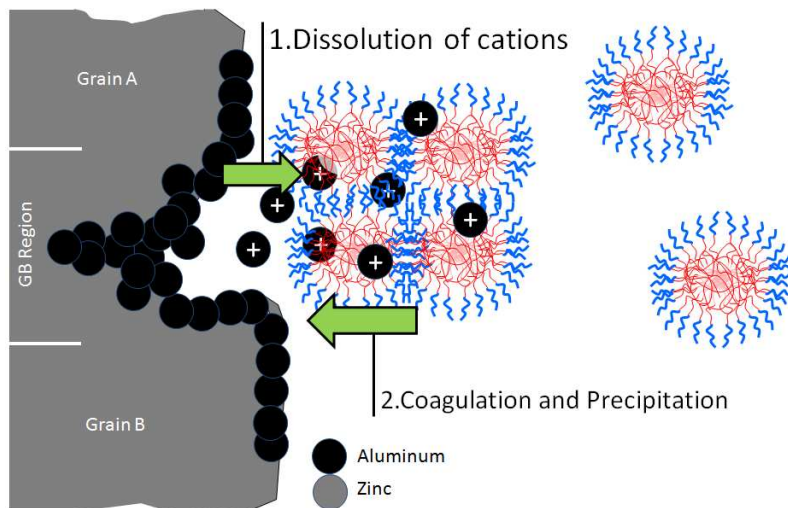


Fig. 3.45: Scheme of the local autophoresis driven polymer precipitation on the grain boundaries.

So far the selective polymer deposition on grain boundaries of HDG steel has been discussed as a local autophoresis driven by the dissolution of cations from grain boundaries. However it might be worth discussing this process under the consideration of alternative possible processes.

It could also be speculated that by anchoring the block-co-polymer functional groups to the solid edges of grain boundaries (see chapter 1). Recent studies have shown that functional groups such as carboxylic acids from polyelectrolytes similar to the block-co-polymers used in this study preferably attach to the edges of polar terminated ZnO (0001)-Zn surfaces [36]. Assuming that all grain surfaces are polar terminated and grain boundaries are the edges of those surfaces, one should also observe polymer particle adsorption on the grain boundaries. Even though the polymer brushes of the DPE dispersions would reach out as anchoring tentacles, only a single particle could cover one adsorption spot that is the size of the particle. As shown in *Fig. 3.45* there is an aggregation and stacking of particles on each other on grain boundaries. Therefore the deposition of the particles may prefer to be driven by local autophoresis. However, the anchoring to the edges of the grain boundaries might be the determining factor for stabilizing them towards electrochemical activity after deposition.

3.4.3.5 Testing results

In order to prove the concept an accelerated corrosion test in a salt spray chamber was provided on non-pretreated and grain boundary treated HDG steel samples. Both the pretreated and non-treated substrates were coated with a coil coating primer from BASF Coatings GmbH, Münster. The test samples were scratched and exposed to the salt spray test for 504 hours. After the exposure the entire coating material was removed from the sample surface and scanning electron microscopy was used to investigate the corrosion propagation along the grain boundaries. *Fig. 3.48* shows the SEM images and combined EDX mappings of non-grain boundary treated and grain boundary treated substrate samples after the corrosive exposure. On the non-treated substrate the grain boundaries connected to the corrosion front show some destruction along the grain boundary stemming from a corrosive attack. The damage along the grain boundary can be measured by chlorine traces detected in the EDX mappings. On

the substrate with the non-treated grain boundaries, the extension of the corrosion path can be measured from 100 to 200 μm based on the border between the plateau corrosion front and the intact HDG surface.

The best results for disabling the grain boundary corrosion were achieved by grain boundary selective deposition of the DPE-TEVS(4.5%) dispersion (see *Fig. 3.46*). To track the corrosion propagation along the grain boundaries the chlorine trace from the EDX mappings was used. In this case, the chlorine trace along the grain boundaries can only be measured to 10 to 30 μm . This would be three to twenty times less than was found on the substrate without selective polymer deposition on the grain boundaries. There is also no visible damage on the treated grain boundaries than can be seen on the non-treated samples in the SEM images.

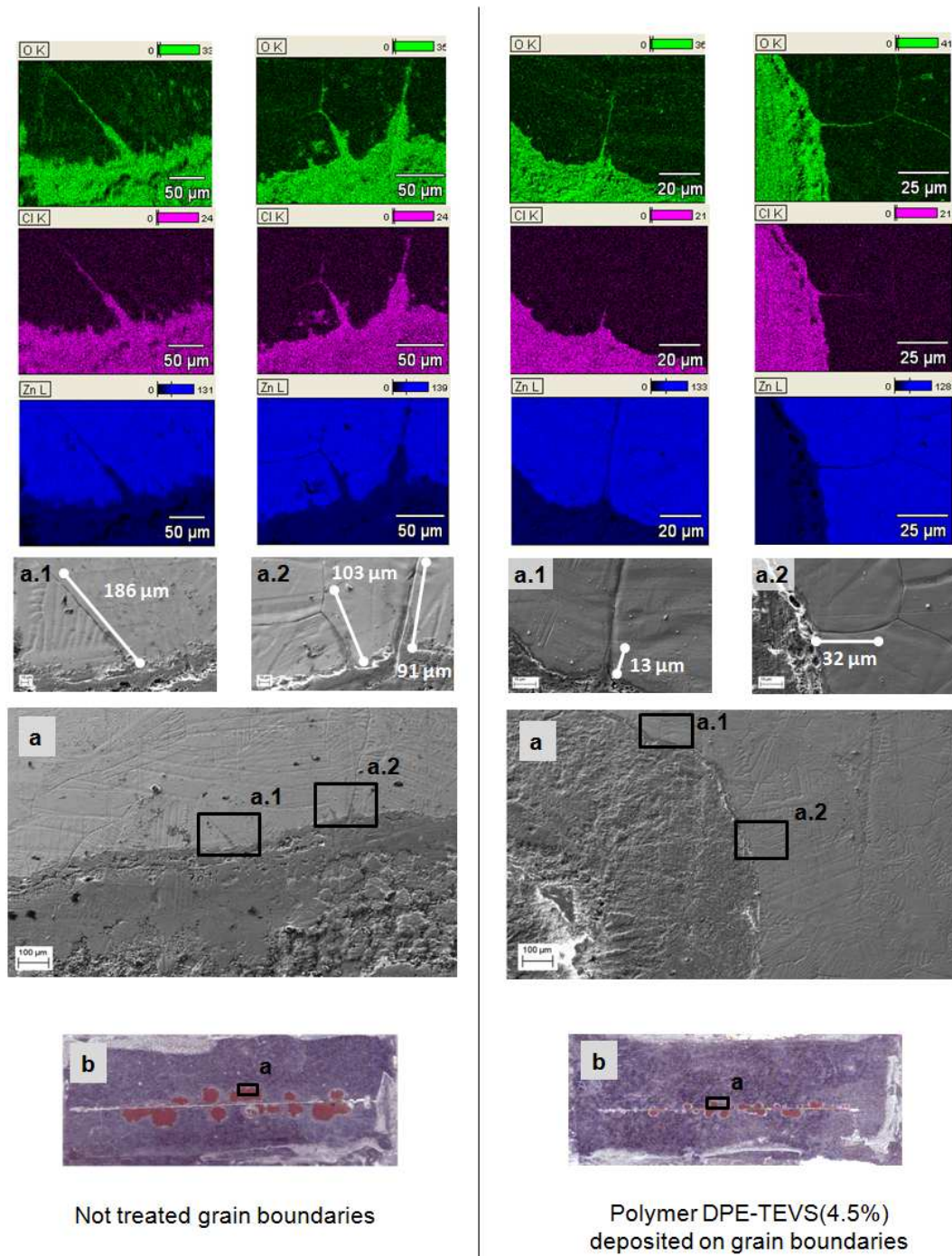


Fig. 3.48: SEM images and EDX mappings of the corrosion front coming from the scratch. Left) Image is obtained from a non-grain boundary treated substrate. Right) Image is obtained from a grain boundary treated substrate with DPE-TEVS(4.5%). The focus is in the border between the corroded and intact surface and on the grain boundaries of that region.

According to the model developed, (see section 3.1), the elimination of grain boundary corrosion should slow down overall corrosion. The results within this chapter could show that a selective polymer deposition on grain boundaries leads to less corrosion along the grain boundaries as is sketched in *Fig. 3.49*.

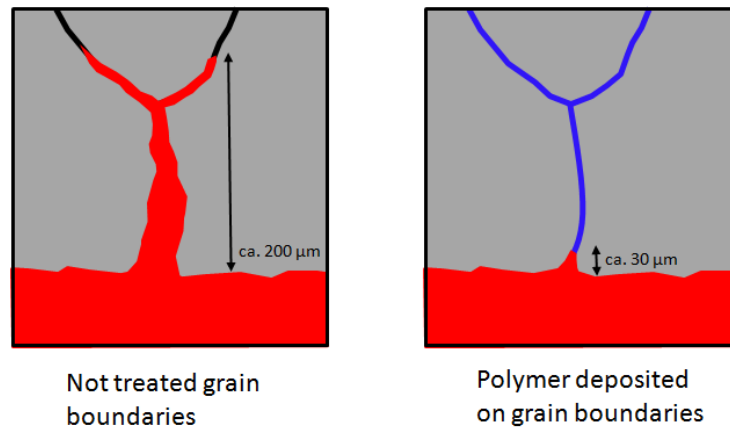


Fig. 3.47: illustrates the results from corrosion on a HDG sample not treated (left) and polymer deposited exclusively on grain boundary (right).

However, on a micro scale these findings support the theory raised about the two corrosion pathways. Unfortunately the overall corrosion performance on a macro scale showed different results. Salt spray tests were carried out and evaluated by total creep from the scratch. While the initial tests showed small statistical improvements on the overall corrosion when grain boundaries are selectively treated with the block-co-polymers, the following results were statistically scattering a lot [37]. The salt spray test itself also scatters with a standard deviation of around 25%. This leads to the assumptions that the grain boundary contribution to corrosion may be within this range and that the salt spray test is not able to resolve the influence of grain boundaries to the overall performance.

In terms of overall performance, the silane functionalized polymer dispersion showed the best results. This behavior is not surprising and is based on the discussions within chapter 1 of this study.

At this point one could also consider that the synthesized polymer dispersions in this study are model polymers for selective grain boundary application. In order to enhance corrosion protection the polymer architecture might bear some potential for improvement.

3.4.4 Conclusions

The main goal of this chapter was to apply the polymer dispersions selectively on the grain boundaries of the hot dipped galvanized steel substrate. Knowing that grain boundaries are aluminum enriched and have a specific structure and therefore a higher susceptibility to electrochemical dissolution the specifically designed water based polymer dispersions were investigated on their coagulation behavior in the presence of aluminum and zinc ions. It was found that the triple charged aluminum ions immediately cause a destabilization of the polymer particles followed by their precipitation. Towards the double charged zinc ions the polymer dispersion showed a tolerance up to a specific ion concentration but then also coagulated and precipitated. This varied influence on the polymer particle stability was further used to evaluate the application window for a selective deposition of the polymer on the grain boundaries. The pH level as a trigger for the dissolution of the aluminum cations was therefore investigated using the surface plasmon resonance spectroscopy. It was found that an ideal window for a selective application exists in the pH value range of 2.0 to 3.0. At higher pH polymer particles could not be deposited on either the aluminum oxide or zinc oxide surfaces. At a pH below that window the polymer dispersion were precipitating on both surfaces. Only in that window were the polymer dispersions precipitating exclusively on the aluminum oxide surfaces. After defining these application parameters the goal of selectively coating grain boundaries of the industrial HDG steel substrate could be realized in a dip coating process. The final proof of concept was provided through a comparison of non-grain boundary treated but coil coated versus grain boundary treated and coil coated HDG substrates in a salt spray test. The results by SEM/EDX imaging showed a significant difference in the condition of the grain boundaries at the corrosion front. It was found that when selectively cover the grain boundaries with a specifically designed polymer the corrosive damage along the grain boundaries is

reduced by a factor of three to twenty. On the micro scale it could be shown that grain boundaries on HDG steel are highly corrosively active. It has also been shown that it is possible to block the grain boundaries and reduce their corrosive activity.

3.4.5 References

- [1] M. Smoluchowski, Phys. Chem. 92 (1917) 129
- [2] H. C. Hamaker, Physica 4 (1937) 1058
- [3] H.-J. Butt, M. Kappl, Surface and Interface Forces, Wiley-VCH (2010)
- [4] Derjaguin, B.V. and Landau, L. (1941) Acta Physicochim. (URSS), 14, 633.
- [5] Verwey, E.J. and Overbeek, J.T.G. (1948) Theory of the Stability of Lyophobic Colloids. Elsevier, Amsterdam.
- [6] K.S. Birdi, Handbook of Surface and Colloid Chemistry, CRC Press, London (2009)
- [7] P.W. Atkins, Physikalische Chemie, Wiley-VCH, Weinheim (2006)
- [8] T. Cosgrove, Colloid Science – Principles, Methods and Applications, Blackwell Publishing, Bristol UK (2005)
- [9] Schulze, J. (1882) pr. Chem., 25, 471.
- [10] Schulze, J. (1883) pr. Chem., 27, 320.
- [11] Hardy, W.B. (1900) Proc. R. Soc., 66a, 110.
- [12] Malvern Instruments
- [13] E. L. Mackor, J. Colloid Sci., 6 (1951) 492
- [14] D. J. Meier, J.Phys.Chem., 71 (1967) 1861
- [15] F. Hesselink, J.Phys.Chem., 75 (1971) 65
- [16] W. Heller, T. L. Pugh, J. Chem. Phys. 22 (1954) 1778
- [17] W. Heller, Pure Appl. Chem. 12 (1966) 249
- [18] D.H. Napper, Trans. Faraday Soc. 64 (1968) 1701
- [19] R. Evans., J.B. Davison, D. H. Napper, J. Polymer Sci. B10 (1972) 449
- [20] R. Evans, D.H. Napper, Kolloid-Z. Z. Polym. 251 (1973) 409
- [21] E.W. Fischer, Kolloid-Z. 160 (1958) 120
- [22] P. Pincus, Macromolecules, 24 (1991) 2912
- [23] J. Hang, L. Shi, X. Feng, L. Xiao, Powder Technology, 192 (2009) 166

- [24] M. Schrunner, B. Haupt, A. Wittemann, Chem. Eng. J. 144 (2008) 138
- [25] H. Ahrens, S. Förster, C. A. Helm, Phys. Rev. Lett. 81 (1998) 4172
- [26] T. Abraham, S. Giasson, J.F. Gohy, R. Jerome, Langmuir 16 (2000) 4286
- [27] M. Balastre, F. Li, P. Schorr, J. Yang, J.W. Mays, M.V. Tirrell, Macromolecules 35 (2002) 9480
- [28] J. Forsman, Curr. Opin. Coll. Interf. Sci. 11 (2006) 290
- [29] S. Viala, Dissertation „Kontrollierte radikalische Heterophasenpolymerisation mit Anwesenheit des Diphenylethylens“ Universität Potsdam (2002)
- [30] B. Weber, Dissertation „Selbststrukturierende Hybridmaterialien für polymer Werkstoffe“ Universität Paderborn (2009)
- [31] P. Thissen, M. Valtiner, G. Grundmeier, Langmuir 26 (2010) 156
- [32] I.L. Liakos, R.C. Newman, E. McAlpine, M.R. Alexander, Langmuir 23 (2007) 995
- [33] N. Fink, B. Wilson, G. Grundmeier, Electrochim. Acta 51 (2006) 2956
- [34] P. Thissen, J. Wielant, M. Köyer, S. Toews, G. Grundmeier, Surf. Coat. Tec. 204 (2010) 3578
- [35] A. F. Holleman, E. Wieberg, Lehrbuch der Anorganischen Chemie, 101 Auflage, deGruyter, Berlin, (1995)
- [36] M. Valtiner, G. Grundmeier, Langmuir 26 (2010) 815
- [37] Salt Spray Test Reports, Internal Documents, BASF Coatings GmbH (2009/10)

Chapter 4 –

Overall Conclusion and Outlook

The motivation for this study is based in contrasts of the general understanding of corrosion and delamination of coated substrates and current technology in substrate treatment for corrosion protection. While it is postulated that corrosion and coating delamination on coated technical substrates starts with and follows weak zones on that substrate, industrial surface treatment applies the same chemistry to the entire substrate surface. The present study followed the scientific approach of identifying the weak spots of corrosive electrochemical processes on hot dipped galvanized steel and created material for selective deposition directly to these spots, with the aim of inhibiting their corrosive activity.

In the first part of this study, investigations of high lateral resolutions on surface element composition and electrochemical micro probe techniques led to the identification of the HDG steel substrate weak zones. It was found that aluminum in HDG alloys segregates not only towards the zinc/iron and zinc/air interface but also towards the grain boundaries of the zinc grains, even at low concentrations of 0.5 w.-%. Furthermore it could be shown that the conventional alkaline cleaning process in contrary to the majority of literature, does not remove all aluminum from the substrate surface. Even though the overall aluminum content becomes negligible it still remains within the grain boundaries. Surface potential mappings utilizing high resolutions of the SKP-FM technique discovered the lower potential of grain boundaries when compared to the surrounding grain surfaces. Spots with lower potential than the surrounding matrix are known to be more corrosively active. The application of the micro capillary cell showed that

grain boundaries tend to dissolve more easily as a result of corrosive currents that could be measured at potential lower than that on the single grains. The final corrosion test on a coil coated and scratched sample in a salt spray chamber, showed higher corrosion activity of the grain boundaries. Corrosion products along grain boundaries beneath the intact coating material could be observed after the coating was removed. These findings collectively led to the development of a model that can predict the occurrence of corrosion on such surfaces; Where the anodic part reaction is quickly propagated forward along grain boundaries and is escorted by the local cathode which delaminates the grains; one could assume that plateau corrosion could follow more easily on delaminated grains. A derivation from this model would be to slowdown the overall corrosion propagation by disabling the grain boundary activity. The proof of this model would lead to new smart coating material that only treated the weak zones of the substrate which are susceptible to corrosion. The pretreatment of the entire substrate surface with the same material would then become obsolete and save the pretreatment material.

In the second part of this study, the design and application of material selectively on grain boundaries was the focus. It was here found that the anodic dissolution ability of grain boundaries and their preferable release of aluminum cations thereof could be used for the selective application of corrosion inhibiting materials exclusively on grain boundaries.

In the first instance a material survey on their controllability of the grain boundary deposition was conveyed. Aside from phosphating procedures and surface spontaneous polymerization, the selective polymer particle deposition showed the most promising results. Selective phosphating could only be achieved with poor crystal densities on grain boundaries and showed poor selectivity towards grain boundaries. Both phosphate and phosphonate precipitation on grain boundaries could only be achieved after special etching of the grain boundaries and the placement of seed crystals. The phosphating route towards inhibited grain boundaries was thus not pursued further in this study.

Spontaneous surface polymerization can be triggered by strong Lewis acids such as aluminum cations. It was assumed that the aluminum cations released from the grain boundaries could initiate the spontaneous polymerization at the grain

boundaries. Unfortunately the polymerization was rather non-selective. One could observe even fewer polymers on the grain boundaries than on the grains themselves. These findings thus also led to an exclusion of the spontaneous polymerization approach for this particular substrate.

The most promising results could be obtained from the autophoretic deposition of dispersions. Among the screened dispersions, the primary anionically stabilized dispersions were the most stable at low pH values as required for the release of cations from the grain boundaries. Acronal 250 D was found to especially provide to some extent initial selectivity towards grain boundaries. Henkel's Aquence is based on similarly polymer particles but is formulated for application on the entire surface and thus it was not possible to deposit Aquence selectively on the grain boundaries. From this survey the approach towards inhibited grain boundaries of HDG steel was focused on local autophoresis of water borne polymer particles.

The most suitable route towards waterborne dispersions was found in the DPE block-co-polymerization process. In some previous work it had been found that monomers such as maleic acid, triethoxyvinylsilane and vinylphosphonic acid provide strong adhesion to metal/metal oxide substrates. For this reason these monomers were incorporated into block-co-polymer dispersions. In the case of vinylphosphonic acid only small amounts, ranging between 17% and 50% of the added monomer could be co-polymerized. The different polymer dispersions ranged in particle size from 40 nm to 230 nm and presented a narrow particle distribution within one batch. The narrow particle distribution was also attributed to the long-term stability of more than one year for these dispersions.

In the last part of this study however the polymer dispersions obtained were investigated in terms of their applicability towards the weak zones of HDG steel substrate surfaces. Considering that grain boundaries are aluminum enriched and have a specific structure and therefore a higher susceptibility to electrochemical dissolution, the specifically designed water based polymer dispersion were investigated for their coagulation behavior in the presence of aluminum and zinc ions. It was found that the triple charged aluminum ions immediately cause a destabilization of the polymer particles followed by their precipitation. Towards the double-charged zinc ions the polymer dispersion showed tolerance up to a specific ion concentration. This varied influence on the

polymer particle stability was further used to evaluate the application window for a selective deposition of the polymer on grain boundaries. The pH was therefore investigated as a trigger for the dissolution of the aluminum cations using surface plasmon resonance spectroscopy. It was found that an ideal window for a selective application exists in the pH range of 2.0 to 3.0. At higher pH polymer particles neither could be deposited on the aluminum oxide surface nor on the zinc oxide surface. At pH below this window, polymer dispersions were precipitating on both surfaces. Only in that window were polymer dispersions precipitating exclusively on the aluminum oxide surface. After defining these application parameters the goal of selectively coating grain boundaries on the industrial HDG steel substrate could be realized through a dip coating process. The final proof of this concept was provided through a comparison of a treated non-grain boundary versus a treated grain boundary of HDG steel substrates in a salt spray test where both samples were coil coated and scratched. The results captured by SEM/EDX imaging showed a significant difference in the condition of the grain boundaries at the corrosion front. It was found that selectively covered grain boundaries with a specifically designed polymer reduced the corrosive damage along the grain boundaries by a factor of three to twenty. On the micro scale it could be shown that grain boundaries on HDG steel are highly corrosively active. It has been also shown that it is possible to block grain boundaries and reduce their corrosive activity. The new method for selective corrosion protection as introduced within this study could save a tremendous amount of material and therefore provide cost benefits. Although the corresponding results from the industrial scale salt spray tests could not show a clear improvement in corrosion creep reduction of grain boundary inhibited HDG steel substrates, the focus on the specific chemistry of industrial surfaces on the micro scale may provide new smart corrosion protection systems.

Based on the results of this study one would recommend that the approach of selective material application for corrosion protection to the specific surface characteristics of technical substrates should be pursued. For HDG steel, as used in this study, one could recommend that different colloidal material towards grain boundaries such as corrosion inhibitor filled nano-containers or capsules should be addressed. One could also combine polymer application for grain boundaries with self-assembling molecules as it is known that SAMs do not

provide adequate barrier properties on the rough structure of grain boundaries, yet they are appropriate for flat topographies as can be found on grains.

All investigations in this study were carried out on one substrate, namely HDG steel Al 0.5 w.-%. Even though this substrate is one of those most commonly used in industrial applications, there are a tremendous number of other technical surfaces that require coating and protection from corrosion degradation. One could make the assumption that benefits could be gained in the transfer of these basic findings to further substrates, creating advanced coating materials adapted to their specific substrate characteristics. Therefore this study underlines the importance of focusing on specific substrate chemistry in order to develop smart coatings and thus improved corrosion protection.

Appendix

Abbreviations

Acronyms

ATRP	Atom Transfer Radical Polymerization
BMA	Butylmethacrylate
CE	Counter Electrode
CRP	Controlled Radical Polymerization
DLS	Dynamic Light Scattering
DPE	1,1-diphenylethylene
EDX	Energy Dispersive X-ray spectroscopy
Eq	Equation
FIB	Focussed Ion Beam
Fig	Figure
GPC	Gel Permeation Chromatography
HDG	hot dipped galvanized
HEMA	Hydroxyethylmethacrylate
HSAB	Hard and Soft Acids and Bases
MA	Maleic Acid
MMA	Methyl Methacrylic Acid
NMP	Nitroxide Mediated Radical Polymerization
pH	potentia Hydrogenii
PVD	Physical Vapor Deposition
RAFT	Reversible Addition Fragmentation Chain Transfer Polymerization
RE	Reference Electrode
SEM	Scanning Electron Spectroscopy
SKP-FM	Scanning Kelvin Probe-Force Microscopy
SPR	Surface Plasmon Resonance spectroscopy
Tab	Table
TEVS	Triethoxyvinylsilane
THF	Tetrahydrofurane
VOC	Volatile Organic Compounds
VPA	Vinylphosphonic Acid
WE	Working Electrode

Symbols

%	percent
°C	degree Celsius
cm	centimeter
cm ²	square centimeter
D	polydispersity
E _c	critical excitation voltage
E ₀	accelerating voltage
g	gram
g/cm ³	density in gram per cubic centimeter
g/mol	molecular weight in gram per mole
keV	kilo electron Volt
kV	kilovolt
mm	millimeter
M _n	weight average Molecular weight
M _w	number average Molecular weight
mV	millivolt
nm	nanometer
s	second
ρ	density
μm	micrometer
θ	theta
ζ	zeta

Publications

M. Dornbusch, H. Hintze-Brüning, S. Toews, W. Bremser, „Verfahren zur Autophoretischen Beschichtung“ Pat.: DE 10 2010 019 245.7 (2010)

S. Toews, W. Bremser, H. Hintze-Bruening, M. Dornbusch, „*Smart Functionalized Polymer Dispersions for effective mapping of heterogeneous metal surfaces: Part 1 - Substrate Characterization*” submitted to Prog. Org. Coat.

S. Toews, W. Bremser, H. Hintze-Bruening, M. Dornbusch, “*New concepts for corrosion protection*” EUROCORR 2010 – The European Corrosion Congress, Moscow, RUS (2010), Oral Presentation

S. Toews, W. Bremser, “*Smart functionalized polymer dispersions for selective adsorption to metal oxide surfaces*” 240th ACS National Meeting, Boston, MA, USA (2010), Poster

S. Toews, W. Bremser, H. Hintze-Bruening, S. Sinnwell, M. Dornbusch, R. Bautista-Mester, W. Kreis, „*Smart Functionalized Polymer Dispersions for effective mapping of heterogeneous metal surfaces: New Concepts for Corrosion Protection*” Coatings Science International Conference Noordwijk, NL (2010), Oral Presentation

S. Toews, W. Bremser, “*Smart Corrosion Protection*” 8th Spring Meeting of the International Society of Electrochemistry, Columbus OH, USA (2010), Oral Presentation

S. Toews, N. Pollmann, O. Seewald, W. Bremser, „*1,1-diphenylethylene a new route to functional block-co-polymers*” 239th ACS National Meeting, San Francisco, CA, USA (2010), Poster

S. Toews, N. Pollmann, O. Seewald, W. Bremser, “*Functional Block-co-Polymers via the DPE Route*” Coatings Science International Conference, Noordwijk, NL (2009), Poster